

# Introduction to Stability and Turbulent Transport in Magnetic Confinement Fusion Plasmas

J. F. Parisi<sup>1,2</sup>

<sup>1</sup> Marathon Fusion, <sup>2</sup> Princeton Plasma Physics Laboratory

jason@marathonfusion.com

July 18, 2025

## Abstract

This tutorial provides an accessible introduction to the principles of stability and turbulent transport in magnetic confinement fusion plasmas. Key concepts, models, and practical implications are discussed to guide researchers new to the field. Some challenges and opportunities are discussed.

## Contents

<b>1</b>	<b>Short Problem Description</b>	<b>3</b>
<b>2</b>	<b>Introduction</b>	<b>6</b>
2.1	Who is This for? . . . . .	6
2.2	What is Instability and Turbulence? . . . . .	6
2.3	Nuclear Fusion Reactions in Plasmas . . . . .	7
<b>3</b>	<b>Energy and Particle Confinement</b>	<b>10</b>
3.1	Lawson Criterion: Energy Confinement . . . . .	10
3.2	Particle Confinement . . . . .	12
<b>4</b>	<b>Magnetic Confinement Schemes</b>	<b>13</b>
<b>5</b>	<b>Transport Mechanisms</b>	<b>16</b>
5.1	Classical Transport . . . . .	16
5.2	Neoclassical Transport . . . . .	17
5.3	Turbulent Transport . . . . .	18
5.4	Power Plant Size Considerations . . . . .	21
5.5	Further Considerations . . . . .	22
<b>6</b>	<b>Transport Framework</b>	<b>22</b>
6.1	Fokker-Planck Equation . . . . .	23
6.2	Maxwell Equilibrium . . . . .	24
6.3	Gyrokinetics . . . . .	25
6.4	Neoclassical . . . . .	28

6.5	Transport . . . . .	28
6.6	Magnetic Equilibrium . . . . .	29
6.7	Example . . . . .	29
6.8	Further Reading . . . . .	30
<b>7</b>	<b>Gyrokinetic Instabilities</b>	<b>30</b>
7.1	Ion Temperature Gradient Instability . . . . .	31
7.2	Electron Temperature Gradient Instability . . . . .	33
7.3	Trapped Electron Mode . . . . .	34
7.4	Microtearing Mode . . . . .	36
7.5	Kinetic Ballooning Mode . . . . .	36
7.6	Parallel Velocity Gradient Instability . . . . .	37
7.7	Universal Instability . . . . .	37
7.8	Nonlinear Phenomena . . . . .	38
7.9	Experimental Measurements . . . . .	39
7.10	Further Reading . . . . .	40
<b>8</b>	<b>Codes and Workflows</b>	<b>41</b>
8.1	Gyrokinetics . . . . .	41
8.2	Neoclassical Transport . . . . .	41
8.3	Integrated Transport Solvers . . . . .	41
8.4	Magnetic Equilibrium Solvers . . . . .	41
<b>9</b>	<b>Tokamak Confinement Regimes</b>	<b>41</b>
9.1	H-mode . . . . .	42
9.2	L-mode . . . . .	43
9.3	Prospects . . . . .	44
9.4	Further Reading . . . . .	44
<b>10</b>	<b>Burning Plasmas</b>	<b>45</b>
<b>11</b>	<b>Other Important Topics</b>	<b>46</b>
<b>12</b>	<b>Summary</b>	<b>46</b>
<b>13</b>	<b>Acknowledgements</b>	<b>47</b>
<b>14</b>	<b>Data Availability</b>	<b>47</b>
<b>A</b>	<b>Appendix: ITG Instability</b>	<b>47</b>
A.0.1	Useful Integrals . . . . .	49
A.0.2	Dispersion Relation . . . . .	50
A.1	Toroidal ITG Instability . . . . .	51
A.2	Slab ITG Instability . . . . .	52
A.2.1	Drift Wave . . . . .	53
A.2.2	Instability . . . . .	53
A.2.3	Landau Damping . . . . .	54
A.2.4	Low $k_{\parallel}$ Growth Rate . . . . .	56
A.2.5	Critical $\eta_i$ . . . . .	57

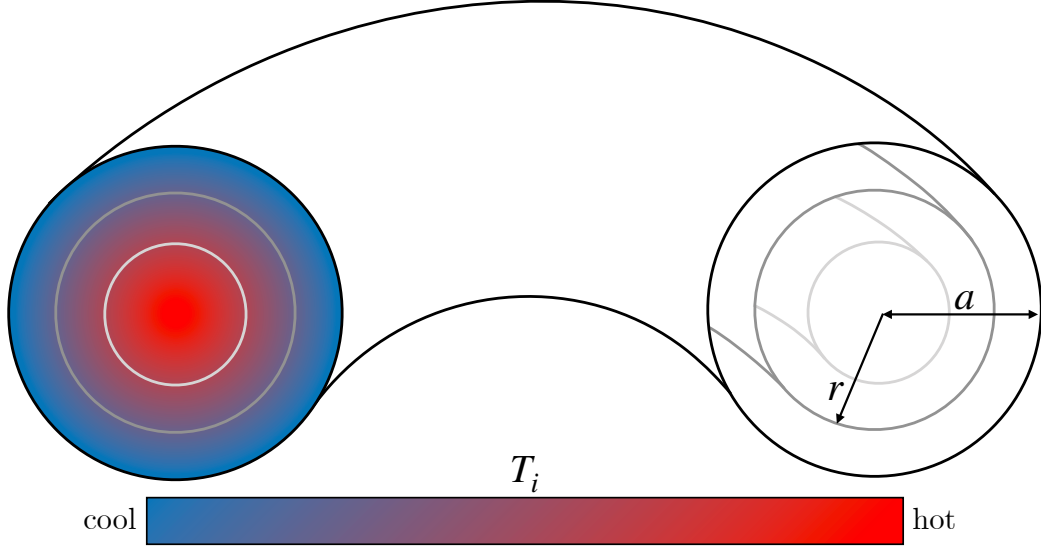


Figure 1: Cartoon of ion temperature profile, radial coordinate  $r$ , and minor radius  $a$  for Equations (1) and (2).

## 1 Short Problem Description

We begin this tutorial with a short motivational problem. A thorough introduction is provided in Section 2. The concepts introduced in this section are described in more detail in later sections.

Building a fusion power plant that produces substantial net energy requires effective confinement of hot plasma, so that fusion reactions occur frequently enough to generate significant power. However, plasma confinement is challenging, as energy continuously escapes through transport processes. For a given heating source, improved confinement – i.e., reduced transport and higher temperature gradients – allows the plasma core to reach higher temperatures. Historically, as fusion devices achieved hotter plasmas, transport losses also increased, limiting further gains in core temperature. The main drivers of these losses are plasma instabilities and turbulence. This tutorial introduces key concepts and tools used to study plasma stability and turbulent transport.

To motivate the importance of these processes in magnetic confinement fusion (MCF) – which includes machines such as tokamaks, stellarators, and mirrors – we begin with a simplified example. This example illustrates how the total fusion power output can depend sensitively on three core transport properties: the critical temperature gradient, the heat diffusivity, and the transport stiffness.

Consider a torus where energy is injected at a volumetric rate  $p_{\text{ext},i}$  (in Watts per cubic meter) around the plasma center. We are interested in the ion temperature  $T_i$  as a function of the radial coordinate  $r$ . A cartoon of  $T_i$  and the radial coordinate  $r$  is shown in Figure 1. In steady-state the plasma ion pressure is constant in time and the conservation equation for radial energy transport is

$$\frac{1}{r} \frac{\partial}{\partial r} (r q_i) = p_{\text{ext},i}, \quad (1)$$

where  $q_i$  is the ion heat flux (in Watts per square meter) and  $r$  is the minor radial coordinate (in meters). The left-hand side of Equation (1) describes energy flux in the radial direction and is equal to a divergence,  $\nabla \cdot \mathbf{q}_i$ . The right-hand side describes an

energy source. Therefore, Equation (1) is similar to Gauss's law  $\nabla \cdot \mathbf{E} = 4\pi\tilde{\rho}$  for charge density  $\tilde{\rho}$  that sources the electric field  $\mathbf{E}$ .

We assume that the normalized, dimensionless heat transport is described by

$$\hat{q}_i = \hat{\chi}_i \left( \frac{a}{L_{T,i}} - \frac{a}{L_{T,i}^{\text{crit}}} \right)^{\alpha_{\text{stiff}}} \text{H} \left( \frac{a}{L_{T,i}} - \frac{a}{L_{T,i}^{\text{crit}}} \right), \quad (2)$$

where the heat flux is normalized by a 'gyroBohm' value  $q_{i,\text{gB}}$ ,

$$\hat{q}_i \equiv \frac{q_i}{q_{i,\text{gB}}}, \quad q_{i,\text{gB}} \equiv \left( \frac{\rho_i}{a} \right)^2 n_i v_{ti} T_i, \quad (3)$$

and the heat diffusivity  $\chi_i$  is also accordingly normalized

$$\hat{\chi}_i \equiv \frac{\chi_i}{\chi_{i,\text{gB}}}, \quad \chi_{i,\text{gB}} \equiv \frac{\rho_i^2 v_{ti}}{a}. \quad (4)$$

The quantity  $a$  is the torus minor radius,  $L_{T,i}$  is the logarithmic ion temperature gradient,

$$L_{T,i} \equiv -(\partial T_i / \partial r)^{-1}, \quad (5)$$

$T_i$  is the ion temperature,  $L_{T,i}^{\text{crit}}$  is the critical ion temperature gradient below which there is zero transport,  $\alpha_{\text{stiff}}$  is a 'stiffness' parameter, H is a Heaviside function,  $n_i$  is the ion density,  $v_{ti} = \sqrt{2T_i/m_i}$  is the ion thermal speed,  $m_i$  is the ion mass,  $\rho_i = v_{ti}/\Omega_{c,i}$  is the ion gyroradius, and  $\Omega_{c,i} = q_i B / cm_i$  is the ion cyclotron frequency where  $q_i$  is the total ion charge,  $B$  is the magnetic field amplitude, and  $c$  is the speed of light. The form of  $\hat{q}_i$  in Equation (2) assumes that turbulence drives all of heat transport; in following sections, we show that other mechanisms also contribute to the heat transport, although they are typically much smaller than turbulence in current machines.

The form of  $\hat{q}_i$  in Equation (2) is motivated by experiments and theory showing that transport (1) has varying 'stiffness' – Equation (2)  $\alpha_{\text{stiff}}$  is typically larger than one but can vary significantly – (2) has a critical gradient  $a/L_{T,i}^{\text{crit}} \neq 0$ , below which there is zero transport – and (3) can be written as proportional to a diffusivity  $\hat{\chi}_i$  [184, 204, 179, 11, 357, 46, 270, 175, 184, 385, 268, 364, 253, 124, 19, 181, 64, 217]. We emphasize that while the transport equation in Equation (1) and the form of  $\hat{q}_i$  in Equation (2) are highly simplified, they illustrate the importance of stability and transport.

We solve Equation (1) using three values of the critical gradient and three values of the diffusivity,

$$\frac{a}{L_{T,i}^{\text{crit}}} \in [1.2, 2.4, 3.6], \quad \hat{\chi}_i \in [0.5, 1.0, 2.0]. \quad (6)$$

The resulting ion temperature profiles are shown in Figure 2(a) for  $\alpha_{\text{stiff}} = 3.0$ : each of the three linestyles corresponds to a different  $\hat{\chi}_i$  value and each of the three colors corresponds to a different  $a/L_{T,i}^{\text{crit}}$  value. In Figure 2(b), we plot the cumulative fusion power up to a given radial location,

$$P_{\text{fus,C}}(r) = \int_0^{V(r)} p_{\text{fus}} dV, \quad (7)$$

where  $p_{\text{fus}}$  is the fusion power density (see Equation (11)) and  $V(r)$  is the plasma volume enclosed by a surface at radius  $r$ . We assume the volume element  $dV$  satisfies circular

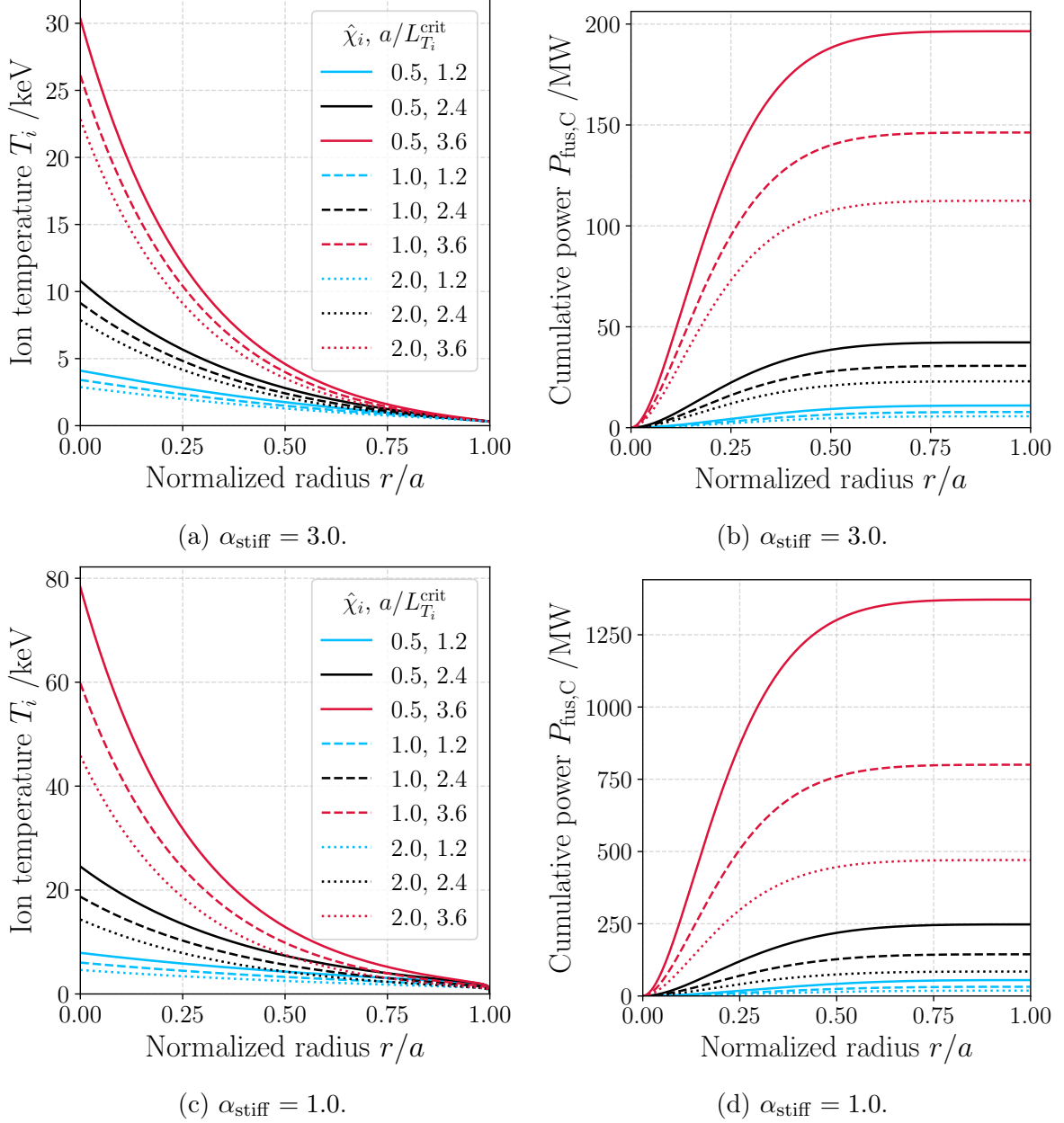


Figure 2: (a), (c) ion temperature profiles for different  $\hat{\chi}_i$  and  $a/L_{T,i}^{\text{crit}}$  values for  $\alpha_{\text{stiff}} = 3.0$  and  $1.0$  respectively; (b), (d) corresponding cumulative fusion power profiles (see Equation (7)).

flux surfaces shown in Figure 1. The results are striking: a 50% change in  $a/L_{T,i}^{\text{crit}}$  changes the total fusion power by roughly a factor of five, whereas a 50% change in  $\hat{\chi}_i$  changes the total fusion power by less than 50%. We repeat this exercise for a less ‘stiff’ transport mechanism,  $\alpha_{\text{stiff}} = 1.0$ , in Figure 2(c) and (d). For transport that is less stiff,  $\hat{\chi}_i$  becomes increasingly important for the variation in the cumulative fusion power but in this simple model, is still less important than  $a/L_{T,i}^{\text{crit}}$ .

This exercise illustrates some important features of turbulent transport. The energy fluxes are determined by at least three important parameters: the critical gradient, the diffusivity, and the stiffness. Plasma ‘stability’ typically determines  $a/L_{T,i}^{\text{crit}}$  and ‘transport’ typically determines  $\hat{\chi}_i$  and  $\alpha_{\text{stiff}}$  although there are turbulent phenomena that can modify

$a/L_{T,i}^{\text{crit}}$  [89, 283, 442, 332, 201, 180, 53]. Therefore, if one is looking to increase the core temperature of fusion power plants, there are multiple approaches: increase the critical gradient, and decrease the turbulent diffusivity, and decrease the stiffness. We are ultimately interested in the total enclosed fusion power; the distribution of the integrated volume in Equation (7) has a big effect on the fusion power [308, 83]. There are many more subtleties, some of which we will cover in later sections.

A second important feature is that predicting profiles can be much less challenging in systems with high transport stiffness. The reason is that finding  $\hat{\chi}_i$  is usually orders of magnitude harder than finding  $a/L_{T,i}^{\text{crit}}$ . This is because finding  $\hat{\chi}_i$  involves nonlinear numerical simulations, whereas  $a/L_{T,i}^{\text{crit}}$  only requires linear simulations, or sometimes even pen and paper theory. Nonlinear simulations are typically much more demanding in numerical resources, implementation, and convergence checks, therefore they require more numerical and human time to complete. If transport is highly stiff ( $\alpha_{\text{stiff}} > 1$ ) then the steady-state temperature gradients might only be marginally above the critical linear gradient  $a/L_{T,i}^{\text{crit}}$ . In this case, using the critical profile gradient would give a close estimate for the profiles. If the transport is not stiff [364], high-fidelity transport simulations are often needed to calculate the achievable temperature gradients. In reality, profiles in devices such as tokamaks are set by many more effects than those laid out in Equations (1) and (2) – high-fidelity plasma turbulence modeling is *sometimes* a necessary, but never sufficient, condition for accurately finding profiles.

## 2 Introduction

### 2.1 Who is This for?

The primary objective of this tutorial is to serve as an accessible entry point for understanding stability and transport in MCF plasmas. While the focus is on plasma stability and turbulence, the intended audience spans the full range of researchers and engineers, and it should be accessible to physics and engineering students at the Sophomore/Junior level of college. In fusion systems, many components are highly interdependent, and plasma confinement is no exception. This tutorial emphasizes practical applications of plasma stability and turbulent transport to MCF devices rather than the theoretical foundations of turbulence, for which there are many excellent resources [40, 304, 119, 184, 227, 370, 185]. Some sections conclude with references for those interested in exploring the material further.

### 2.2 What is Instability and Turbulence?

First, let us define precisely what we mean by instability and turbulence in the context of fusion plasmas. Instability is when an initially small perturbation such as density or temperature grows over time. If this instability grows to become sufficiently large, the resulting plasma state can become turbulent. Turbulence, *multiscale disorder* (a description borrowed from [365]), is a state where energy can be transferred across a range of spatial and temporal scales. One particularly interesting, and often challenging, aspect of turbulence in plasmas is that it is *kinetic* – that is, in addition to the problem having spatial and temporal dependence, there is also a velocity-space dependence.

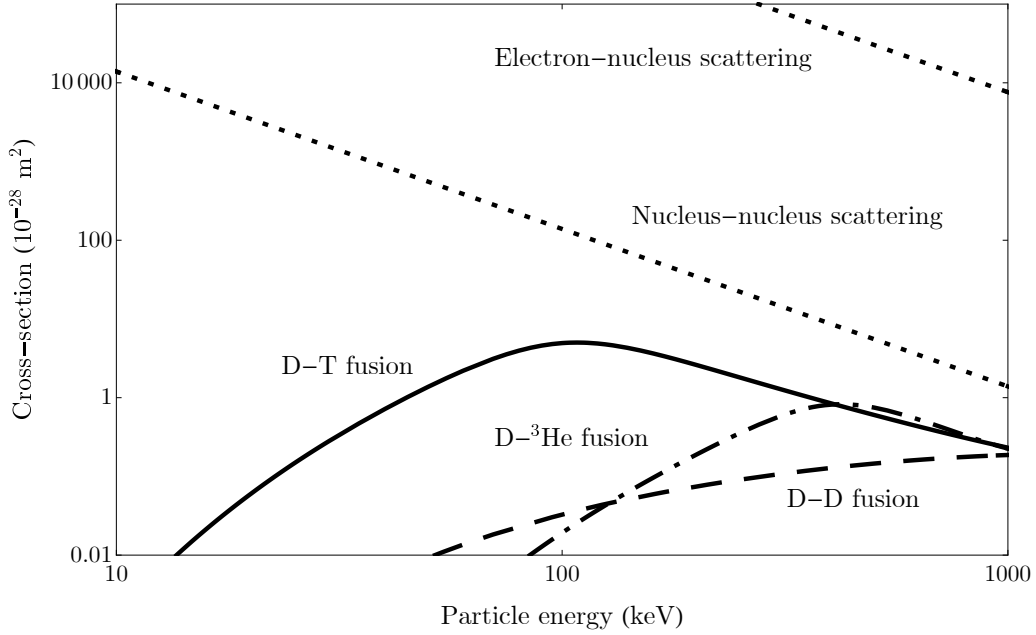
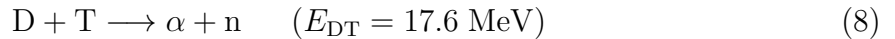


Figure 3: Cross sections for Coulomb scattering and fusion reactions versus particle energy. Adapted from [307].

### 2.3 Nuclear Fusion Reactions in Plasmas

The practical motivation to study stability and transport in MCF plasmas is that it is a powerful tool for improving the viability of fusion energy. Nuclear fusion energy promises to produce energy through nuclear reactions with the highest energy released per unit mass of any known physical mechanism with the exception of matter anti-matter annihilation. Nuclear fusion reactions release energy by fusing two nuclei into new configurations with a lower total nuclear binding energy. A particularly attractive fusion reaction is the deuterium-tritium (D-T) fusion reaction [387, 214, 430], which fusions a deuterium and tritium nucleus into a fast helium-4 (alpha particle) and a fast neutron,



where  $E_{\text{DT}}$  is the energy released from a D-T fusion reaction. The neutron carries roughly four fifths of the energy released. Because helium-4 has an exceptionally high binding energy per nucleon, the energy released per D-T reaction is very high. The difference in binding energy between the incoming and outgoing particles is released as kinetic energy, which can be converted to heat and/or electricity.

Because the cross section for electrostatic repulsion between ions - shown by the nucleus-nucleus scattering cross section in Figure 3 - is so much higher than fusion reactions, a viable fusion energy generation scheme must allow particles to scatter many times before fusion occurs. The probability of a deuterium and tritium tunneling through the electrostatic Coulomb potential barrier increases exponentially with energy [286]. However, above a certain energy - for D-T fusion approximately 100 keV - the probability of fusion decreases [249]. Therefore according to Figure 3 ideally our D-T fuel will have energies in the tens to hundreds of keV. At such high energies, the electrons and nuclei are disassociated, leaving a collection of positively charged nuclei (ions) and electrons called a plasma. In most magnetically confined plasmas, the ion distribution function is

approximately a Maxwellian,

$$F_{Ms}(\mathcal{E}) = n_s \left( \frac{m_s}{2\pi T_s} \right)^{3/2} \exp \left( - \frac{\mathcal{E}}{T_s} \right), \quad (9)$$

where  $s$  is the species label,  $\mathcal{E} = m_s v^2/2$  is the particle energy with speed  $v$  and mass  $m_s$ , and  $n_s$  and  $T_s$  are the density and temperature.

In plasmas with temperatures of tens of keV, despite the higher fusion cross section, Coulomb collisions between ions are still orders of magnitude more frequent than D-T fusion reactions – see nucleus-nucleus scattering in Figure 3. This necessitates the plasma be *confined* so that particles can be scattered many times before eventually undergoing fusion. In addition to the particles constituting the fusion fuel being well-confined, we also require that energy be well-confined. A fairly good analogy to confinement in a fusion plasma is a wood fire. The wood fire needs particles to burn. And heat must be sufficiently well-confined, otherwise the fire will eventually stop. On the other hand, the waste products from the fire must also be ventilated, otherwise there will be insufficient oxygen for ignition. Analogously, alpha particles from D-T fusion reactions must deposit their energy and then be removed from the plasma to prevent them from diluting the fusion fuel. Just as there are techniques for improving a wood fire’s heat output, wood burn-up, and longevity, there are many techniques in development for improving the properties of fusion fire. These requirements – and others we introduce later – necessitate a *confinement scheme*.

Because magnetic fields permeate plasma, one mainstream fusion energy confinement approach is to use strong magnetic fields to confine plasma in a toroidal cage. The plasma needs to be hot in the center of the torus – so that the fusion rate is high – and cold at the edge – so that the machine walls do not melt. These are two of the most stringent boundary conditions for MCF, but alone, are insufficient information to build a power plant: some of the next most important questions are how to configure the plasma temperature and pressure profiles given that we wish to generate significant fusion power and not melt the walls.

According to Figure 3, only particles with energies

$$20 \text{ keV} \lesssim \mathcal{E} \lesssim 500 \text{ keV}, \quad (10)$$

have a significant likelihood of undergoing fusion reactions. In fusion plasmas, this usually means that the overwhelming majority of fusion reactions come from ions in the high energy tails of  $F_{Ms}$  in Equation (9) – the remainder have insufficient energy to have a high likelihood of tunneling through the Coulomb barrier. Intuitively, one strategy to increase fusion power might be to increase the plasma temperature so that most particles satisfy Equation (10). However, this is usually a fruitless task for at least three reasons.

First, for D-T fusion reactions, the fusion power peaks around  $T \simeq 60 \text{ keV}$ , meaning that if many particles can significantly more energy than  $\sim 500 \text{ keV}$ , the cross section and therefore the fusion power drops. The D-T fusion power per unit volume is

$$p_{\text{fus}} = \frac{1}{4} n^2 \langle \sigma v \rangle E_{\text{DT}}, \quad (11)$$

where  $n$  is the fuel number density,  $\sigma$  is the cross section, and  $\langle \sigma v \rangle$  is the fusion reactivity – a velocity integral over the Maxwellian distribution function  $F_{Ms}$  in Equation (9). We plot the reactivity of some common fusion reactions in Figure 4 – while plasmas that



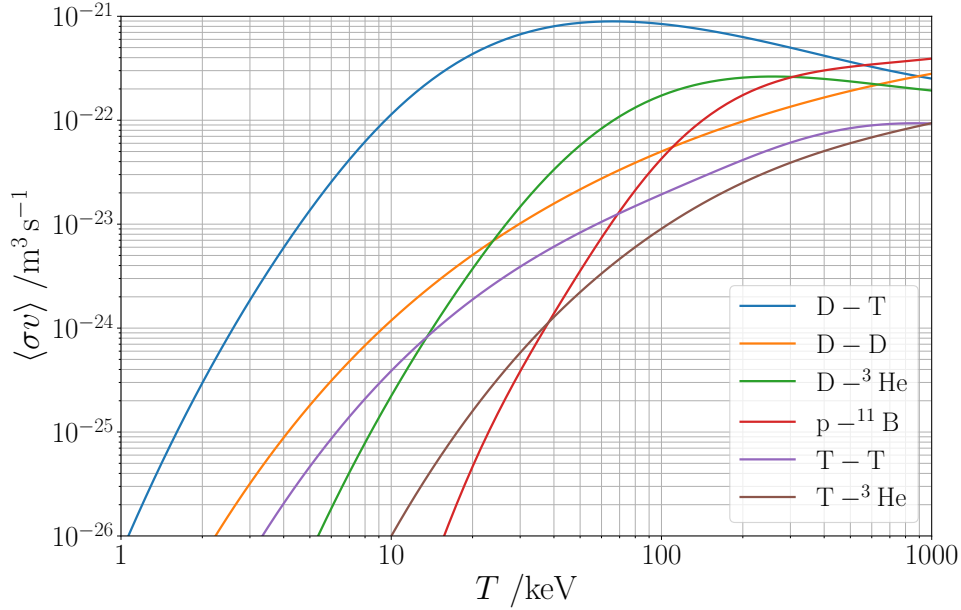


Figure 4: Reactivity of some fusion reactions with Maxwellian energy distributions.

burn too hot will have lower fusion power with increasing temperature, achieving such high temperatures in a MCF device is very challenging due to energy loss mechanisms such as radiation.

Second, because the ion and electron temperatures are usually quite similar, a plasma with higher ion temperature will also have higher electron temperature and therefore a higher Brehmstrahlung power per unit volume

$$p_B = C_B n n_e T_e^{1/2}. \quad (12)$$

Here  $n$  is total hydrogen density,  $n_e$  is the electron density, and  $C_B = 3.34 \times 10^{-21} \text{ keV m}^3/\text{s}$  is a constant. Therefore, while Equation (11) and Figure 4 show that higher power density might be achievable with higher temperature, the radiative power losses can become prohibitive.

Third, plasma confinement typically degrades with higher temperature. This is due to two main reasons: (1) Because of the requirement that a plasma is cool at the edge and hot in the center, an increasingly hot center results in steeper temperature gradients. These steep temperature gradients are a source of free energy that drive plasma instabilities, which cause further plasma losses – sustaining a plasma with very high temperature gradients usually requires prohibitively high power; (2) Charged particles in a magnetic field undergo gyromotion in the plane perpendicular to the field; as a particle becomes more energetic, its gyroradius increases and the particle confinement time decreases due to various transport mechanisms. We will discuss this in detail in coming sections.

It is important to distinguish the transport discussed in this tutorial from other transport mechanisms. Here, we focus on ‘diffusive’-like transport as opposed to larger disruptive events. For example, magnetohydrodynamic (MHD) instability can cause very large displacements of energy and particles through events such as edge-localized modes (ELMs) [114, 77, 287, 262, 193, 229, 409] and plasma disruptions [420, 170, 439, 30, 388, 211].

This tutorial is organized as follows: we introduce the Lawson criterion and other confinement considerations in Section 3. In Section 4, we introduce magnetic confine-

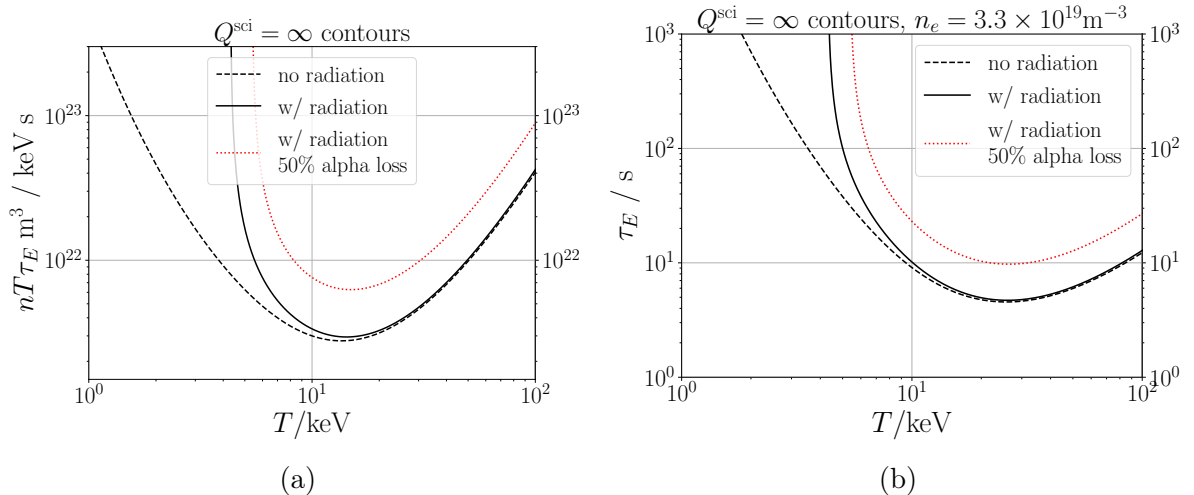


Figure 5: (a) Lawson triple product and (b) energy confinement time, both for an ignited plasma. In (b), we assume a constant plasma density of  $n = 3.3 \times 10^{19} \text{m}^{-3}$ .

ment schemes. In Section 5, we give an overview of the various transport mechanisms. In Section 6, we describe the theoretical framework for self-consistent transport calculations. In Section 7, we review the gyrokinetic instabilities that give rise to turbulent transport. In Section 8, we introduce some commonly used codes for gyrokinetic, neoclassical, transport, and magnetic equilibrium calculation. In Section 9, we cover the main tokamak confinement regimes. In Section 10, we discuss some challenges and questions. Due to time constraints, I have omitted many important topics – some of these are briefly covered in Section 11. We conclude in Section 12.

### 3 Energy and Particle Confinement

In order to estimate the required quality of energy confinement in a fusion device, we defer to a derivation called the Lawson criterion [242, 430]. The result will be a quantitative measure of the conditions required for fusion ignition, analogous to what we intuitively know for a wood fire: a roaring fire needs enough wood fuel (fusion fuel), temperature, and the heat must be confined for sufficiently long. We will also present an analogous argument for particle confinement.

#### 3.1 Lawson Criterion: Energy Confinement

Here, we determine the required quality of energy confinement in a fusion plasma. The argument [242, 430] begins with the requirement that power losses  $p_L$  should balance the power sources from alpha heating  $p_\alpha$  and external heating  $p_{\text{ext}}$ ,

$$p_L = p_\alpha + p_{\text{ext}}. \quad (13)$$

We define the energy confinement time as

$$\tau_E \equiv \frac{w}{p_L}, \quad (14)$$

where  $w = 3nT/2$  is the stored thermal energy per unit volume for a plasma composed of ion density  $n$  with ion temperature  $T$ .  $\tau_E$  measures the time for a unit of energy

deposited in the plasma center to leave the plasma. As formulated in Equation (14),  $\tau_E$  includes the effects of any physical mechanism that causes energy to leave the plasma.

A self-sustaining fusion plasma uses the alpha particles produced from D-T reactions to keep it hot. Because an alpha particle is approximately four times the neutron mass, roughly one fifth of the total fusion power is carried as kinetic energy of alpha particles. Therefore, the heating power provided by alpha particles  $p_\alpha$  assuming no alpha particle losses is

$$p_\alpha = \frac{p_{\text{fus}}}{5}. \quad (15)$$

Using Equation (13), the external heating power required to sustain a plasma is

$$p_{\text{ext}} = \frac{3nT}{\tau_E} - \frac{1}{4}n^2\langle\sigma v\rangle\frac{E_{\text{DT}}}{5}. \quad (16)$$

When the plasma can supply all of its heating requirements from alpha particles the external power requirement vanishes,  $p_{\text{ext}} = 0$ . Such a plasma is said to have *ignited*. For an ignited plasma, the value of  $n\tau_E$  must satisfy

$$n\tau_E > \frac{60}{\langle\sigma v\rangle} \frac{T}{E_{\text{DT}}}. \quad (17)$$

It is customary to multiply Equation (17) by  $T$  in order to obtain a triple product,

$$nT\tau_E > \frac{60}{\langle\sigma v\rangle} \frac{T^2}{E_{\text{DT}}}. \quad (18)$$

It is often used that for temperature in the range 10-20 keV, the D-T fusion reactivity satisfies

$$\langle\sigma v\rangle = 1.1 \times 10^{-24} \frac{T^2}{(\text{keV})^2} \text{m}^3\text{s}^{-1}, \quad (19)$$

with a maximum of 10% error. In this range,  $nT\tau_E$  in Equation (18) is temperature independent. We plot solutions to Equation (18) on the ‘no radiation’ curve in Figure 5(a) using realistic cross section data. However, there are other important loss mechanisms such as Bremsstrahlung radiation (Equation (12)). We show the modified triple product to include Bremsstrahlung power in the ‘w/ radiation’ curve in Figure 5(a), where we have added the Bremsstrahlung loss term in power balance (Equation (13)). In Equation (18) we also assumed that 100% of the alpha particles deposit all of their power. In the ‘w/ radiation 50% alpha loss’ curve in Figure 5(a), we show the effect of 50% of the alpha particle energy being lost. This significantly increases the  $nT\tau_E$  required for ignition [79, 219].

We can finally make a very rough quantitative estimate of how large  $\tau_E$  must be in order for the plasma to ignite. We plot  $\tau_E$  versus  $T$  in Figure 5(b) for a plasma with  $n = 3 \times 10^{19} \text{m}^{-3}$ , which is the density of a record JET D-T experiment 42976 with [214]. For the ‘w/ radiation’ curve at a minimum with  $T \simeq 20 - 30$  keV, the confinement time for ignition satisfies  $\tau_E \gtrsim 4$  seconds. The JET D-T discharge had a predicted ion temperature of  $T = 28$  keV and a predicted confinement time of  $\tau_E = 0.90$  seconds.

A common measure of plasma performance is the scientific gain parameter  $Q^{\text{sci}} = P_{\text{fus}}/P_{\text{ext}}$  where  $P_{\text{fus}}$  is the total fusion power. At  $t = 13.13$  seconds, JET discharge 42976 achieved  $Q^{\text{sci}} = 0.60$ . Yet, according to the simple arguments that gave the curve in Figure 5(b), only a factor of four to five increase in  $n\tau_E$  is required to bring the plasma

to ignition (where  $Q^{\text{sci}} = \infty$ ). It is important to keep in mind that the Lawson criterion makes several approximations – higher fidelity modeling is required to more accurately determine the plasma conditions required for very high fusion gain [196, 27, 302, 348].

We need to understand what determines  $\tau_E$  so that we might increase its value, which in tokamaks is set largely by turbulent transport. The first step is to write power balance in Equation (13) as an energy continuity equation,

$$\frac{3}{2} \frac{\partial nT}{\partial t} + \nabla \cdot \mathbf{q} = p_\alpha + p_{\text{ext}}, \quad (20)$$

where the quantity  $\mathbf{q}$  is the heat flux. The transport term  $\nabla \cdot \mathbf{q}$  measures the rate of heat being transported into or out of a volume. In steady state where  $\partial T / \partial t = 0$ , we can write

$$\tau_E = \frac{w}{\nabla \cdot \mathbf{q}}. \quad (21)$$

Therefore, the energy confinement time increases as the rate of heat leaking out of a volume  $\nabla \cdot \mathbf{q}$  decreases in size. In the limit of perfect heat insulation,  $\nabla \cdot \mathbf{q} = 0$ , the energy confinement time tends to infinity. The study of energy confinement in fusion plasmas centers on making  $\nabla \cdot \mathbf{q}$  as small as possible.

### 3.2 Particle Confinement

Controlling particle confinement is also crucial for a workable confinement scheme [339, 361, 265, 8, 424, 312]. For D-T MCF power plants, the conditions for particle confinement are more complicated than for energy confinement. For energy confinement, it is almost always more desirable to achieve a higher particle confinement time. For particle confinement, there is a more complicated set of tradeoffs [437]. On the one hand, if the particle fueling rate is constant, it is desirable for deuterium and tritium to remain in the hot core for as long as possible to increase the probability of them undergoing fusion reactions. Furthermore, tritium is very expensive and challenging to handle, so it is undesirable to have large tritium flows through the plasma and ancillary power plant systems [209, 3, 354, 103, 202, 224, 31, 2, 281, 424, 312]. Additionally, it is desirable for alpha particles born from D-T reactions to stay confined to the plasma core while they slow down, depositing their energy into the hot core. On the other hand, once alpha particles are slow and thermalized, they become helium ash, which dilute the core fuel and decrease the total fusion power – it is desirable for the helium ash to be transported from the fusion core as quickly as possible [404, 396, 122, 338, 395, 163, 372, 347, 220, 282]. There are also further requirements that non-fuel impurities be transported from the core [161, 177, 99, 41, 166, 7], but sometimes confined in the outer-core to edge region to radiate power [206, 210, 109, 104, 66, 428].

In this section, we focus on D-T fuel confinement, neglecting the subtleties discussed above for the other particle species. We basic require D-T fuel to stay in the core for as long as possible to maximize the probability of fusion occurring. We can write a similar equation to power balance in Equation (13) for D-T particle balance. To simplify the arguments, the following equations will be for the deuterium species in a D-T plasma, although they will also be applicable to tritium. The particle balance equation is

$$S_L = S_{\text{fus}} + S_{\text{ext}}, \quad (22)$$

where  $S_L$  is the loss of deuterium particles by transport (units of particles per second),  $S_{\text{fus}}$  is a sink of deuterium particles into D-T fusion reactions, and  $S_{\text{ext}}$  is external fueling of

deuterium provided by neutral beams [96, 382, 183] and pellet injectors [68, 21, 169, 285]. We define the particle confinement time as

$$\tau_p \equiv \frac{n_D}{S_L}, \quad (23)$$

where  $n_D$  is the deuterium particle density. As we did before for the Lawson criterion, we assume that the plasma density and temperature profiles are constant. The sink of deuterium particles is equal to minus the D-T fusion reaction rate

$$S_{\text{fus}} = -n_D^2 \langle \sigma v \rangle, \quad (24)$$

where we have assumed equal densities of deuterium and tritium. Rearranging particle balance in Equation (22) gives a required deuterium particle confinement time

$$\tau_p = \frac{n_D}{S_{\text{ext}} - n_D^2 \langle \sigma v \rangle} = \frac{n_D}{S_{\text{ext}} - P_{\text{fus}}/E_{\text{DT}}}. \quad (25)$$

There is a fundamental difference between particle confinement and energy confinement: for energy confinement, a plasma can ‘ignite’ since fusion reactions release energy that can heat the plasma. However, a D-T plasma cannot ‘ignite’ for the particle supply, because D-T fusion reactions are a sink of D-T fuel. Therefore, for a fusion plasma with perfect particle confinement,  $\tau_p \rightarrow \infty$ , the particle fueling source  $S_{\text{ext}}$  must balance the D-T particle consumption rate  $P_{\text{fus}}/E_{\text{DT}}$ . In reality, there are always mechanisms that cause particle transport, which means we require the denominator of Equation (25) to be positive definite over sufficiently long time periods,

$$S_{\text{ext}} > P_{\text{fus}}/E_{\text{DT}}. \quad (26)$$

Therefore, Equation (25) shows that in a burning plasma, particle and energy transport are coupled by fusion reactions. There are many more subtle ways that particle and energy transport are coupled, some of which we will review in this article.

Finally, in addition to particle and energy transport, we are also often interested in momentum transport. Tokamak plasmas can rotate, often very quickly [37, 355, 381, 194]. Both the rotation and the spatial gradient of the rotation (‘rotation shear’) can have a significant impact on the stability properties of toroidal plasmas [412, 143, 399, 414, 140, 59, 17, 435]. Angular momentum can even be redistributed internally in tokamaks [344, 86, 317]. In this article, we will focus on particle and energy transport, generally omitting momentum transport.

## 4 Magnetic Confinement Schemes

In Section 2 we claimed that Coulomb scattering being much faster than any fusion reaction rate motivates a confinement scheme. Mainstream fusion research efforts are centered on two distinct confinement schemes: inertial confinement fusion and magnetic confinement fusion. In inertial confinement fusion, the fusion fuel is rapidly compressed and heated, relying on its own inertia to hold it together briefly until fusion reactions occur. The goal is for the fuel to have undergone many fusion reactions at extremely high densities before the fuel flies apart. In contrast, magnetic confinement fusion occurs at roughly ten orders of magnitude lower density, using strong magnetic fields to contain a hot plasma for extended periods.

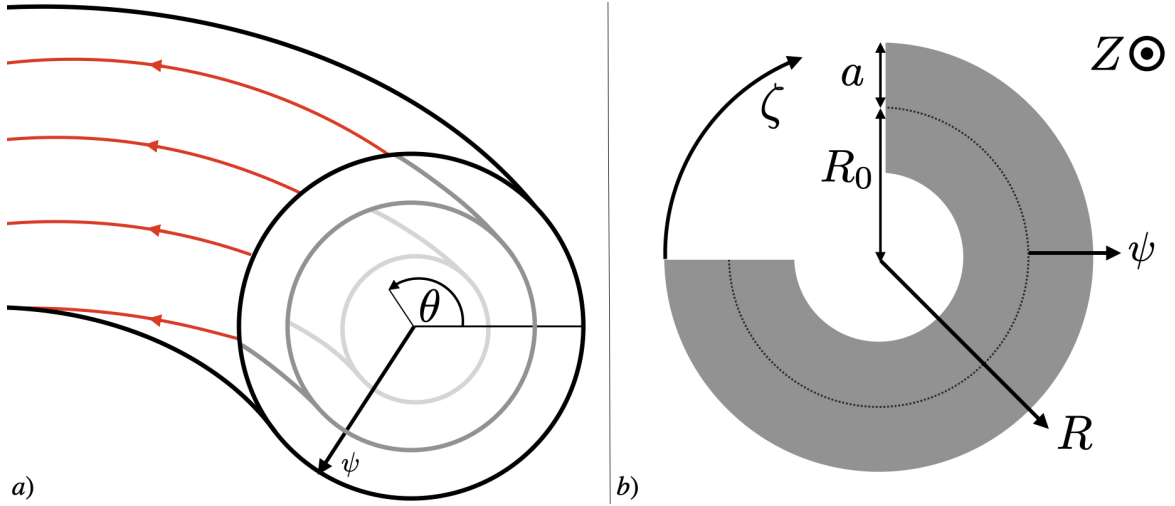


Figure 6: (a): Three nested magnetic flux surfaces. Red lines on the outermost surface represent a field line sampling the surface;  $\theta$  is a poloidal angle and  $\psi$  is the poloidal flux divided by  $2\pi$ . (b): Bird's eye view of a tokamak;  $R$  is the major radial coordinate,  $Z$  is the axial coordinate,  $\zeta$  is the toroidal angle,  $R_0$  is the  $R$  location of the LCFS, and  $a$  is the minor radius.

This tutorial focuses on magnetic confinement fusion. We will generally use the coordinate system in tokamaks, although many concepts will also carry over to other magnetic confinement schemes such as stellarators. A tokamak is a donut-shaped (toroidal) machine designed to confine plasma. Inside a tokamak, magnetic fields force the charged particles to move along circular paths, tracing out layers called magnetic flux surfaces. Think of these flux surfaces as nested donut-shaped layers inside the tokamak – see Figure 6(a) for an illustration. Charged particles move rapidly along these surfaces but move much more slowly from one surface to another.

The relatively slow particle motion across flux surfaces occurs because charged particles spiral around magnetic field lines, a motion called Larmor gyration. An ion with thermal speed

$$v_{ti} = \sqrt{\frac{2T}{m}} \quad (27)$$

has a gyroradius

$$\rho_i = \frac{v_{ti}}{\Omega_i} \quad (28)$$

with gyrofrequency

$$\Omega_i = \frac{Z_i e B}{m_i}, \quad (29)$$

for a charge number  $Z_i$ , proton charge  $e$ , magnetic field strength  $B$ , and mass  $m_i$ . Although particles can move freely and quickly along magnetic field lines, their perpendicular motion across lines is much more limited. This is the basic premise of magnetic confinement.

Because particles mostly remain confined to their flux surfaces, certain properties of the plasma, such as temperature, density, and electric potential, remain nearly uniform on each surface. These properties are called ‘flux functions’ because they are constant a single flux surface. Flux functions  $g$  therefore satisfy

$$\mathbf{B} \cdot \nabla g = 0, \quad (30)$$

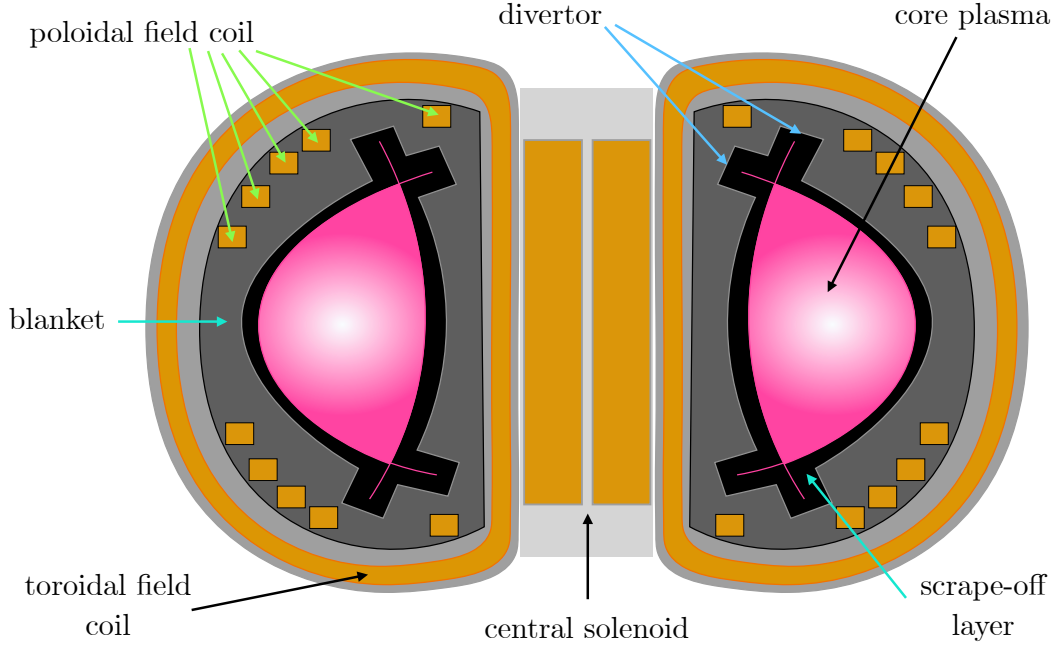


Figure 7: Some key features of a tokamak.

where  $\mathbf{B}$  is the magnetic field vector. The equilibrium magnetic field for tokamaks can be written as

$$\mathbf{B} = I\nabla\zeta + \nabla\zeta \times \nabla\psi. \quad (31)$$

Here,  $I(\psi(R, Z)) = RB_T$  is a flux function where  $B_T$  is the toroidal component of the magnetic field,  $R$  is the major radial coordinate,  $Z$  is the axial coordinate,  $\psi$  is the poloidal flux divided by  $2\pi$ , and  $\zeta$  is the toroidal angle. The toroidal field in Equation (31) is  $\mathbf{B}_T = I\nabla\zeta$  and the poloidal field is  $\mathbf{B}_p = \nabla\zeta \times \nabla\psi$ . The variables  $(R, Z, \zeta)$  form a cylindrical coordinate system, shown in Figure 6(a).

The outer boundary of the nested magnetic surfaces is called the Last Closed Flux Surface (LCFS). In the region beyond the LCFS called the scrape-off layer (SOL), particles stream along open field lines until they intersect with a divertor. Inside the LCFS, however, particles remain well-contained, significantly reducing heat loss and making efficient confinement possible. Other useful quantities are  $a$ , the minor radius, and  $R_0$ , the  $R$  location of the LCFS, illustrated in Figure 6(b).

Before moving ahead, it is worth placing the problem we are studying in context. As described in the Lawson criterion in Section 3, the fusion power, confinement, plasma heating, and other losses are strongly coupled. However, there are more strong couplings: in Figure 7 we show a schematic of a tokamak, showing the core plasma and scrape-off layer. This review will primarily be focused on turbulence within the LCFS, although SOL turbulence is also an important research area. Surrounding the vacuum vessel containing the plasma is a blanket where tritium fuel is bred by lithium neutron capture reactions. These neutrons are produced by D-T reactions in the plasma core, and so the neutron product rate and their spatial trajectories in the plasma core impacts tritium breeding. There are poloidal field coils used mainly for plasma shaping, the central solenoid for current drive and heating, and toroidal field coils for generating the toroidal field. There are many other important systems we have omitted. We emphasize that stability and transport in the plasma core should not be studied in isolation – many of the power plant

systems are coupled in interesting and challenging ways. These couplings will become stronger as we move toward routine operation of burning plasmas.

## 5 Transport Mechanisms

In this section, we describe the physical mechanisms causing transport in MCF plasmas: classical, neoclassical, and turbulent. Since the main subject of this tutorial is turbulent transport, we will spend only a short amount of time covering classical and neoclassical transport.

The task of transport calculations is to self-consistently find the evolution of the magnetic equilibrium and plasma profiles. This is an involved task, accomplished by solving a system of equations across a range of time and spatial scales: (1) the gyrokinetic equation, which describes the evolution of fast plasma perturbations on small gyroradius scales, (2) the neoclassical equation, which describes the evolution of slow plasma perturbations on large equilibrium scales, (3) the transport equation, which describes the slow evolution of the magnetic equilibrium and plasma profiles and (4) Maxwell's equations. We will cover these equations in detail in Section 6.

In this section, we focus on order of magnitude estimates of the transport coefficients in the transport equation. This involves calculating the particle and heat fluxes  $\mathbf{\Gamma}_s$  and  $\mathbf{q}_s$  that enter the particle and heat transport equations,

$$\frac{\partial n_s}{\partial t} + \nabla \cdot \mathbf{\Gamma}_s = S_s, \quad \frac{3}{2} \frac{\partial n_s T_s}{\partial t} + \nabla \cdot \mathbf{q}_s = P_s, \quad (32)$$

where  $n_s$  is the number of particles per unit volume for a species  $s$  (an ion or electron species),  $T_s$  is the temperature, and  $S_s$  and  $P_s$  are the particle and energy sources. Typically, the fluxes can be written in ‘diffusive’ form,

$$\mathbf{\Gamma}_s = -D_s \nabla n_s, \quad \mathbf{q}_s = -\chi_s n_s \nabla T_s, \quad (33)$$

$\mathbf{\Gamma}_s$  and  $\mathbf{q}_s$  in Equation (33) describe the radial transport of particles and heat that tends to flatten density and temperature gradients  $\nabla n_s$  and  $\nabla T_s$ .

In the following subsections, we will estimate the relative size of  $\chi_s$  for classical, neoclassical, and turbulent heat transport. For each of these three transport mechanisms, our mental model for transport will be as follows: transport occurs as a spatially two-dimensional random walk with step size  $l$ , and each step occurs with a frequency  $f$ . The random walk is two dimensional because the plasma is magnetized, and within the LCFS motion along the field lines does not lead to radial transport. We estimate the diffusion coefficient as a random walk,

$$\chi_s \sim l^2 f. \quad (34)$$

We will see that for tokamaks, only turbulent transport gives sufficiently fast radial energy diffusion to explain the observed energy confinement time in high-performance experiments. Recall that

### 5.1 Classical Transport

The first regime of transport that causes particles and energy to diffuse from the plasma core to the edge is called *classical* transport [36, 12, 246, 168]. In the classical transport regime, particles undergo a random walk with a step size of the Larmor radius  $\rho_i$  and a



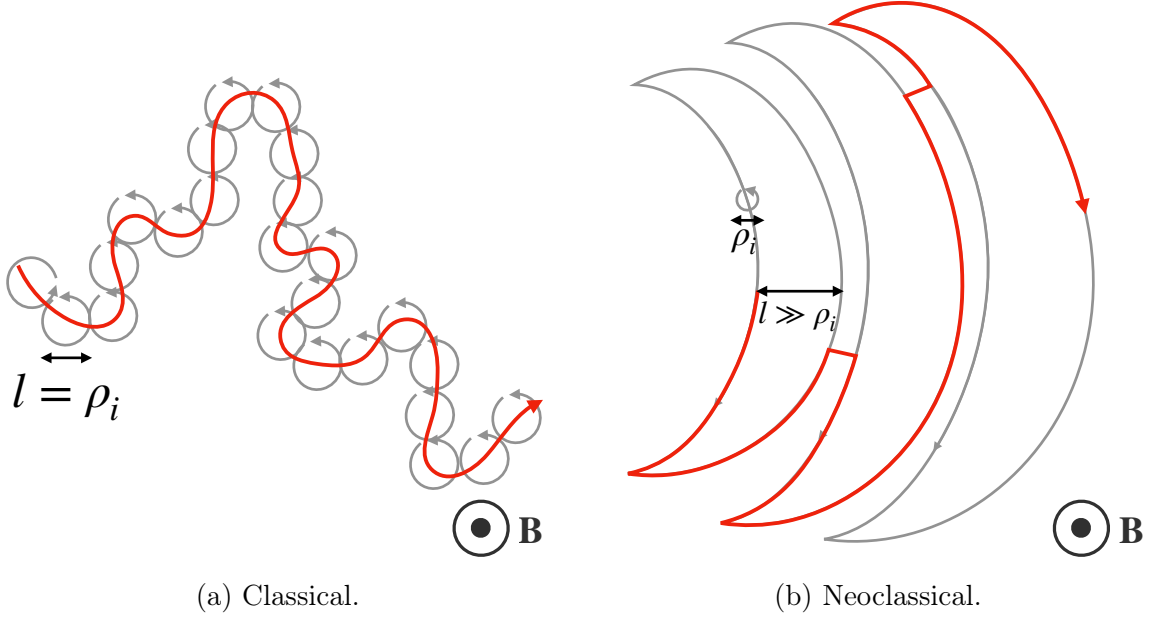


Figure 8: Heuristic random walk models for (a) classical and (b) neoclassical transport.

frequency of the collision frequency – a cartoon of this process is shown in Figure 8(a). Collisional transport gives relatively low transport levels and so is tolerable within MCF schemes such as tokamaks. If this were the only transport mechanism, energy confinement would be excellent, and as of 2025, we would almost certainly have fusion power plants delivering electricity to the grid.

The transport coefficient estimate in Equation (34) using a step size equal to the ion gyroradius  $\rho_i$  and a step frequency equal to the ion-ion collision frequency  $\nu_{ii}$  gives

$$\chi_i^{\text{classical}} \sim \rho_i^2 \nu_{ii}. \quad (35)$$

Revisiting the JET discharge 42976 [214] we introduced earlier, we now estimate the energy confinement time in a plasma where energy transport is dominated by collisional transport. Heuristically, we can estimate the collisional confinement time as

$$\tau_E^{\text{classical}} \approx \frac{a^2}{\chi_i^{\text{classical}}} = \left( \frac{a}{\rho_i} \right)^2 \frac{1}{\nu_{ii}}. \quad (36)$$

For this JET discharge,  $\rho_i \approx 0.0015$  meters,  $\nu_{ii} \approx 600$  Hertz, the minor radius is  $a = 0.95$  meters, and toroidal field  $B_T = 3.6$  Tesla. This gives

$$\tau_E^{\text{classical}} \approx 670 \text{ seconds}. \quad (37)$$

Given that the experimental value is  $\tau_E = 0.90$  seconds, the classical rough estimate gives a confinement time over 700 times larger than the experimental value. Additional transport mechanisms are required to explain the experimental  $\tau_E$  value.

## 5.2 Neoclassical Transport

Unfortunately, there are additional transport mechanisms with much larger diffusivity than classical transport. One is *neoclassical* transport [177, 13, 168]. The toroidicity of

tokamaks and stellarators causes the diffusive step size to increase, which increases the diffusivity significantly. In tokamaks, a large fraction of particles will bounce between maxima in the magnetic field, tracing out particle trajectories called banana orbits. The width of the banana orbit is approximately the new step size and the step frequency is the ion-ion collision frequency. The physical picture is approximately as follows, shown in Figure 8(b): trapped particles execute banana orbits. In a collision, the particle will be scattered into a new banana orbit.

Estimating the diffusion coefficient for neoclassical transport is more involved than for classical transport [168]. We concern ourselves with trapped particles undergoing banana orbits. The fraction of particles that are trapped is  $f_t \approx \sqrt{2\epsilon}$ , where  $\epsilon = r/R$  is the inverse aspect ratio. The effective collision frequency is  $\nu_{ii}/\epsilon$  and the new step size is  $l \approx \rho_{p,i}\sqrt{\epsilon}$ . Here,  $\rho_{p,i}$  is the poloidal gyroradius, which involves using the poloidal magnetic field rather than the total magnetic field in the gyrofrequency in Equation (29). Putting these together, we find

$$\chi_i^{\text{neoclassical}} \sim \sqrt{2\epsilon}\rho_{p,i}^2\nu_{ii}. \quad (38)$$

Therefore, the ratio of neoclassical to classical diffusivity is

$$\frac{\chi_i^{\text{neoclassical}}}{\chi_i^{\text{classical}}} \sim \sqrt{2\epsilon} \left( \frac{B}{B_p} \right)^2 \sim \sqrt{2}q^2\epsilon^{-3/2}, \quad (39)$$

where  $q \approx \epsilon B/B_p$  is the safety factor. In tokamaks,  $q$  is typically much larger than one.

We now estimate  $\tau_E^{\text{neoclassical}}$  using

$$\tau_E^{\text{neoclassical}} \approx \frac{a^2}{\chi_i^{\text{neoclassical}}}, \quad (40)$$

for the JET discharge 42976. Assuming that  $q^2 \approx 4$  for this discharge and taking a typical aspect ratio  $\epsilon \approx 1/5$ , we find

$$\tau_E^{\text{neoclassical}} \approx 11 \text{ seconds}. \quad (41)$$

Therefore, comparing with the experimental  $\tau_E = 0.90$  seconds, the neoclassical estimate of confinement time is still an order of magnitude too long compared with experiment. Another transport mechanism is required to explain the experimentally observed confinement time.

### 5.3 Turbulent Transport

The remaining transport mechanism to explain the shorter-than-expected energy confinement time is *turbulent* transport [250, 429, 89, 50, 123, 29]. The nature of turbulent transport is qualitatively different from classical and neoclassical, which were predictable from the equilibrium profiles. Turbulent transport, in contrast, arises from plasma perturbations that deviate from the equilibrium. Because of the requirement for high core pressure and low edge pressure, there are *pressure gradients* across the radial profiles. Pressure gradients provide a source of free energy, which can drive *instabilities*. These instabilities consist of electromagnetic, density, and temperature perturbations. These perturbations grow until they *saturate*, leaving the plasma in a turbulent state. Turbulence in MCF devices gives rise to *gyroBohm* transport. Such transport has a step size at

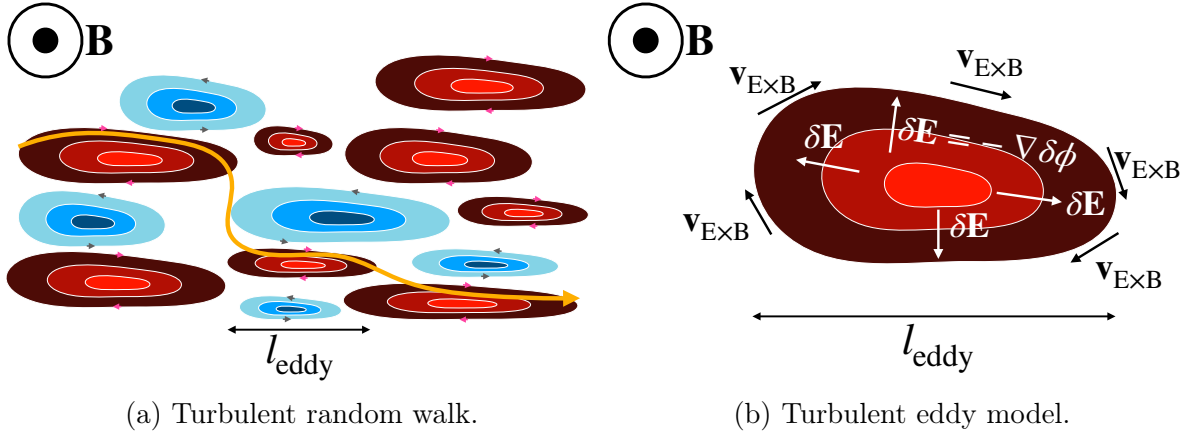


Figure 9: Heuristic models for a turbulent random walk (a) and a turbulent eddy (b). Red eddies have a density slightly higher than the background mean density and blue eddies have a density slightly lower than the mean density.

least as large – and often much higher – as the ion or electron gyroradius, and a frequency much faster than collisions.

One mental model for turbulent transport consists of radially connected turbulent eddies shown in Figure 9(a). These eddies consist of overperturbations and underperturbations to the mean density, temperature, etc. For reasons that we explain shortly, these eddies rotate in the direction of the pink and grey arrows indicated in Figure 9(a). Because the eddies are formed of particles themselves, they are dynamic, short-lived structures with a lifetime  $\tau_{nl}$  which we call the eddy turnover time. The orange arrow in Figure 9(a) shows the trajectory of a particle as it moves along different eddies. Red eddies have a density slightly higher than the background mean density and blue eddies have a density slightly lower than the mean density.

We now present an argument to estimate the turbulent transport coefficient for ion heat transport. The step size is the radial scale of a turbulent eddy  $l_{\text{eddy}}$  and the frequency is the eddy turnover time  $\tau_{nl}$ ,

$$\chi_i^{\text{turb}} \sim l_{\text{eddy}}^2 / \tau_{nl}. \quad (42)$$

We define the nonlinear time as the time it takes particles to move across the radial eddy extent,

$$\tau_{nl} \equiv l_{\text{eddy}} / v_{E \times B}, \quad (43)$$

where  $v_{E \times B}$  is the  $E \times B$  velocity,

$$v_{E \times B} \equiv \left| \frac{\mathbf{B} \times \nabla \delta\phi}{B^2} \right| \sim \frac{\delta\phi}{B l_{\text{eddy}}}. \quad (44)$$

Physically,  $v_{E \times B}$  is a drift arising from a magnetic and electric field that have a non-vanishing perpendicular component. Here,  $\delta\phi$  is the fluctuating electrostatic potential. To estimate the final term in Equation (44), we need to estimate  $\delta\phi$ . First, use that the normalized potential fluctuations are proportional to the eddy size divided by the device size  $a$ ,

$$\frac{e\delta\phi}{T} \sim \frac{l_{\text{eddy}}}{a}. \quad (45)$$

We invoke the ambient pressure gradient argument: the perturbed potential energy

$(a/l_{\text{eddy}})e\delta\phi$  is comparable to the plasma thermal energy,

$$\frac{a}{l_{\text{eddy}}}e\delta\phi \sim T = \frac{1}{2}mv_t^2. \quad (46)$$

Inserting Equation (46) into Equation (44) gives

$$v_{E \times B} \sim \frac{T}{aeB}. \quad (47)$$

This gives a nonlinear time  $\tau_{nl} \sim (l_{\text{eddy}}/\rho)(a/v_t)$ , and therefore the turbulent diffusivity,

$$\chi_i^{\text{turb}} \sim \frac{l_{\text{eddy}}}{\rho_i} \rho_{*i} \rho_i v_t = \frac{l_{\text{eddy}}}{\rho_i} \chi_{gB}, \quad (48)$$

where the gyroBohm diffusivity is

$$\chi_{gB} \equiv \rho_{*i} \rho_i v_t, \quad (49)$$

and

$$\rho_{*i} \equiv \rho_i/a. \quad (50)$$

The diffusivity expression in Equation (48) shows that when turbulent eddies have a length equal to the ion gyroradius, transport is gyroBohm. Physically, gyroBohm diffusivity corresponds to eddies the size of the gyroradius, where the eddies themselves have an  $\mathbf{E} \times \mathbf{B}$  drift that carries particles across the eddy structure. GyroBohm transport can be much higher than collisional transport because particles typically move across eddies much faster than they collide. A cartoon for how energy is transported around a turbulent eddy is shown in Figure 9(b).

Crucially, the gyroBohm transport diffusivity in Equation (48) scales with  $\rho_{*i}$ . This observation has informed much of the thinking about how to improve confinement in future devices by decreasing  $\rho_{*i}$ : (1) since  $\rho_i \sim 1/B$ , use strong magnetic fields to increase  $B$  [383, 426, 445], and (2) increase  $a$  by making the machine larger [375].

The ratio of turbulent to neoclassical diffusivity is

$$\frac{\chi_i^{\text{turb}}}{\chi_i^{\text{neoclassical}}} \sim \frac{1}{\sqrt{2\epsilon}} \frac{l_{\text{eddy}}}{\rho_i} \left( \frac{B}{B_p} \right)^2 \frac{v_{ti}}{a} \frac{1}{\nu_{ii}}. \quad (51)$$

For ion heat transport, typically

$$\frac{\chi_i^{\text{turb}}}{\chi_i^{\text{neoclassical}}} \gtrsim 1. \quad (52)$$

where  $v_{ti}/a \gtrsim \nu_{ii}$ . However, for electron heat transport, the turbulent eddy size is typically on the order of the ion, not the electron gyroradius [93],  $l_{\text{eddy}} \sim \rho_i \sim (m_i/m_e)\rho_e$ , giving a surprisingly high electron heat transport

$$\frac{\chi_e^{\text{turb}}}{\chi_e^{\text{neoclassical}}} \gg 1, \quad (53)$$

despite initial estimates that turbulent electron heat transport is small due to the small electron gyroradius. The turbulent energy confinement time is thus approximately

$$\tau_E^{\text{turb}} \approx \frac{a^2}{\chi_i^{\text{turb}}}. \quad (54)$$

$\tau_E^{\text{experiment}} / \text{s}$	$\tau_E^{\text{classical}} / \text{s}$	$\tau_E^{\text{neoclassical}} / \text{s}$	$\tau_E^{\text{turb}} / \text{s}$
0.90	670	11	0.4

Table 1: Comparison of experimental confinement time for JET discharge 42976 at  $t = 13.13$  seconds versus heuristic classical (Equation (37)), neoclassical (Equation (41)), and turbulent (Equation (56)) confinement times. The experimental confinement time  $\tau_E^{\text{experiment}}$  is reported in [214].

Comparing again with JET discharge 42976 [214] with the experimental  $\tau_E = 0.90$  seconds, using a thermal velocity  $v_{\text{ti}} \approx 10^6$  meters / second, the turbulent diffusivity estimate is

$$\chi_i^{\text{turb}} \approx 2 \text{ meters/second}, \quad (55)$$

and the corresponding confinement time is

$$\tau_E^{\text{turb}} \approx 0.4 \text{ seconds}. \quad (56)$$

We summarize the comparison of experimental, classical, neoclassical, and turbulent confinement times in Table 1. The classical, neoclassical, and turbulent times in Table 1 are only intended as order-of-magnitude estimates to demonstrate that energy confinement in JET is very likely determined by turbulent transport mechanisms. We emphasize that this is a very rough estimate, but it captures enough detail to be useful.

## 5.4 Power Plant Size Considerations

Taking as given that ion thermal transport is driven primarily by turbulence, we can estimate the required size of a burning plasma in a fusion power plant. The total plasma thermal energy  $W$  is roughly

$$W \sim nTL^3, \quad (57)$$

where  $L$  is the device spatial length scale and we used the previous form of the radial heat flux  $q_i \sim \chi_i^{\text{turb}} n_i T_i / L$ . The total power loss due to turbulent transport is  $P_{\text{loss}} \sim q_i L^2 \sim \chi_i n_i T_i L$ . The global energy confinement time  $\tau_E$  is

$$\tau_E \equiv \frac{W}{P_{\text{loss}}} \sim \frac{L^2}{\chi_i^{\text{turb}}}. \quad (58)$$

One way to measure the performance of a FPP is with the Lawson criterion, requiring  $n_i T_i \tau_E$  to exceed a certain bound for the plasma to ignite [242, 430], which we estimated in Equation (18),

$$n_i T_i \tau_E > C_{\text{Lawson}}. \quad (59)$$

Ignoring any scalings of  $n_i$  or  $T_i$  with  $L$  or  $B$ , we see that  $\chi_i^{\text{turb}} \sim 1/B^2$ . Also writing a confinement enhancement/degradation  $H$  in  $\tau_E$  relative to a fixed nominal  $\tau_{E,\text{nominal}}$  as [133, 212, 438]

$$\tau_E = H \tau_{E,\text{nominal}}, \quad (60)$$

we obtain

$$\tau_E \sim HL^2 B^2. \quad (61)$$

Therefore Equation (59) becomes

$$n_i T_i \tau_E \sim HL^2 B^2 > C_{\text{Lawson}}, \quad (62)$$

giving a size scaling of

$$L > \left( \frac{C_{\text{Lawson}}}{HB^2} \right)^{1/2}. \quad (63)$$

Therefore, for a fixed  $C_{\text{Lawson}}$  increasing  $H$  and  $B$  can both reduce device size. Note that these are very heuristic arguments, and integrated systems codes are required to predict how changes in parameters such as  $H$ ,  $L$ , and  $B$  feed through to plasma performance and ultimately the predicted cost as a fusion power plant. For example, in [411] it was found that increasing the parameter  $H$  from 0.9 to 1.7 halved the estimated cost of a fusion power plant from \$8 billion USD to \$4 billion USD, which was a much bigger effect than any other parameter variation in the system. These are tantalizing hints that ideas for improving confinement could have a significant impact on the cost of FPP. These are physics ideas, falling under the purview of fusion scientists. While the scaling exponents of  $H$ ,  $L$ , and  $B$  in Equation (62) are highly approximate, they capture the basic ideas. See [373, 383, 75, 279, 445, 411, 369] for a variety of more sophisticated approaches to these questions.

## 5.5 Further Considerations

Despite the optimistic message of Equation (63) and studies such as [411] showing that improving energy confinement through higher  $H$  would lead to smaller fusion power plants, it is important to emphasize that increasing confinement indefinitely is not useful, and might actually be harmful. This is because there are other constraints that come into play.

One constraint is that power must be exhausted in a way that does not melt the vacuum vessel. In a burning power there will be much more power relative to the surface area available for dissipation. In D-T fusion, 1/5 of the total fusion power is carried by alpha particles that deposit power into the plasma. The total enclosed fusion power  $P_{\text{fus}}$  scales as  $P_{\text{fus}} \sim L^3$  but the surface area through which heat leaves the plasma only scales as  $L^2$ . However, the actual area where the plasma touches the divertor likely scales even more pessimistically with  $L$  [405, 102, 39]. Other techniques are being developed to radiate heat within the plasma and to protect the divertor.

In addition to heat transport, there are particle transport constraints. Further to those already mentioned in Section 3.2 (helium ash and impurity removal), a pertinent constraint all tokamaks are subject to is a plasma density limit [139] where the volume-averaged density normalized to the total plasma current cannot exceed a certain value.

## 6 Transport Framework

In this section we introduce the theoretical background required for finding the time evolution of the magnetic equilibrium and plasma profiles. Despite the evolution of the equilibrium and profiles being slow, on transport timescales  $\tau_E$ , it is necessary to simulate much faster dynamics included in the gyrokinetic and neoclassical equations, which we introduce in this section.

We first introduce kinetic theory through the Fokker-Planck equation. We then describe the evolution of smaller turbulent and equilibrium dynamics in the gyrokinetic and neoclassical equations. Slower transport timescale dynamics are described in the transport and magnetic equilibrium equations. We will use a simplified treatment, neglecting

certain physical effects such as rotation that are often important.

We will use the ‘ $\delta f$ ’ (pronounced ‘delta f’) formalism [22], which assumes small fluctuations compared with the equilibrium,

$$\frac{\delta f_s}{f_s} \sim \frac{\delta B}{B} \sim \frac{\delta E}{E} \sim \rho_{*s} = \frac{\rho_s}{a} \ll 1. \quad (64)$$

Here,  $f_s$  is a particle distribution function for a species  $s$  and  $\delta f_s$  is its fluctuating component. This approximation is usually good in the plasma core where fluctuations are indeed small. However, this approximation usually breaks down in the edge where fluctuations can be comparable in size to the equilibrium – one approach to solve this is ‘full f’ gyrokinetics [135, 165, 195, 319, 144], which we don’t study here.

The approach for finding the transport equations with the assumptions in Equation (64) is to exploit scale separation using an order-by-order asymptotic expansion in the parameter  $\rho_{*s}$ . Starting from the Fokker-Planck kinetic equation, one typically investigates at three temporal scales  $\mathcal{O}(\rho_{*s}\Omega_s f_s)$ ,  $\mathcal{O}(\rho_{*s}^2\Omega_s f_s)$ , and  $\mathcal{O}(\rho_{*s}^3\Omega_s f_s)$ . Terms of the size  $\mathcal{O}(\rho_{*s}\Omega_s f_s)$  change fastest. Most notably, one learns that the lowest order distribution function is a Maxwellian. Terms of the size  $\mathcal{O}(\rho_{*s}^2\Omega_s f_s)$  change slower, and at these scales one finds the gyrokinetic and neoclassical equations. Terms of the size  $\mathcal{O}(\rho_{*s}^3\Omega_s f_s)$  change slowest. These are the transport equations. The transport equations cannot be solved without information from terms found in the  $\mathcal{O}(\rho_{*s}\Omega_s f_s)$  and  $\mathcal{O}(\rho_{*s}^2\Omega_s f_s)$  equations. The pedagogy of this presentation is similar to that in [4], but we only produce the main results.

There are also other approaches for deriving gyrokinetics, most notably the Hamiltonian approach; [38] is an excellent starting point.

## 6.1 Fokker-Planck Equation

In this subsection, we introduce the Fokker-Planck equation, which describes the evolution of a system subject to electromagnetic forces. A very useful quantity is the particle distribution function  $f_s(\mathbf{r}, \mathbf{v}, t)$  for a species  $s$ , which describes the number of particles in position space  $\mathbf{r}$  and velocity space  $\mathbf{v}$  at a given time  $t$ . For example, the total particle density is a velocity space integral of  $f_s(\mathbf{r}, \mathbf{v}, t)$ ,

$$n_s(\mathbf{r}, t) = \int f_s(\mathbf{r}, \mathbf{v}, t) d\mathbf{v}, \quad (65)$$

and the momentum  $m_s \mathbf{u}_s$  and temperature  $T_s$  are higher order ‘moments,’

$$m_s \mathbf{u}_s(\mathbf{r}, t) = \int \mathbf{v} f_s(\mathbf{r}, \mathbf{v}, t) d\mathbf{v}, \quad T_s(\mathbf{r}, t) = \int \frac{m_s v^2}{2} f_s(\mathbf{r}, \mathbf{v}, t) d\mathbf{v}. \quad (66)$$

Other useful quantities such as fluxes can also be obtained from moments of  $f_s(\mathbf{r}, \mathbf{v}, t)$ . We will discuss these later.

We are interested in the time evolution of  $f_s(\mathbf{r}, \mathbf{v}, t)$ , which is given by the Boltzmann equation

$$\frac{df_s}{dt} = \frac{\partial f_s}{\partial t} + \frac{\partial}{\partial \mathbf{r}} \cdot \left( \frac{d\mathbf{r}}{dt} f_s \right) + \frac{\partial}{\partial \mathbf{v}} \cdot \left( \frac{d\mathbf{v}}{dt} f_s \right) = C_s + G_s, \quad (67)$$

where  $C_s$  is a *collision operator* and  $G_s$  are sources. In a plasma, we concern ourselves with forces on charged particles due to an electric field  $\mathbf{E}$  and a magnetic field  $\mathbf{B}$ ,

$$m_s \frac{d\mathbf{v}}{dt} = Z_s e \left( \mathbf{E} + \frac{\mathbf{v} \times \mathbf{B}}{c} \right), \quad (68)$$

where  $Z_s$  is the particle charge number and  $e$  is the proton charge. This gives the Fokker-Planck equation,

$$\frac{\partial f_s}{\partial t} + \mathbf{v} \cdot \nabla f_s + \frac{Z_s e}{m} \left( \mathbf{E} + \frac{\mathbf{v} \times \mathbf{B}}{c} \right) \cdot \frac{\partial f}{\partial \mathbf{v}} = C_s + G_s. \quad (69)$$

Because Equation (69) has three unknowns –  $f_s(\mathbf{r}, \mathbf{v}, t)$ ,  $\mathbf{E}(\mathbf{r}, t)$ , and  $\mathbf{B}(\mathbf{r}, t)$ , we close it with Maxwell's equations,

$$\begin{aligned} \nabla \cdot \mathbf{E} &= 4\pi e \sum_s Z_s \int f_s d\mathbf{v}, \\ \nabla \cdot \mathbf{B} &= 0, \\ \nabla \times \mathbf{E} &= -\frac{1}{c} \frac{\partial \mathbf{B}}{\partial t}, \\ \nabla \times \mathbf{B} &= \frac{1}{c} \frac{\partial \mathbf{E}}{\partial t} + \frac{4\pi e}{c} \sum_s Z_s \int \mathbf{v} f_s d\mathbf{v}. \end{aligned} \quad (70)$$

The system of equations in Equations (69) and (70) form the basis for solving the transport problem: finding  $f_s$ ,  $\mathbf{E}$ , and  $\mathbf{B}$  over transport timescales on the order of  $\tau_E$ .

## 6.2 Maxwell Equilibrium

Taking only terms of order  $\mathcal{O}(\rho_{*s} \Omega_s f_s)$  in Equation (69) and performing a gyroaverage shows that parallel particle streaming balances particle collisions,

$$v_{\parallel} \hat{\mathbf{b}} \cdot \frac{\partial f_s}{\partial \mathbf{R}_s} = \langle C \rangle_{\mathbf{R}_s}, \quad (71)$$

where the magnetic field unit vector is  $\hat{\mathbf{b}} = \mathbf{B}/B$  and the parallel velocity is  $v_{\parallel}$ . After some algebraic manipulations [4], one arrives at

$$\left\langle \int d^3v \ln f_s C \right\rangle_{\psi} = 0, \quad (72)$$

which means that to leading order the distribution function is Maxwellian,

$$f_s = F_{Ms} + \dots \quad (73)$$

The Maxwellian equilibrium distribution function (reproduced from Equation (9)) is

$$F_{Ms}(v) = n_s \left( \frac{m_s}{2\pi T_s} \right)^{3/2} \exp \left( -\frac{m_s v^2}{2T_s} \right). \quad (74)$$

In Equation (72) a useful operation called a flux-surface average is performed,

$$\langle g \rangle_{\psi}(\psi) \equiv \oint \frac{g}{|\nabla V|} dS, \quad (75)$$

where the integral is performed over a closed flux surface with area element  $dS$  and  $V$  is the volume enclosed by the flux surface. This operation is used a lot in deriving the transport equations because it simplifies many expressions. After performing the average, the only spatial dependence for a quantity  $g$  is flux-surface coordinate  $\psi$ .



### 6.3 Gyrokinetics

Gyrokinetics is a system of equations that is often a good approximation of turbulence in MCF devices [55, 118, 391, 318, 4]. It is a very useful formalism because it can reduce computational complexity by orders of magnitude without significant loss of accuracy. This speedup is obtained by reducing velocity space from 3D to 2D, which considerably speeds up computation [22]. Physically the reduction from 3D to 2D corresponds to modeling ‘rings’ of charge rather than following the exact location of a particle throughout its gyromotion. This is achieved with the ‘guiding center’ coordinate transformation [55],

$$\mathbf{R}_s = \mathbf{r} - \boldsymbol{\rho}_s, \quad (76)$$

where  $\mathbf{r}$  is the particle position, and

$$\boldsymbol{\rho}_s = \frac{\hat{\mathbf{b}} \times \mathbf{v}}{\Omega_s}, \quad (77)$$

is the cyclotron motion. By subtracting  $\boldsymbol{\rho}_s$  from the particle position,  $\mathbf{R}_s$  describes the guiding center position of the particle. Modeling the guiding center is generally an excellent approximation because turbulence does not usually change appreciably on the gyrofrequency timescale. Mathematically, the turbulent frequency  $\omega$  is ordered to be much slower than the cyclotron frequency  $\Omega_s$ ,

$$\omega \ll \Omega_s. \quad (78)$$

However, while we model particle guiding center trajectories with  $\mathbf{R}_s$ , we still include the spatial physics of a nonzero particle gyroradius, known as Finite Larmor Radius (FLR) effects. Spatially, the perpendicular wavenumber of turbulence  $k_\perp$  is expected to be comparable to the gyroradius,

$$k_\perp \rho_s \sim 1. \quad (79)$$

This is a particularly important ‘kinetic’ effect that vanishes when  $k_\perp \rho_s \rightarrow 0$ . For  $k_\perp \rho_s \gg 1$ , turbulence is damped because particles average over many small structures during their fast gyromotion. Mathematically, FLR effects arise from gyroaveraging a quantity  $g$  over its gyrophase  $\varphi$ ,

$$\langle g \rangle_{\mathbf{R}_s} \equiv \int_0^{2\pi} g d\varphi / 2\pi. \quad (80)$$

The  $\mathbf{R}_s$  subscript in  $\langle g \rangle_{\mathbf{R}_s}$  indicates that the gyroaverage is performed at constant  $\mathbf{R}_s$ . To see how FLR effects enter physically, consider a Fourier mode  $k_\perp$  of  $g$ , where  $g$  represents some fluctuating quantity such as the electrostatic potential,

$$\hat{g}(k_\perp) = \int g(\mathbf{r}) \exp(i\mathbf{k}_\perp \cdot \mathbf{r}) d\mathbf{r} = \int g(\mathbf{r}) \exp(i\mathbf{k}_\perp \cdot \mathbf{R}_s) \exp(i\mathbf{k}_\perp \cdot \boldsymbol{\rho}_s) d\mathbf{r}, \quad (81)$$

where we used Equation (76) for the final term. Performing the gyroaverage (Equation (80)) of the Fourier mode  $\hat{g}(k_\perp)$  converts the  $\exp(i\mathbf{k}_\perp \cdot \boldsymbol{\rho}_s)$  term into  $J_0$ , a Bessel function of the first kind,

$$\langle \hat{g}(k_\perp) \rangle_{\mathbf{R}_s} = \int g(\mathbf{r}) \exp(i\mathbf{k}_\perp \cdot \mathbf{R}_s) J_0 \left( \frac{k_\perp v_\perp}{\Omega_s} \right) d\mathbf{r}. \quad (82)$$

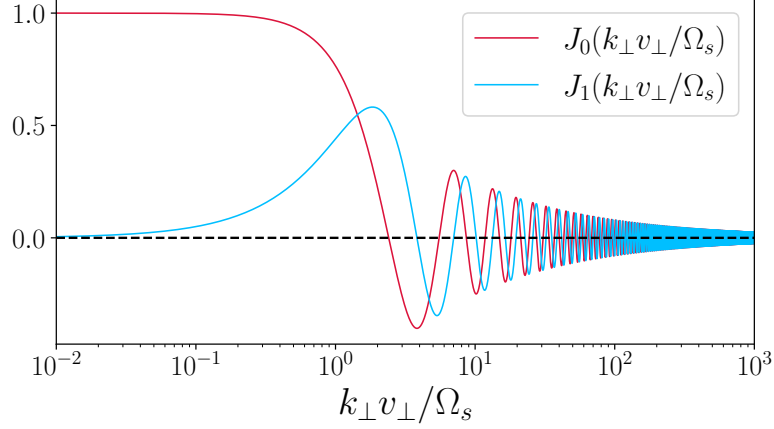


Figure 10: Bessel functions  $J_0(k_\perp v_\perp / \Omega_s)$  and  $J_1(k_\perp v_\perp / \Omega_s)$  that arise from gyroaveraging.

The Bessel function is obtained by

$$J_0\left(\frac{k_\perp v_\perp}{\Omega_s}\right) = \int_0^{2\pi} \exp(i\mathbf{k}_\perp \cdot \boldsymbol{\rho}_s) d\varphi / 2\pi. \quad (83)$$

The higher order Bessel function  $J_1$  also often appears in the gyrokinetic system of equations, occurring with higher  $v_\perp$  moments of the plasma distribution function. We plot  $J_0$  and  $J_1$  in Figure 10. As  $x$  increases for  $J_0(x)$ , the turbulence wavenumber  $k_\perp$  becomes increasingly smaller, causing the mode to average over more perturbations, decreasing the ‘drive’ for linear instability. For  $k_\perp \rho_s \ll 1$ , a particle samples a roughly constant fluctuation amplitude during its gyromotion (see Figure 11 (a)), meaning that FLR effects are unimportant. As the turbulent wavenumber increases to be comparable to the gyroradius,  $k_\perp \rho_s \sim 1$ , the particle samples multiple fluctuations during its gyromotion (see Figure 11 (b)), which can start to damp the turbulence. When the particle gyroradius is large compared with the turbulent wavelength,  $k_\perp \rho_s \gg 1$ , the particle averages over a large number of fluctuations during its gyromotion (see Figure 11 (c)), causing turbulence to be significantly weaker.

Dynamics parallel to the magnetic field line are also important. In toroidal devices such as tokamaks and stellarators, particles move much faster along field lines than across them. This results in turbulence typically being more extended along magnetic field lines. Therefore, the parallel wavenumber associated with turbulence  $k_\parallel$  is typically much smaller than the perpendicular wavenumber  $k_\perp$ , giving rise to turbulence that is spatially anisotropic,

$$k_\parallel \ll k_\perp. \quad (84)$$

The next step is to find the gyrokinetic equation. For brevity, we don’t perform a full derivation but highlight the main steps. A formal ordering of quantities is performed with the small parameter

$$\rho_{*s} \equiv \frac{\rho_s}{L} \ll 1, \quad (85)$$

where  $L$  is the device size. The standard gyrokinetic ordering is

$$\frac{\delta f_s}{f_s} \sim \frac{Z_s e \delta \phi}{T_s} \sim \frac{\omega}{\Omega_s} \sim \frac{\nu_s}{\Omega_s} \sim \frac{k_\parallel}{k_\perp} \sim \frac{\delta B}{B} \sim \frac{\delta E}{E} \sim \rho_{*s}, \quad (86)$$

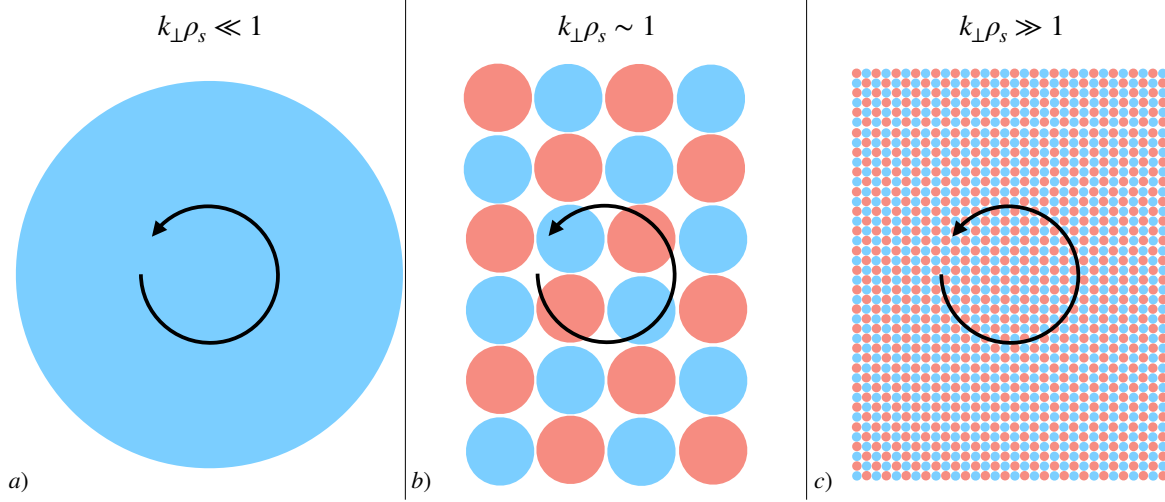


Figure 11: FLR effects at different perpendicular wavenumbers. Red and blue blobs represent turbulent overdensities and underdensities, respectively. Black arrows represent the particle's gyromotion. (a): The gyroradius is small compared with the turbulent wavelength and hence the particle sees a fairly constant density during a single gyroperiod. (b): The gyroradius is comparable to the turbulent wavelength and therefore the particle averages over several perturbations per gyroperiod, affecting its growth rate. (c): The gyroradius is large compared with the turbulent wavelength and hence the particle sees a rapidly changing turbulent density. Adapted from [310].

where  $\nu_s$  is the Coulomb collision frequency. Quantities are split into mean and fluctuating components. For example the total electric field  $\tilde{\mathbf{E}}$  has a mean component  $\mathbf{E}$  and fluctuating component  $\delta\mathbf{E}$

$$\tilde{\mathbf{E}} = \mathbf{E} + \delta\mathbf{E}. \quad (87)$$

We use gyrokinetic variables: the guiding center spatial coordinate  $\mathbf{R}_s$ , the energy  $\mathcal{E}_s = m_s v^2/2$ , the magnetic moment  $\mu_s = m_s v_\perp^2/2B$ , the gyrophase  $\varphi$ , and the sign of the parallel velocity  $\sigma = v_\parallel/|v_\parallel|$ . With these new coordinates, we write the kinetic equation for the fluctuating distribution function in a similar manner as Equation (67),

$$\frac{d\delta f_s}{dt} = \frac{\partial\delta f_s}{\partial t} + \mathbf{R}_s \cdot \frac{\partial\delta f_s}{\partial \mathbf{R}_s} + \dot{\mu}_s \frac{\partial\delta f_s}{\partial \mu_s} + \dot{\mathcal{E}}_s \frac{\partial\delta f_s}{\partial \mathcal{E}_s} + \dot{\varphi} \frac{\partial\delta f_s}{\partial \varphi} = C_s. \quad (88)$$

It is useful to define a ‘non-adiabatic’ distribution function

$$h_s = \delta f_s + \frac{Z_s e \delta \phi}{T_s} F_{Ms}, \quad (89)$$

which is the non-Boltzmann part of the perturbed distribution function. In order to eliminate the  $\partial\delta f_s/\partial\varphi$  term, we gyroaverage Equation (88), giving

$$\left\langle \frac{\partial\delta f_s}{\partial t} \right\rangle_{\mathbf{R}_s} + \mathbf{R}_s \cdot \frac{\partial\delta f_s}{\partial \mathbf{R}_s} + \left\langle \dot{\mathcal{E}}_s \right\rangle_{\mathbf{R}_s} \frac{\partial\delta f_s}{\partial \mathcal{E}_s} = \langle C_s \rangle_{\mathbf{R}_s}, \quad (90)$$

where we also used that  $\langle \dot{\mu}_s \rangle_{\mathbf{R}_s}$  is small. Equation (90) has an oscillating and equilibrium component. The oscillating component of Equation (90) is called the gyrokinetic equation

$$\frac{\partial h_s}{\partial t} + \left( v_\parallel \hat{\mathbf{b}} + \mathbf{v}_{Ms} + \langle \mathbf{v}_\chi \rangle_{\mathbf{R}_s} \right) \cdot \nabla h_s = \frac{Z_s e F_{Ms}}{T_s} \frac{\partial \langle \delta \chi \rangle}{\partial t} - \langle \mathbf{v}_\chi \rangle_{\mathbf{R}_s} \cdot \nabla F_{Ms} + C_s. \quad (91)$$

The gyrokinetic potential is

$$\delta\chi = \delta\phi - \frac{\mathbf{v} \cdot \delta\mathbf{A}}{c}, \quad (92)$$

the magnetic particle drifts are

$$\mathbf{v}_{Ms} = \frac{\hat{\mathbf{b}}}{\Omega_s} \times \left( \left[ v_{\parallel}^2 + \frac{v_{\perp}^2}{2} \right] \nabla \ln B + v_{\parallel}^2 \frac{4\pi}{B^2} \frac{dp}{dr} \nabla r \right), \quad (93)$$

and the fluctuating velocity field is

$$\mathbf{v}_{\chi} = \frac{c}{B} \hat{\mathbf{b}} \times \nabla \chi. \quad (94)$$

The quantity  $\mathbf{v}_{\chi}$  can be thought of as a generalized  $\mathbf{E} \times \mathbf{B}$  drift, the difference being that the vector potential is also included in  $\mathbf{v}_{\chi}$ . Note that in Equation (91) we have omitted plasma rotation, which is often important in MCF plasmas. See [392] for the gyrokinetic equation with rotation.

The gyrokinetic equation must be coupled to its equivalent order in Maxwell's equations, found by performing a similar expansion in Equation (70).

## 6.4 Neoclassical

The equilibrium component of Equation (90) is called the neoclassical drift-kinetic equation

$$\left( \mathbf{v}_M \cdot \nabla + \frac{Z_s e}{cT} v_{\parallel} \hat{\mathbf{b}} \cdot \frac{\partial \mathbf{A}_0}{\partial t} \right) f_0 = C[\langle f_1 \rangle_{\mathbf{R}_s}] - v_{\parallel} \hat{\mathbf{b}} \cdot \nabla \langle f_1 \rangle_{\mathbf{R}_s}, \quad (95)$$

found by averaging Equation (90) over time and space scales much longer than turbulent timescales  $\omega$ . The neoclassical equation describes slow perturbations at large scales to the equilibrium, in contrast to the gyrokinetic equation, which describes fast perturbations at gyroradius scales to the equilibrium. The neoclassical equation must be coupled to its equivalent order in Maxwell's equations, found by performing a similar expansion in Equation (70).

## 6.5 Transport

The gyrokinetic system of equations describe the time evolution of fluctuating quantities such as  $h_s$ ,  $\delta f_s$ ,  $\delta\phi$ , and  $\delta\mathbf{A}$ . While this describes a plasma over fast timescales, the turbulent fluxes driven by turbulent fluctuations can modify the plasma profiles and the magnetic equilibrium. In order to describe this behavior self-consistently, we study the transport equations, which describe the evolution of the equilibrium distribution function  $f_0$ . In this tutorial, the regime with zero plasma flows. It is customary to study quantities in the transport equations averaged over both gyrophase and flux surface.

The evolution of  $f_0$  is given by the particle transport equation and the energy transport equation (and also the momentum equation if plasma rotation is included). The particle equation is

$$\frac{\partial n_s}{\partial t} + \frac{1}{V'} \frac{\partial V' \langle \Gamma_s \rangle_{\psi}}{\partial \psi} = \langle s_s \rangle_{\psi}, \quad (96)$$

where

$$V' \equiv \frac{dV}{d\psi}, \quad (97)$$

and  $S_s$  is the sum of particle sources and sinks for species  $s$ . The energy equation is

$$\frac{3}{2} \frac{\partial n_s T_s}{\partial t} + \frac{1}{V'} \frac{\partial V' \langle q_s \rangle_\psi}{\partial \psi} = \langle p_s \rangle_\psi, \quad (98)$$

where  $P_s$  is the sum of energy sources and sinks.

The radial particle and heat fluxes are now scalar quantities indicating radial fluxes, containing contributions from classical, neoclassical, and turbulent transport,

$$\langle \Gamma_s \rangle_\psi \equiv \nabla \psi \cdot \int d^3v (\mathbf{v}_\chi \delta f_1 + \mathbf{v}_{Ms} \langle f_1 \rangle_\psi + \rho C [\boldsymbol{\rho} \cdot \nabla f_0]), \quad (99)$$

$$\langle q_s \rangle_\psi \equiv \nabla \psi \cdot \int d^3v \frac{m_s v^2}{2} (\mathbf{v}_\chi \delta f_1 + \mathbf{v}_{Ms} \langle f_1 \rangle_\psi + \rho C [\boldsymbol{\rho} \cdot \nabla f_0]). \quad (100)$$

The  $\mathbf{v}_\chi \delta f_1$  term describes radial energy transport arising from turbulent perturbations contained within  $\mathbf{v}_\chi$  and  $\delta f_1$ ; the  $\mathbf{v}_M \langle f_1 \rangle_\psi$  describes radial energy transport arising from magnetic drifts from neoclassical effects contained within  $\langle f_1 \rangle_\psi$ ; the  $\rho C [\boldsymbol{\rho} \cdot \nabla f_0]$  term describes radial energy transport arising from collisions.

## 6.6 Magnetic Equilibrium

Finally, the evolution of the magnetic equilibrium must also be calculated since the magnetic equilibrium enters the gyrokinetic, neoclassical, and transport equations. This involves finding the evolution of the toroidal and poloidal fluxes (see Equation (31)) by solving the Grad-Shafranov equation

$$R^2 \nabla \cdot \left( \frac{\nabla \psi}{R^2} \right) + I \frac{dI}{d\psi} = -4\pi R^2 \sum_s \frac{dp_s}{d\psi}, \quad (101)$$

to update  $\psi$  that enters the particle and energy transport equations, and solving the toroidal component of Faraday's law

$$\frac{\partial}{\partial \psi} \left\langle \frac{I}{R^2} \right\rangle_\psi = -\frac{1}{V'} \frac{\partial}{\partial \psi} \left( V' \left\langle \frac{\partial \mathbf{A}_0}{\partial t} \cdot \frac{\mathbf{B}}{c} \right\rangle_\psi \right), \quad (102)$$

and obtaining  $\partial \mathbf{A}_0 / \partial t \cdot \mathbf{B} / c$  from the neoclassical equation.

We now have all of the components for studying the evolution of the plasma profiles and magnetic equilibrium.

## 6.7 Example

In this section, we show an example output from a transport solver called TRANSP [306]. In order to calculate power balance, the electron energy equation is volume-integrated from the magnetic axis up to a given flux surface,

$$P_{e,\text{gain}} + P_{e,\text{loss}} = P_{e,\text{source}}. \quad (103)$$

The change in electron thermal energy is

$$P_{e,\text{gain}} = \frac{3}{2} \int \frac{\partial n_e T_e}{\partial t} dV, \quad (104)$$

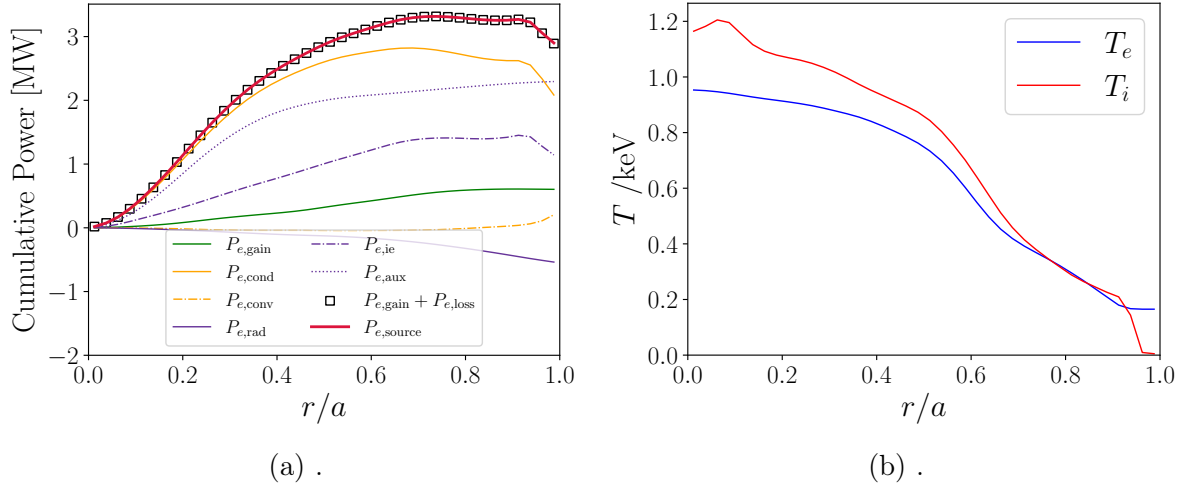


Figure 12: For NSTX discharge 132543 at  $t = 0.614$  seconds, (a) terms in the volume-integrated electron energy transport equation versus normalized minor radius  $r/a$ , (b) ion and electron temperature. In (a), the time derivative term is green, the heat losses are in orange, and the sources and sinks are in purple. See Equation (103) for further explanation.

the conductive and convective losses are

$$P_{e,\text{loss}} = P_{e,\text{cond}} + P_{e,\text{conv}} = \int \nabla \cdot \mathbf{q}_e dV, \quad (105)$$

and the source terms are

$$P_{e,\text{source}} = P_{e,\text{aux}} + P_{e,\text{rad}} + P_{e,\text{ie}} = \int \sum_k s_{e,k} dV. \quad (106)$$

Here,  $P_{e,\text{heat}}$  is the auxiliary electron heating power,  $P_{e,\text{rad}}$  is the electron radiated power, and  $P_{e,\text{ie}}$  is the ion-electron coupling power from electrons to ions.

In Figure 12(a), we plot these terms for NSTX discharge 132543 [26] at  $t = 0.614$  seconds. In Figure 12(b), we plot the electron and ion temperature profiles.

## 6.8 Further Reading

An excellent tutorial on gyrokinetics can be found in Appendix A of [190]. For readers with more background, classic gyrokinetics references are [55, 118, 392, 318, 4]. For collisional and neoclassical transport [168] is a good resource. For transport equations, see [393, 16].

## 7 Gyrokinetic Instabilities

We have covered the main equations that describe transport in MCF devices. However, we have said very little about the physical mechanisms that give rise to turbulence. In this section, we present the most common plasma instabilities that drive heat (and some particle) transport in tokamaks and stellarators.

The physical picture for radial heat transport in tokamaks is as follows. Steep temperature and density gradients can destabilize linear instabilities. These instabilities cause

plasma fluctuations to grow until they saturate in magnitude. The mechanisms that cause this saturation are an ongoing area of research.

Fusion scientists care about the transport properties of turbulence resulting from different microinstabilities. For each instability, we will provide a summary of the transport characteristics in terms of the relative heat and particle transport diffusivities,  $\chi_s$  and  $D_s$  for different species  $s$ . In Table 2 we list some features of the gyrokinetic instabilities covered in this section.

Table 2: Some features of the main gyrokinetic instabilities.

Mode	$\chi_i/\chi_e$	$D_e/\chi_e$	$D_i/\chi_i$	Free Energy Source	Resonance	Section
ITG	$\gg 1$	-	$\ll 1$	$\nabla T_i$	$v_{\parallel}, v_{Mi}$	7.1
ETG	$\ll 1$	$\ll 1$	-	$\nabla T_e$	$v_{\parallel}, v_{Me}$	7.2
TEM	$\sim 1$	$\sim 1$	$\sim 1$	$\nabla T_e$	$v_{Me}$	7.3
MTM	$\ll 1$	$\ll 1$	-	$\nabla T_e$	$v_{Me}$	7.4
KBM	$\sim 1$	$\sim 1$	$\sim 1$	$\nabla p$	$v_{Mi}, v_{Me}$	7.5
PVG	$\gg 1$	-	$\sim 1$	$\nabla u_{\parallel}$	$v_{\parallel}$	7.6
Universal	$\gg 1$	-	$\sim 1$	$\nabla n$	$v_{\parallel}, v_{Mi}, v_{Me}$	7.7

## 7.1 Ion Temperature Gradient Instability

In this section, we describe one of the most common and virulent instabilities in magnetized toroidal devices: the ion temperature gradient (ITG) instability [356, 298, 148, 76, 299]. ITG instability is concerning for fusion power plants because it can lower the core ion temperature, which reduces the fusion power. Analytic calculations, even for the simplest ITG instability, are quite involved. We will not reproduce the calculation in the main text; those who wish to read the technical details can read Appendix A.

There are generally two ‘branches’ of ITG instability. The toroidal ITG branch is destabilized by the effect of ion magnetic drifts arising from toroidicity. The slab ITG branch is destabilized by the motion of ions moving along magnetic field lines. These modes have different features beyond the scope of this tutorial. See [313] for an in-depth discussion of toroidal and slab branches. In this section, we briefly describe the features of the toroidal ITG mode.

The toroidal ITG mode that is destabilized by ion magnetic drifts and steep ion temperature gradients. In Figure 13 we present a cartoon picture of the ITG instability. In Figure 13 (a), we show a wave at the low-field side with a poloidal wavenumber in the presence of a background temperature gradient. We represent peaks and troughs in the wave by red and blue horizontal ovals, depicting positive and negative ion temperature fluctuations, respectively. The temperature fluctuations due to the wave cause variations in the size of the ion magnetic particle drifts in the vertical direction, shown in (b). Due to particle conservation, this causes ion density compressions and rarefactions, causing positive charge buildup and depletion due to the ion having a positive charge. Shown in (c), this creates a perturbed electric field  $\delta \mathbf{E}$  that also creates a perturbed  $\mathbf{E} \times \mathbf{B}$  drift. Due to the direction of the  $\mathbf{E} \times \mathbf{B}$  drift, hot plasma is sucked radially outwards from the core to where there are temperature overperturbations, and cold plasma is sucked radially inwards from the edge to where there are temperature underperturbations. This exacerbates the instability, whose amplitude can eventually grow sufficiently large to

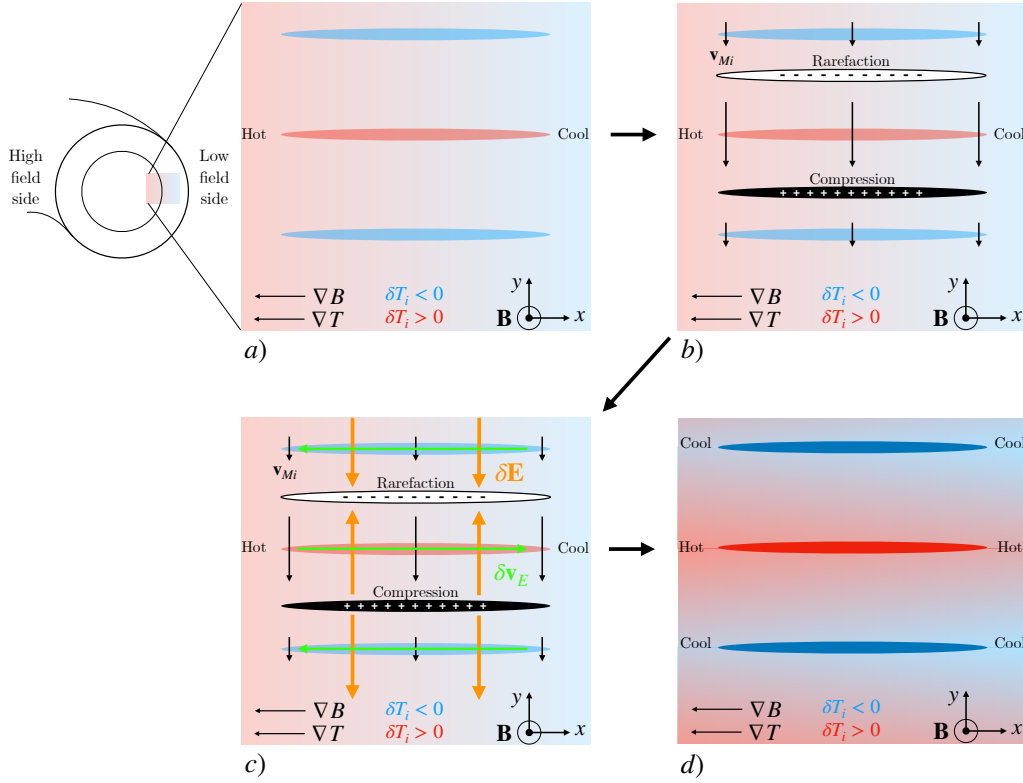


Figure 13: Mechanism for the toroidal ITG instability. (a): At the low-field side, a wave with a poloidal wavenumber creates regions of slightly hotter and colder temperature perturbations,  $\delta T_i$ , shown by red and blue contours. (b): The ion magnetic drift  $\mathbf{v}_{Mi}$  is larger in the regions where  $\delta T_i > 0$  and smaller where  $\delta T_i < 0$ . This makes regions of compressed and rarified plasma. In compressed regions there will be a net positive electric charge and in rarified regions a net negative electric charge. (c): The charge overdensities and underdensities create a perturbed electric field  $\delta \mathbf{E}$ , resulting in a perturbed  $\mathbf{E} \times \mathbf{B}$  drift,  $\delta \mathbf{v}_E$ . This causes hot plasma to be sucked into regions where  $\delta T_i > 0$ , and cool plasma to be sucked into regions where  $\delta T_i < 0$ , creating a positive feedback loop. This creates the unstable state in (d), which can grow to become turbulent.

cause turbulence. Note that this mechanism does not drive instability at the low-field side since the temperature gradient is in the opposite direction. This has a stabilizing effect when combined with the ion magnetic drifts. The toroidal ITG instability is usually most virulent when the magnetic curvature and temperature gradient are aligned, which occurs at the low-field side.

An important result from linear gyrokinetic analysis is the growth rate  $\gamma$  of a perturbation such as the non-adiabatic ion distribution function  $h_i$  (see Equation (91)). Given  $h_i$  at an initial time  $t_0$ , if there is an instability  $h_i$  can grow with linear dependence at  $t > t_0$

$$h_i(t) = h_i(t_0)e^{i\gamma t}, \quad (107)$$

until nonlinear effects become sufficiently strong for the plasma to enter a turbulent state (see Section 7.8). Generally speaking, the higher the linear growth rate, the more strongly driven the turbulence is. In Appendix A we derived an expression for the toroidal ITG



growth rate (Equation (182)),

$$\gamma \approx \sqrt{\omega_{\kappa i} \omega_{*e}^T} \simeq k_y \rho_i \sqrt{-\frac{v_{ti}^2}{L_\kappa L_{T_i}}}, \quad (108)$$

where the magnetic drift frequency  $\omega_{\kappa i}$  and the drift wave frequency  $\omega_{*e}^T$  are

$$\omega_{\kappa i} \sim -k_y \rho_i \frac{v_{ti}}{L_\kappa}, \quad \omega_{*e}^T \sim k_y \rho_i \frac{v_{ti}}{L_{T_i}}, \quad (109)$$

$L_\kappa$  is the magnetic curvature length scale typically comparable in size to the major radius  $R_0$ , and  $k_y$  is a wavenumber in direction binormal to the magnetic field. A necessary condition for instability is

$$\omega_{\kappa i} \omega_{*e}^T > 0, \quad (110)$$

which require the magnetic curvature and ion temperature gradient have the opposite sign,  $L_\kappa L_{T_i} < 0$ . The region where  $L_\kappa L_{T_i} < 0$  is known as ‘bad curvature’ and  $L_\kappa L_{T_i} > 0$  is ‘good curvature.’ The bad curvature region is generally on the low-field side in Figure 13 and the good curvature region is on the high-field side.

The ITG mode typically produces significant ion heat transport, but little particle transport. Therefore,

$$\frac{D_i}{\chi_i} \ll 1. \quad (111)$$

Finally, because electrons do not typically respond kinetically, ITG produces very little electron heat transport. This results in

$$\frac{\chi_i}{\chi_e} \gg 1. \quad (112)$$

## 7.2 Electron Temperature Gradient Instability

Linearly, electron temperature gradient (ETG) instability [205, 93, 401, 443, 158, 313, 5] is identical (‘isomorphic’) to ITG instability under the substitution,

$$\rho_i \rightarrow \rho_e, \quad m_i \rightarrow m_e, \quad h_i \rightarrow h_e, \quad Z_i \rightarrow Z_e. \quad (113)$$

In the presence of ETG driven turbulence, the plasma core electron temperature can decrease. However, there are certain features that break the isomorphism between ITG and ETG, so that the nonlinear state is quite different. A 1991 paper on ITG instability [76] and turbulence predicted that under certain conditions, the transport due to ITG turbulence would be radially elongated and cause extremely high heat transport. Thankfully, due to some technicalities ITG turbulence is not radially elongated. However, simulations of ETG turbulence found that the transport arising from ETG turbulence is radially elongated [205, 93]. This means that the ETG transport can be comparable in size to ITG turbulence. This is predicted to be the case for present-day tokamaks.

Nonlinear gyrokinetic simulations of drift-wave turbulence show a crucial distinction between ITG-driven and ETG-driven turbulence: the way in which the zonal (flux-surface-averaged) component of the electrostatic potential feeds back on density fluctuations. In ITG turbulence, electrons are typically treated as adiabatic on ion-gyroradius scales.

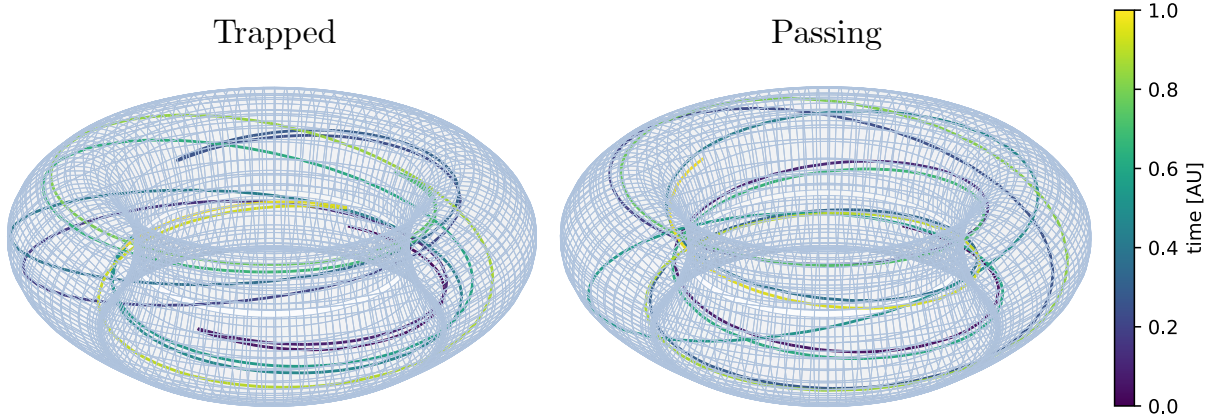


Figure 14: Trapped and passing guiding-center orbits in the ASDEX Upgrade tokamak (shot 26884 at 4300 ms) [172]. Both trapped and passing particles begin at the same location with the same energy but have different pitch. Trajectories are calculated using GORILLA [100, 101].

Their density perturbation is given by a modified Boltzmann response that enforces zero net electron charge on each flux surface:

$$\frac{\delta n_e}{n_e} = \frac{e}{T_e} [\delta\phi - \langle\delta\phi\rangle_\psi], \quad (114)$$

where  $\delta\phi$  is the fluctuating potential and  $\langle\delta\phi\rangle_\psi$  is its flux-surface average. Subtracting  $\langle\delta\phi\rangle_\psi$  guarantees that the integrated electron density perturbation over the surface vanishes, preventing any unbalanced zonal charge from appearing in the adiabatic closure. In contrast, ETG turbulence occurs at electron-gyroradius scales, where ions are effectively adiabatic and respond according to a simple Boltzmann law without any zonal subtraction:

$$\frac{\delta n_i}{n_i} = -\frac{Z_i e}{T_i} \delta\phi, \quad (115)$$

The subtraction in (114) has no effect until a nonzero zonal potential is present, which can only occur in a nonlinear turbulent state. In a linear analysis,  $k_y = 0$  is ignored because the growth rate is zero, which forces  $\langle\delta\phi\rangle_\psi = 0$  and reduces both (114) and (115) to a simple proportionality between  $\delta n_s/n_{s0}$  and  $\delta\phi$ . Only when nonlinear mode-mode coupling is retained does energy transfer into the  $k_y = 0$  ‘zonal’ mode, generating a non-zero  $\langle\delta\phi\rangle_\psi$ . Physically, the resulting zonal shear  $\partial_x \langle\delta\phi\rangle_\psi$  plays a dominant role in regulating ITG turbulence. We discuss zonal flows more in Section 7.8

ETG-driven turbulence typically produces significant electron heat transport, but little particle transport. Therefore,

$$\frac{D_e}{\chi_e} \ll 1. \quad (116)$$

Finally, because ions do not typically respond kinetically, ITG produces very little ion heat transport. This results in

$$\frac{\chi_i}{\chi_e} \ll 1. \quad (117)$$

### 7.3 Trapped Electron Mode

In this section, we describe another common instability called the trapped electron mode (TEM) [105, 160]. It is challenging to obtain analytic results for the TEM. The TEM

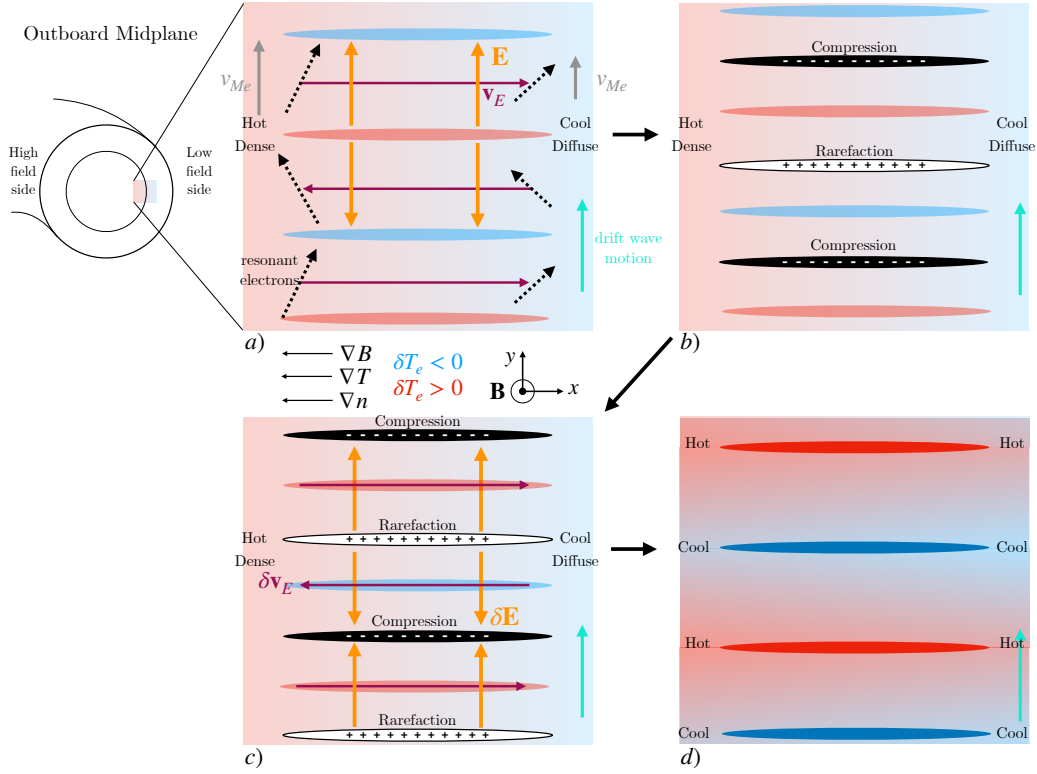


Figure 15: Mechanism for the TEM instability. See discussion above Equation (119) for explanation of the physical mechanism.

is destabilized by both temperature and density gradients, and is driven primarily by ‘trapped’ electrons. In tokamaks, some particles are trapped due to variation in the magnetic field strength as they follow field lines. Trapping occurs due to conservation of two quantities: (1) the magnetic moment,  $\mu = v_{\perp}^2/2B$ , and (2) the particle energy  $E = m\mu B + mv_{\parallel}^2/2$  where the pitch is  $\lambda = m\mu B_0/E$  and the total speed is  $v = \sqrt{2E/m}$ . The parallel velocity for a particle is

$$v_{\parallel} = \pm v \sqrt{1 - \frac{B}{B_0} \lambda}. \quad (118)$$

Any particle with  $v_{\parallel} = 0$  during its motion along field lines will be trapped, and if its speed  $v$  is sufficiently large, will bounce back. In Figure 14 we plot trapped and passing orbits for two particles with  $T = 10$  keV but different pitch. The orbit trajectories are calculated in a realistic geometry for the ASDEX upgrade tokamak using the GORILLA guiding center code [100, 101].

The intuition for the TEM is that a subpopulation of trapped electrons can resonate with drift waves. Drift waves are stable waves that are common in plasmas with density gradients, and have a wave frequency  $\omega = \omega_{*e}$  called the drift frequency. In Figure 15 we consider a cartoon for the TEM instability. In (a), a drift wave is propagating in the  $y$  direction on the low-field side of a tokamak. A fraction of trapped electrons also move in the  $y$  direction at the same speed as the drift wave – these resonant electrons always see the same  $\mathbf{E} \times \mathbf{B}$  drift from the drift wave. Because of a radial density gradient, the  $\mathbf{E} \times \mathbf{B}$  drift will create regions of more trapped electrons (labeled as ‘Compression’) and regions of fewer trapped electrons (labeled as ‘Rarefaction’). Compression regions will have a net

negative charge and Rarefaction regions will have a net positive charge, shown in (b). A perturbed electric field  $\delta\mathbf{E}$  will form between the Compression and Rarefaction regions, giving rise to a perturbed  $\mathbf{E} \times \mathbf{B}$  drift  $\delta\mathbf{v}_E$ . The perturbed drift  $\delta\mathbf{v}_E$  causes hot, dense plasma to be sucked into regions where  $\delta T_i > 0$ , and cool, diffuse plasma to be sucked into regions where  $\delta T_i < 0$ , creating a positive feedback loop. This creates the unstable state in (d), which can grow to become turbulent. In this physical picture, we have assumed that density and temperature perturbations for TEM instability are in phase, that is

$$\frac{\delta n_e}{\delta T_e} > 0. \quad (119)$$

Because the kinetic response of both ions and electrons matters for TEM, there is no reason to expect that the electrons or ions dominate heat transport,

$$\frac{\chi_i}{\chi_e} \sim 1. \quad (120)$$

Similarly, because both the electron and ion kinetic response are sizable, both species can produce comparable particle and heat transport,

$$\frac{D_i}{\chi_i} \sim 1, \quad \frac{D_e}{\chi_e} \sim 1. \quad (121)$$

## 7.4 Microtearing Mode

In this section, we describe microtearing modes (MTMs) [94, 151], which are destabilized by electron temperature gradients. Microtearing modes *reconnect* magnetic field lines [433] and require collisionality to be sufficiently high to be unstable. The instability drive relies on a resonant interaction with electron parallel motion. Magnetic reconnection forms magnetic islands that enhance radial electron transport. This reconnection process allows magnetic field topology to change, breaking the frozen-in condition of ideal MHD.

The MTM produces significant electron heat transport, primarily through the electromagnetic channel (the heat flux generated by  $\delta\mathbf{A}$  fluctuations is much larger than the flux generated by  $\delta\phi$  fluctuations), but little particle transport. Therefore,

$$\frac{D_e}{\chi_e} \ll 1. \quad (122)$$

Finally, because ions do not typically respond kinetically, MTM produces very little ion heat transport. This results in

$$\frac{\chi_i}{\chi_e} \ll 1. \quad (123)$$

MTMs have been observed on many devices, and are thought to play a particularly important role in heat transport at the plasma edge [9, 90, 88, 157, 337, 208, 155, 159, 151, 92, 320].

## 7.5 Kinetic Ballooning Mode

In this section, we describe the kinetic-ballooning-mode (KBM) [398, 378, 6, 215], which is destabilized by pressure gradients. The KBM is the kinetic analogue of the ideal ballooning mode [71]. The KBM is typically characterized by a very strong stiffness [379]

and so it is thought that any plasma profile subject to KBM instability will have the gradients strongly clamped to those values. This is the basis for the widely used EPED model [378], which predicts the edge profiles in H-mode plasmas. Recently, non-stiff KBM-driven turbulence has been reported in stellarators [288].

Because the kinetic response of both ions and electrons matters for KBM, there is no reason to expect that the electrons or ions dominate heat transport,

$$\frac{\chi_i}{\chi_e} \sim 1. \quad (124)$$

Similarly, because both the electron and ion kinetic response are sizable, both species can produce comparable particle and heat transport,

$$\frac{D_i}{\chi_i} \sim 1, \quad \frac{D_e}{\chi_e} \sim 1. \quad (125)$$

Recently, experimental measurement of KBM was reported [207] on the DIII-D tokamak [255].

## 7.6 Parallel Velocity Gradient Instability

In this section, we describe the parallel velocity gradient (PVG) instability, which is destabilized by a radial gradient in the particle flow [56, 218, 323, 54, 345, 296, 17, 366]. As mentioned briefly in the introduction, tokamak plasmas can rotate toroidally with external angular momentum input using neutral beams, or in the absence of external input by redistributing momentum across flux surfaces [317]. Because magnetic field lines are not fully in the toroidal direction, the toroidal flow associated with rotation has a component parallel to the magnetic field as well as a perpendicular component. A radial gradient in the perpendicular flow can stabilize unstable modes and reduce turbulent transport [42, 17] whereas a radial gradient in the parallel flow drives PVG.

Physically, the PVG instability is driven by adjacent plasma layers moving past each other along with different parallel flow velocities. This velocity shear is similar to the velocity jump across a shear layer in the Kelvin–Helmholtz (KH) instability in fluids. In the KH instability, perturbations at the boundary of two fluid streams can grow if there’s a velocity difference. Eddies form and grow by extracting energy from the shear flow.

The PVG instability typically produces significant ion heat transport, but less particle transport,

$$\frac{D_i}{\chi_i} \ll 1. \quad (126)$$

Because electrons do not typically respond kinetically for PVG, it produces very little electron heat transport,

$$\frac{\chi_i}{\chi_e} \gg 1. \quad (127)$$

## 7.7 Universal Instability

In this section, we describe the universal instability. Because many microinstabilities are stabilized by steep pressure gradients, it is tempting to use steep density gradients to stabilize turbulence. Furthermore, because the fusion power scales with the square of the fuel ion density (see Equation (11)), higher density in the plasma core resulting from

steep density gradients gives much higher power. This is particularly true for stellarators that appear to not be subject to the Greenwald density limit [390, 129].

However, there is an instability destabilized by steep density gradients [225, 353, 234], the universal instability. [234] demonstrated the universal instability can be unstable a wide range perpendicular scales, from wavelengths longer than the ion gyroradius to those shorter than the electron gyroradius. This instability could limit the achievable core density values if the density gradients are too steep.

The kinetic response of both ions and electrons is important for universal modes, and therefore

$$\frac{\chi_i}{\chi_e} \sim 1. \quad (128)$$

Because both the electron and ion kinetic responses are sizable, both species can produce comparable particle and heat transport,

$$\frac{D_i}{\chi_i} \sim 1, \quad \frac{D_e}{\chi_e} \sim 1. \quad (129)$$

## 7.8 Nonlinear Phenomena

In this section, we briefly describe some nonlinear phenomena arising in turbulent magnetized fusion plasmas. Nonlinear physics is important because it is responsible for the turbulence that causes transport. All of the instabilities described in earlier subsections are predictable using linear equations. Only if the perturbations resulting from these instabilities grow sufficiently large in amplitude for nonlinear physics to matter, do these instabilities cause significant transport.

First, what is nonlinearity? In the gyrokinetic equation, nonlinearity arises from terms that are not linear in perturbed quantities. From the gyrokinetic equation (Equation (91)), there is only a single term,  $\langle \mathbf{v}_\chi \rangle_{\mathbf{R}_s} \cdot \nabla h_s$ . Because both  $\mathbf{v}_\chi$  and  $h_s$  are proportional to perturbed quantities, this term is quadratic in perturbations. Taking the electrostatic form of  $\mathbf{v}_\chi$ , the nonlinearity is

$$\langle \mathbf{v}_E \rangle_{\mathbf{R}_s} \cdot \nabla h_s = \frac{c}{B} \left( \hat{\mathbf{b}} \times \nabla_\perp \langle \delta \phi \rangle_{\mathbf{R}_s} \right) \cdot \nabla h_s, \quad (130)$$

which is the  $\mathbf{E} \times \mathbf{B}$  advection of the perturbed distribution  $h_s$ . Because advection in real space corresponds to a convolution in Fourier space, this nonlinearity couples different wavenumbers in the plasma.

To see why the nonlinear term couples different modes, Fourier decompose  $\delta \phi$  and the distribution function

$$\langle \delta \phi \rangle_{\mathbf{R}_s} = \sum_{\mathbf{k}'} \Phi_{\mathbf{k}'} e^{i\mathbf{k}' \cdot \mathbf{R}_s}, \quad h_s = \sum_{\mathbf{k}''} H_{\mathbf{k}''} e^{i\mathbf{k}'' \cdot \mathbf{R}_s}. \quad (131)$$

Substituting into Equation (130) gives

$$\langle \mathbf{v}_E \rangle_{\mathbf{R}_s} \cdot \nabla h_s = \frac{c}{B} \sum_{\mathbf{k}', \mathbf{k}''} (\mathbf{k}' \times \mathbf{k}'') \cdot \hat{\mathbf{b}} \Phi_{\mathbf{k}'} H_{\mathbf{k}''} e^{i(\mathbf{k}' + \mathbf{k}'') \cdot \mathbf{R}_s}. \quad (132)$$

Fourier transforming,  $\mathcal{F}$ , gives the nonlinear term for a single wavenumber  $\mathbf{k}$

$$\mathcal{F}\{\langle \mathbf{v}_E \rangle_{\mathbf{R}_s} \cdot \nabla h_s\}(\mathbf{k}) = \frac{c}{B} \sum_{\mathbf{k}' + \mathbf{k}'' = \mathbf{k}} (\mathbf{k}' \times \mathbf{k}'') \cdot \hat{\mathbf{b}} \Phi_{\mathbf{k}'} H_{\mathbf{k}''}. \quad (133)$$

Therefore, the interpretation is that two “pump” modes  $\mathbf{k}'$  (from  $\phi$ ) and  $\mathbf{k}''$  (from  $h_s$ ) nonlinearly couple to the mode at  $\mathbf{k} = \mathbf{k}' + \mathbf{k}''$ .

An important question is why the nonlinear term doesn’t keep growing bigger and bigger over time in the presence of linear instabilities such as ITG that continuously pump energy into the perturbed fields from the equilibrium. Part of the answer is that the equilibrium gradients might eventually become sufficiently weak such that there is no further free energy available to drive instability. However, another interesting phenomenon is that the turbulence can self-regulate transport via zonal flows.

A zonal flow in gyrokinetics is a shear flow, i.e. a mode with purely radial wavenumber. The wavenumber  $\mathbf{k}$  can be decomposed into a radial component  $x$  and binormal component  $y$ ,

$$\mathbf{k} = k_x \nabla x + k_y \nabla y. \quad (134)$$

For a zonal flow,  $\mathbf{k} = k_x \nabla x$ , and therefore the sum in Equation (133) must satisfy

$$k'_y = -k''_y. \quad (135)$$

Consider coupling two drift-wave modes that satisfy  $k'_y = -k''_y$ .  $\mathbf{k}' = (k'_x, k'_y)$  and  $\mathbf{k}'' = (-k'_x, -k'_y)$ . This injects energy into the zonal mode at  $\mathbf{k} = (2k'_x, 0)$ :

$$\partial_t \Phi_{ZF}(2k'_x) \propto \frac{c}{B} \sum_{k'_y \neq 0} (\mathbf{k}' \times (-\mathbf{k}')) \cdot \hat{\mathbf{b}} \Phi_{\mathbf{k}'} H_{-\mathbf{k}'} \sim 2k'_x k'_y \frac{c}{B} \Phi_{\mathbf{k}'} H_{-\mathbf{k}'}.$$

Thus, nonlinear drift-wave interactions can generate  $k_y = 0$  shear flows, which in turn can regulate turbulence by shearing apart eddies. There is an extensive literature on zonal flows [81, 277, 87, 198, 120, 446, 176, 325, 441].

A potentially very useful phenomenon has been observed in simulations of driven driven by certain instabilities such as ITG: the critical temperature gradient that the plasma can support (with a very weak energy source) is higher than the linear critical gradient. This is known as the Dimits shift, referring to the upshift in the nonlinear critical gradient [89]. Because critical temperature gradients are logarithmic, not linear, a small increase in the critical ion temperature gradient can lead to a significant increase in ion temperature in the plasma core, which 1) increases the core fusion reactivity and therefore fusion power, and 2) increases  $T_i/T_e$  (which stabilizes ITG turbulence). There is extensive work on the Dimits shift [352, 283, 270, 267, 188, 63, 442, 363, 146, 201, 291, 248, 297].

## 7.9 Experimental Measurements

Experimental validation of theoretical and computational transport and turbulence predictions is crucial for building next-step devices. For fusion machines we are interested in the transport resulting from turbulent fluctuations. In order for turbulent fluctuations to produce significant transport, they must broadly do three things: (1) have large fluctuation amplitudes, (2) have appropriate fluctuation cross-phases, and (3) be coherent (maintain an appropriate cross-phase) for a sufficiently long time. The cross-phase angle between fluctuating quantities  $A$  and  $B$  is

$$\alpha_{A,B} = \Theta_A - \Theta_B, \quad (136)$$

where  $\Theta_A = \arg(A)$  and  $A = |A| \exp(i\Theta_A)$ . The electrostatic heat flux has two components that arise from the relative fluctuations of the potential and temperature, and the of the potential and density [331, 403],

$$Q \sim \sum_{k_y} k_y \left( n |\delta T_{k_y}| |\delta \phi_{k_y}| \gamma_{T,\phi} \sin \alpha_{T,\phi} + T |\delta n_{k_y}| |\delta \phi_{k_y}| \gamma_{n,\phi} \sin \alpha_{n,\phi} \right), \quad (137)$$

where  $\delta T_{k_y}$ ,  $\delta \phi_{k_y}$ , and  $\delta n_{k_y}$  are the Fourier coefficients of fluctuating temperature, potential, and density for a binormal wavenumber  $k_y$ . The quantities  $\gamma_{T,\phi}$  and  $\gamma_{n,\phi}$  are the coherencies for temperature-potential and density-potential fluctuations. Heat transport vanishes when the cross phase angle satisfies  $\alpha_{A,B} = n\pi$  for an integer  $n$ . Simultaneously measuring cross-phases, coherencies, and their corresponding amplitudes in experiment is challenging [108, 154, 423]. The first comparison of gyrokinetic turbulence simulations with measurements of the cross phase was reported in [422].

We briefly describe some turbulence imaging techniques routinely used in modern machines. Beam-emission spectroscopy (BES) [98, 276, 368, 376, 116] detects electron density fluctuations by measuring D- $\alpha$  light (Balmer-series emission from excited neutral deuterium atoms) produced by an injected neutral beam. Gas-puff imaging (GPI) injects a hydrogen or helium puff and films the resulting atomic line emission with fast cameras, mapping two-dimensional filamentary ‘blob’ structures and drift-wave eddies [447, 374, 448, 301]. Doppler backscattering (DBS) launches a millimeter-wave beam that backscatters from density perturbations to measure the fluctuation power [171, 173, 342, 284, 145]. Microwave-imaging reflectometry (MIR) extends this concept to 2-D by using an antenna array, producing real-time movies of density fluctuations [275, 289, 315, 434, 244]. Correlation electron-cyclotron emission (CECE) cross-correlates electron-cyclotron emission to measure electron temperature fluctuations [82, 421, 117, 252].

## 7.10 Further Reading

- Ion temperature gradient instability [356, 243, 298, 76, 148, 299], nonlinear simulations [416, 349, 419, 57, 19, 182], experiment [136, 408, 410, 423, 422].
- Electron temperature gradient instability [245, 401, 443, 313, 5, 341], nonlinear simulations [93, 67, 314, 60], experiment [340, 269].
- Trapped electron mode instability [142, 65], nonlinear simulations [105, 78, 431, 160], experiment [423, 422].
- Microtearing mode instability [131, 94, 70, 159, 152], nonlinear simulations [141, 91, 157, 208].
- Kinetic ballooning mode instability [398, 418, 6, 215], nonlinear simulations [334, 260, 197, 231, 278].
- Parallel velocity gradient instability [56, 366], nonlinear simulations [17, 273].
- Universal instability [241, 167, 234, 74].
- Multiscale turbulence [187, 259, 189, 261, 62, 150, 333, 24, 258], experiment [343, 174].
- General gyrokinetic mode considerations [223].



## 8 Codes and Workflows

In this section, we describe a non-exhaustive selection of commonly used codes for turbulence, neoclassical, transport, and equilibrium calculations in tokamaks and stellarators. As discussed in Section 6, self-consistently solving the transport problem requires coupling equations that describe physical phenomena across a wide range of spatial and temporal scales.

### 8.1 Gyrokinetics

On fast timescales, gyrokinetic codes solve the system of equations described in Section 6.3, either linearly or nonlinearly. These codes differ in two key ways: local versus global domains, and  $\delta f$  versus full- $f$  formulations. Local codes compute turbulence within a narrow radial region (a flux-tube), while global codes simulate a larger radial extent.  $\delta f$  codes assume fluctuations are small compared to the equilibrium ( $\sim \rho_*$ ), whereas full- $f$  codes make no such assumption.

**Local  $\delta f$  gyrokinetic codes:** CGYRO [51, 48], GENE [132], GKX [322], GS2 [93], GX [266], STELLA [18].

**Global  $\delta f$  gyrokinetic codes:** GENE [132], ORB5 [238], XGC [228].

**Global full- $f$  gyrokinetic codes:** GKEYLL [144], GTC [251], XGC [228].

### 8.2 Neoclassical Transport

Several codes specialize in computing neoclassical transport in both tokamaks and stellarators. These typically solve the drift-kinetic equation with appropriate collision operators.

**Neoclassical codes:** FORTEC-3D [272], NEO [23], PERFECT [236], SFINCS [237].

### 8.3 Integrated Transport Solvers

These codes evolve profiles over confinement timescales by coupling turbulence, neoclassical, and source models.

**Transport codes:** T3D [359], TANGO [85], TGYRO [49], TRANSP [306], Trinity [20].

### 8.4 Magnetic Equilibrium Solvers

Magnetic equilibrium codes provide the background geometry for both gyrokinetic and transport simulations. Different tools are used for tokamaks and stellarators.

**Tokamak equilibrium codes:** CHEASE [254], EFIT [239], Tokamaker [149].

**Stellarator equilibrium codes:** DESC [305], VMEC [178].

## 9 Tokamak Confinement Regimes

In this section, we describe the three main confinement regimes in tokamaks, H-mode, L-mode, and I-mode.

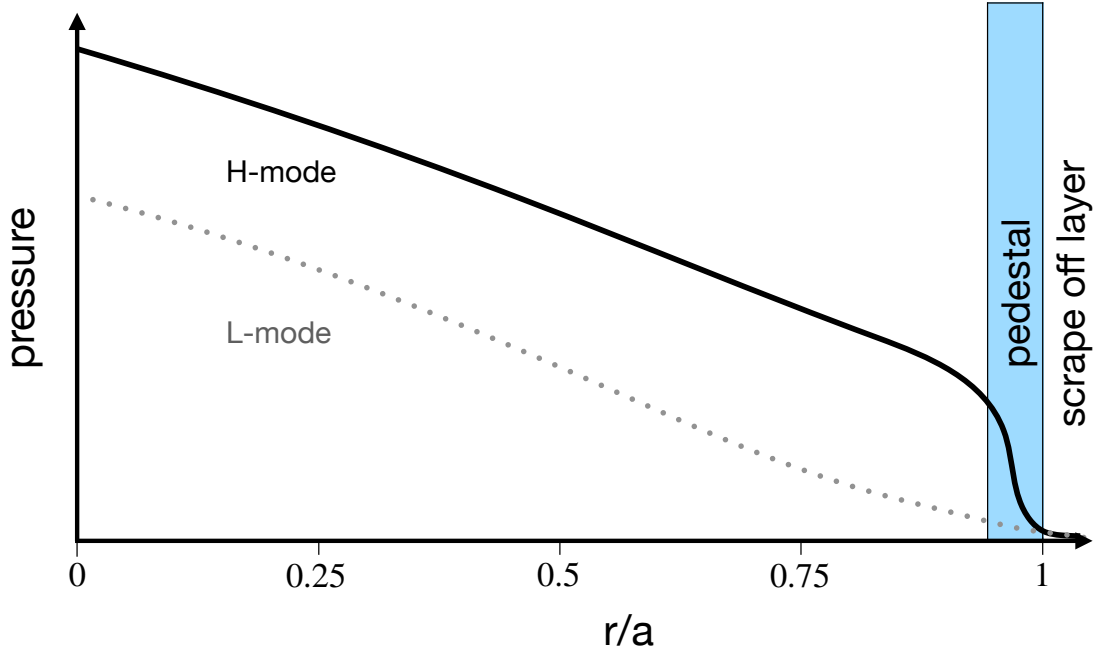


Figure 16: Cartoon of the different pressure profiles for H-mode and L-mode.

## 9.1 H-mode

Until the early 1980s, tokamak experiments operated in a regime now known as L-mode, or low-confinement mode. In 1982, a landmark paper [413] reported ASDEX discharges that had roughly double the energy confinement time of similar L-mode discharges and much higher core plasma pressure. These high-performance discharges, later named ‘H-mode’, bifurcated from the L-mode discharges once the plasma heating power exceeded a threshold value, subject to other parameters values such as magnetic field strength and plasma density.

H-mode has some very desirable characteristics, most of which can be attributed to the transport barrier that forms at the plasma edge called the pedestal, illustrated in Figure 16. In the pedestal, the particle and density gradients are typically an order of magnitude or more higher than in L-mode discharges. This is particularly helpful because even if the critical gradients remain unchanged across the core profiles between L-mode and H-mode, the higher pressure at the pedestal top in H-mode can significantly increase the core pressure, which increases the fusion power. Second, the global energy confinement time roughly doubles in H-mode [413], meaning that the energy diffusion coefficients decrease significantly across the plasma profiles. Third, in the highest-performing H-modes, plasma impurities (that radiate power and dilute the fuel) are flushed from the core [335] due to instabilities called edge-localized modes (ELMs) [444, 72, 380, 222, 247].

Unfortunately, ELMs are also a serious barrier to H-mode being a viable operating regime for fusion power plants. ELMs are periodic bursts of energy that can deposit tens of percent of the stored thermal plasma energy onto the divertor. While ELMs are tolerable in today’s smaller machines, they are not tolerable in fusion power plants due to the much greater stored energy in the plasma [114, 77, 287, 262, 193, 229, 409]. There are signs of hope, however – ELM-free or small-ELM regimes are a subject of intense investigation [409], which if successful could allow power plants to have higher core power density without ELMs. ELMs do have a useful feature, which is they flush

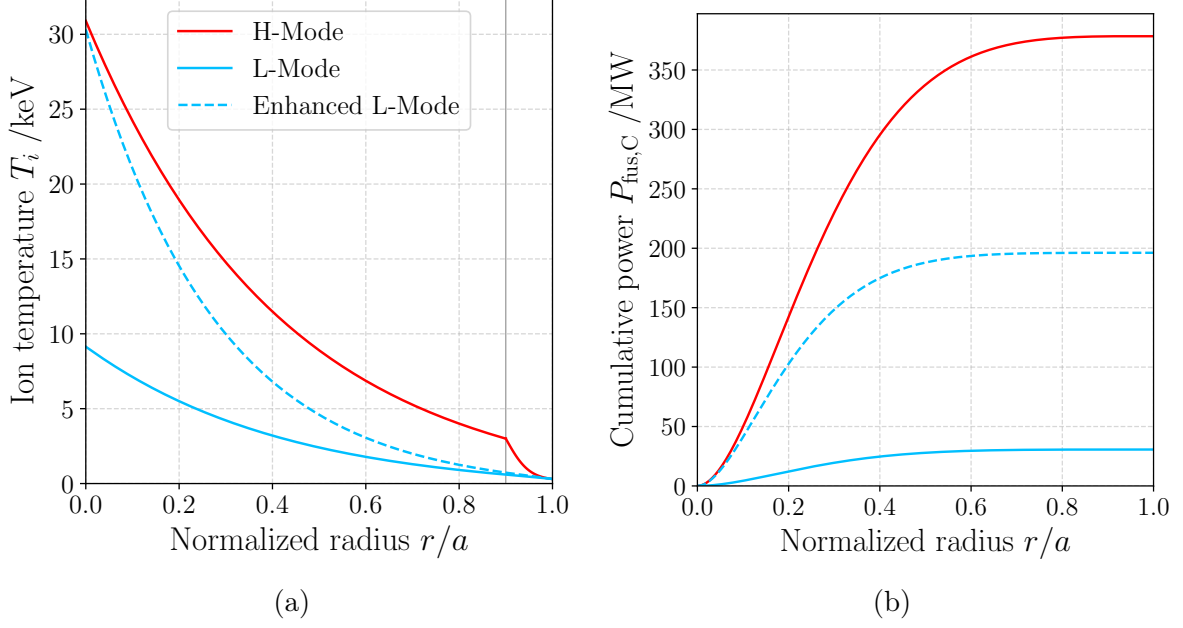


Figure 17: (a) Calculated ion temperature profiles and (b) corresponding cumulative fusion power profiles for L-Mode, Enhanced L-mode, and H-mode (see Equation (7)). For L-Mode and H-mode, we use  $\alpha_{\text{stiff}} = 3.0$ ,  $\hat{\chi}_i = 1.0$ , and  $a/L_{T,i}^{\text{crit}} = 2.4$ . For Enhanced L-Mode, we use  $\hat{\chi}_i = 0.5$  and  $a/L_{T,i}^{\text{crit}} = 3.6$ . Density and geometry profiles are identical for all cases.

out impurities that accumulate in the plasma core. Finding mechanisms for impurity flushing in the absence of ELMs is an essential research area.

## 9.2 L-mode

Despite the advantages of H-mode, in the past decade there has been a renaissance for L-mode operation, the main driver being an operating mode called negative triangularity (NT) [10]. The principal idea behind negative triangularity is that it forces the plasma to stay in H-mode. The leading hypothesis is that instabilities at the plasma edge prevent steep gradients from forming, preventing the emergence of a pedestal [292, 293, 295, 294], although there are other explanations [45, 58, 367, 34, 226]. While L-mode discharges cannot benefit from a high pedestal pressure, NT L-modes are reported to have certain transport advantages such as higher critical gradients, lower turbulent diffusivity, and lower plasma stiffness.

Recall that the primary motivation for H-mode is that it can significantly increase the total fusion power within the plasma,

$$P_{\text{fus}} = \int p_{\text{fus}} dV. \quad (138)$$

It is argued that H-mode is an efficient way to pack high power density regions into the plasma core – by increasing pressure as quickly as possible in the plasma edge, there is a larger volume in the plasma core where  $p_{\text{fus}}$  is large. L-mode takes a different approach, which is to use higher critical gradients and lower turbulent transport to obtain a higher  $p_{\text{fus}}$  in the core.

Because the magnetic geometry of positive and negative triangularity also differs, the volume profile  $V(r)$  can vary significantly [308], especially at low aspect ratio – negative triangularity configurations may enclose more volume near the magnetic axis, which is where  $p_{\text{fus}}$  is typically highest. This could have beneficial consequences for the total fusion power in L-mode discharges, even with the disadvantage of not having a pedestal.

We now perform a simple demonstration of the differences between L-mode and H-mode using the transport model in Section 1. For H-mode, we set the ion temperature  $T_i = 3.0$  keV at  $r/a = 0.9$ , whereas in L-mode we have no pedestal and use an edge temperature  $T_i = 0.3$  keV. H-mode achieves nearly four times the core ion temperature despite the stiffness, turbulent diffusivity, and critical temperature gradient being identical to L-mode. We also show an Enhanced L-mode with half the turbulent diffusivity and a fifty percent higher critical gradient. Enhanced L-mode achieves a similar core temperature to H-mode but the total fusion power is roughly half that of H-mode. This demonstrates the importance of volume-integrated fusion power rather than the peak power density. We have assumed the same stiffness value, density profiles and geometry profiles for all three cases.

Finally, we mention a third promising and relatively under-explored regime, I-mode. I-mode has a temperature pedestal but not a density pedestal, and is generally ELM-free [138, 358, 425, 191]. I-mode therefore has relatively long energy confinement time but short particle confinement time. A short particle confinement time can be useful for quickly flushing helium ash from the plasma core where it dilutes the fusion power.

### 9.3 Prospects

Where does this leave us for tokamak confinement regimes going forward? Machines such as ITER, designed in the 1980s and 1990s, required H-mode to obtain sufficient power density for them to obtain high plasma gain. However, given the risk of ELMs, even if the modeling demonstrates otherwise, we will not know whether we can produce FPP-relevant ELM-free H-modes until the experiment is operated, which are multi-billion dollar machines with long construction times. Given that we have new tools at our disposal to increase fusion power density such as high magnetic field [383] and plasma shaping [293], L-mode and I-mode merit continued investigation as serious alternatives to H-mode.

### 9.4 Further Reading

- Quasi-continuous exhaust regime [111, 153, 336, 112, 97].
- Enhanced-pedestal H-mode [264, 263, 52, 127].
- Enhanced D-alpha H-mode [192, 232, 130, 257].
- I-mode [138, 358, 425, 191].
- Quiescent H-mode [43, 360, 394, 126, 106, 44, 61, 427, 186].
- Active ELM suppression strategies: resonant magnetic perturbations [221], vertical kicks [80], ELM pacing [107], supersonic molecular beam injection [436].
- L-mode [203, 216, 10, 293, 321, 428].

- Impurity flushing [335, 7].

## 10 Burning Plasmas

In this section, we provide a survey on some of the most important outstanding confinement questions for burning plasmas [122, 137, 134, 162, 300, 113, 282]. A burning plasma is one where the fusion products constitute a significant fraction of the total plasma heating. For D-T fusion, alpha heating constitutes 50% of all heating when the plasma gain  $Q^{\text{sci}} = 5$  (recall  $Q^{\text{sci}} = P_{\text{fus}}/P_{\text{ext}}$  where  $P_{\text{fus}}$  is the fusion power and  $P_{\text{ext}}$  is the external heating power) and constitutes 100% of all heating when the plasma has ignited ( $Q^{\text{sci}} = \infty$ ). The burning regime represents a new regime not yet seen in MCF plasmas (as of 2025) – every MCF machine so far has operated with  $Q^{\text{sci}} < 1$ .

Why is this significant? The first reason is that there are new couplings between transport and sources in burning plasmas due to alpha particles produced from D-T fusion reactions. The higher the core temperature and density, the stronger the alpha heating source. And a stronger alpha heating source leads to more alpha heating and a range of fast particle instabilities. Second, the alphas are a particle source that dilute the main ion species, which reduces the fusion power. Coupling these effects is an unsolved problem because of its immense computational and theoretical complexity and uncertainty. One limiting factor is that the effect of fast particles on transport is complicated and no experiments exist for burning plasmas where we can benchmark, although there is much work from TFTR [386] and JET [214], as of 2025, the only two magnetic confinement plasmas to produce significant fusion power. A recent study [411] showed the capital cost of a fusion power plant is most sensitive to the energy confinement quality factor  $H$  (see Equation (60)). This is reason both for both caution and optimism: if burning plasmas have improved energy confinement, they could be cheaper and faster to build. But if confinement is degraded, they could be more expensive and slower. This is an area where advances in transport physics and energy confinement could be a large lever for accelerating the deployment of fusion power.

Another interesting question for burning plasmas is particle transport. A burning plasma burns deuterium and tritium fuel to produce fusion power. A critical engineering and regulatory question for fusion power is the quantity of tritium onsite, called the tritium inventory. Reducing the tritium inventory size can significantly ease engineering and regulatory requirements. It is predicted that the most effective way to decrease tritium inventory is to increase the tritium burn efficiency [2, 281, 424]. Tritium burn efficiency can be increased by increase tritium particle confinement time [2, 31, 32, 424, 312], more rapidly removing helium ash from the core [339, 424], increasing the reactivity of fusion fuel [230, 309], and increasing fueling efficiency [397, 2]. Similar to the discussion of energy confinement above, these are largely areas where plasma physics can drive progress.

While we largely avoided discussion of momentum transport and plasma rotation, this is an area of very high uncertainty for MCF power plant design because energy confinement is sensitive to rotation and generally benefits from higher rotation [42, 17]. The largest driver of plasma rotation in modern machines is with neutral beam injection (NBI). However, it is unclear whether NBI will be used in MCF power plants, and even if it were, it is unlikely it will drive as much rotation as it currently does in current devices. This is important, because in the absence of NBI and other momentum inputs, it is

predicted that the size of self-generated plasma flows scales with  $\rho_* = \rho/a$  [317]. This is pessimistic. Because future machines will be larger and have higher magnetic field strength (smaller  $\rho_*$ ) than current machines, the available rotation and rotation shear will be much lower than is currently available.

## 11 Other Important Topics

In this section, I briefly summarize some topics that are important, but for which I did not have time to include.

**Reduced Models.** Using gyrokinetics to calculate the turbulent fluxes in the transport equations can be prohibitively expensive computationally. In order to reduce computational cost, reduced models for the turbulent fluxes have been developed [69, 417, 384, 329, 33, 290, 156, 128] in order to allow larger parameter scans and lower computational cost.

**Plasma Geometry.** Tokamaks and stellarators come in a wide range of shapes and sizes. These different geometric configurations have a substantial effect on confinement [133, 212, 402, 25, 271, 15, 280, 10, 293, 14, 428, 26, 217, 235, 311].

**Scrape-Off-Layer (SOL) Turbulence.** Beyond the last-closed-flux-surface, magnetic field lines are *open*: following a magnetic field line from just beyond the last-closed-flux-surface will intersect with a plasma wall. This magnetic field configuration is distinct from within the last-closed-flux-surface, where field lines are closed and trace out flux surfaces. The SOL transport can have a significant impact on plasma exhaust and core plasma fueling [432, 303, 400, 121, 106, 440, 371, 324].

**Experimental Confinement Scalings.** A useful approach for predicting future tokamak energy confinement time is based on database analysis of past experiments. There are many scalings [133, 212, 438, 389, 213, 73, 407]. A big question is the accuracy of the current scaling laws as future experiments enter new parameter regimes.

**Fast Particles.** Fast particles (with energy  $E \gtrsim 1$  MeV) have been reported to both drive and suppress turbulence and other instabilities [330, 164, 351, 84, 274, 125]. In burning plasmas, fast particles will constitute a significant fraction of the plasma energy and density [163, 134]. Self-consistently including the effect of fast particles in the system of transport equations discussed in Section 6 is challenging.

**Machine Learning.** Machine learning approaches are used commonly in confinement research, for example in accelerating turbulence simulations [256, 406], magnetic equilibrium reconstruction [115, 240, 47], plasma heating modeling [415, 362], plasma stability prediction [326, 327] and profile prediction [35, 1, 95], among other topics [377, 235].

## 12 Summary

In this tutorial, I have attempted to provide an accessible entry point for students and researchers interested in plasma stability and transport in magnetic confinement plasmas.

Section 1 motivated the transport problem with a simple example. We demonstrated how apparently small changes in energy transport properties could lead to big changes in the total fusion power. Section 2 showed how the physics of nuclear fusion reactions and Coulomb collisions generally require a hot plasma and a confinement scheme. The deuterium-tritium nuclear fusion cross section plays a central role in determining the temperature and confinement schemes required for a successful fusion power plant. Section 3

discussed the Lawson Criterion for energy confinement and an analogous argument for particle confinement. We found the minimum density and confinement time required for fusion ignition and the minimum particle sources for a plasma with a given fusion power. Section 4 discussed the basics of magnetic confinement and introduced the coordinate system for tokamaks. Section 5 estimated the confinement times of a tokamak discharge based on classical, neoclassical, and turbulent transport. We then found an approximate scaling for the minimum power plant size on the energy confinement quality. Section 6 introduced the main equations required for finding the magnetic equilibrium and plasma profiles on long timescales. We described some features of the gyrokinetic, neoclassical, transport, and magnetic equilibrium equations. Section 7 covered some of gyrokinetic instabilities giving rise to turbulent transport in tokamaks and stellarators. We briefly discussed nonlinear physics and turbulence measurements. A detailed derivation of the ion-temperature-gradient instability is provided in Appendix A. Section 8 introduced some commonly used numerical tools used to solve the transport problem. Section 9 described the most common tokamak confinement regimes. We compared H-Mode and L-Mode fusion power profiles. Section 10 discussed some of the challenges and opportunities in burning plasmas. Section 11 listed some important topics that I didn't have time to describe in detail.

## 13 Acknowledgements

I am indebted to Felix Parra, Michael Barnes, Steve Cowley, Paul Dellar, Walter Guttenfelder, Stan Kaye, Colin Roach, and Alex Schekochihin for their instruction in turbulence and transport. This work was supported by the U.S. Department of Energy under contract numbers DE-AC02-09CH11466, DE-SC0022270, DE-SC0022272. The United States Government retains a non-exclusive, paid-up, irrevocable, world-wide license to publish or reproduce the published form of this manuscript, or allow others to do so, for United States Government purposes.

## 14 Data Availability

Data sharing is not applicable to this article as no new data were created or analyzed in this study.

## A Appendix: ITG Instability

In this section we derive a dispersion relation for linear ion-temperature-gradient (ITG) instability in toroidal geometry. The goal is to find an expression for the complex frequency and the critical gradient.

We keep the effects of both magnetic drifts and parallel streaming, whose effects correspond to ‘toroidal’ and ‘slab’ ITG respectively. The slab ITG of this derivation closely follows [316, 147] and is based on lecture courses given at Massachusetts Institute of Technology and Princeton University by F.I. Parra.

We work in the electrostatic limit where  $\delta\mathbf{A}$  fluctuations are neglected, we neglect collisions, and we neglect the nonlinear term. We assume a single ion species. In this

limit, the non-adiabatic distribution function from Equation (91) is

$$h_i = \frac{\omega - \omega_{*i} \left[ 1 + \eta_i \left( \hat{v}_{\parallel}^2 + \hat{v}_{\perp}^2 - \frac{3}{2} \right) \right]}{\omega - k_{\parallel} v_{\parallel} - \omega_{\kappa i} \hat{v}_{\parallel}^2 - \omega_{Bi} \hat{v}_{\perp}^2 / 2} J_0 \left( \frac{k_{\perp} v_{\perp}}{\Omega_i} \right) \frac{Z_i e \delta \phi}{T_i} F_{Mi}. \quad (139)$$

To make analytic progress, we order the parallel streaming as much faster than the magnetic drifts (see [200] where this was not assumed),

$$|\omega - k_{\parallel} v_{\parallel}| \gg |\omega_{\kappa i} \hat{v}_{\parallel}^2 + \omega_{Bi} \hat{v}_{\perp}^2 / 2|. \quad (140)$$

Using Equation (140), the ion distribution function assuming  $Z_i = 1$  is

$$h_i = \frac{\omega \tau + \omega_{*e} \left[ 1 + \eta_i \left( \hat{v}_{\parallel}^2 + \hat{v}_{\perp}^2 - \frac{3}{2} \right) \right]}{\omega - k_{\parallel} v_{\parallel}} J_0 \left( \frac{k_{\perp} v_{\perp}}{\Omega_i} \right) \frac{e \delta \phi}{T_e} F_{Mi} \left( 1 + \frac{A}{\omega - k_{\parallel} v_{\parallel}} + \dots \right), \quad (141)$$

where

$$A \equiv \omega_{\kappa s} \hat{v}_{\parallel}^2 + \omega_{Bs} \hat{v}_{\perp}^2 / 2, \quad \tau \equiv \frac{T_e}{T_i}. \quad (142)$$

For this analysis of ITG instability, we limit ourselves to the perpendicular scales  $k_{\perp} \rho_e \ll 1$ . At these scales, we expect  $|k_{\parallel} v_{\parallel}| \gg \omega_{*e}, \omega$ . Using this assumptions, the electrons are ‘adiabatic’:  $h_e = 0$ . Physically, this corresponds to electrons rapidly streaming along field lines with a modified Boltzmann response,

$$\delta f_e = -\frac{e \delta \phi}{T_e} F_{Me}. \quad (143)$$

The perturbed quasineutrality equation is

$$\sum Z_s \delta n_s = 0. \quad (144)$$

Using Equations (141) and (143), perturbed quasineutrality is

$$\sum Z_s \delta n_s = \sum Z_s \int \delta f_s d^3 v = -\frac{e \delta \phi}{T_i} \int F_{Mi} d^3 v + \int h_i d^3 v - \frac{e \delta \phi}{T_e} \int F_{Me} d^3 v, \quad (145)$$

We also consider quasineutrality for the equilibrium density,

$$\sum Z_s n_s = 0, \quad (146)$$

which gives  $n_i = n_e$ . Therefore, perturbed quasineutrality in Equation (145) is

$$\int h_i d^3 v - \frac{e \delta \phi}{T_e} n_e (1 + \tau) = 0. \quad (147)$$

The next step is to split the integral for  $h_i$  into three parts corresponding to the term independent of magnetic drifts, the curvature drift term, and the grad-B drift term,

$$\int h_i d^3 v = \int T_1 d^3 v + \int T_1 \frac{\omega_{\kappa i}}{\omega - k_{\parallel} v_{\parallel}} \hat{v}_{\parallel}^2 d^3 v + \int T_1 \frac{\omega_{\nabla Bi}}{\omega - k_{\parallel} v_{\parallel}} \frac{\hat{v}_{\perp}^2}{2} d^3 v \quad (148)$$

where

$$T_1 = \frac{\omega \tau + \omega_{*e} \left[ 1 + \eta_s \left( \hat{v}_{\parallel}^2 + \hat{v}_{\perp}^2 - \frac{3}{2} \right) \right]}{\omega - k_{\parallel} v_{\parallel}} J_0 \left( \frac{k_{\perp} v_{\perp}}{\Omega_s} \right) \frac{e \delta \phi}{T_s} F_{Ms}. \quad (149)$$



### A.0.1 Useful Integrals

Before evaluating the three integrals in Equation (148), we introduce a few useful relations. The first is the well-known plasma dispersion function [110]

$$Z(\zeta) = \frac{1}{\sqrt{\pi}} \int_{-\infty}^{\infty} \frac{dx e^{-x^2}}{x - \zeta}, \quad (150)$$

for  $\text{Im}(\zeta) > 0$  where

$$\zeta \equiv \frac{\omega}{k_{\parallel} v_{ts}} \quad x \equiv \frac{v_{\parallel}}{v_{ts}}. \quad (151)$$

Because we will taking integrals with moments of  $v_{\parallel}$ , it is also helpful to use

$$\frac{1}{\sqrt{\pi}} \int_{-\infty}^{\infty} \frac{dx x^2 e^{-x^2}}{x - \zeta} = 2\zeta + \zeta^2 Z(\zeta), \quad \frac{1}{\sqrt{\pi}} \int_{-\infty}^{\infty} \frac{dx x^4 e^{-x^2}}{x - \zeta} = 6\zeta^2 + \zeta^4 Z(\zeta). \quad (152)$$

There will also be integrals with two powers of  $\omega - k_{\parallel} v_{\parallel}$  in the denominator, giving integrals of the form

$$\frac{1}{\sqrt{\pi}} \int_{-\infty}^{\infty} \frac{x^a e^{-x^2}}{(x - \zeta)^2} dx, \quad (153)$$

where  $a \geq 0$  is an even integer. To handle these integrals, we take derivatives of the dispersion function. The  $n$ -th derivative of  $Z(\zeta)$  is

$$Z^{(n)}(\zeta) = (-1)^n n! \frac{1}{\sqrt{\pi}} \int_{-\infty}^{\infty} \frac{e^{-x^2}}{(x - \zeta)^{n+1}} dx, \quad (154)$$

which give the handy recurrence relation valid for  $n \geq 1$ ,

$$Z^{(n+1)}(\zeta) = -2 \left( Z^{(n)}(\zeta) + \zeta Z^{(n-1)}(\zeta) \right), \quad (155)$$

where

$$Z^{(0)}(\zeta) = Z(\zeta), \quad Z^{(1)}(\zeta) = -2(1 + \zeta Z(\zeta)). \quad (156)$$

Therefore, the zeroth moment is

$$\frac{1}{\sqrt{\pi}} \int_{-\infty}^{\infty} \frac{e^{-x^2}}{(x - \zeta)^2} dx = 2(1 + \zeta Z(\zeta)). \quad (157)$$

After some more algebra, we find the second moment

$$\frac{1}{\sqrt{\pi}} \int_{-\infty}^{\infty} \frac{x^2 e^{-x^2}}{(x - \zeta)^2} dx = 1 + 2\zeta Z - 2\zeta^2 - 2\zeta^3 Z, \quad (158)$$

and the fourth moment

$$\frac{1}{\sqrt{\pi}} \int_{-\infty}^{\infty} \frac{x^4 e^{-x^2}}{(x - \zeta)^2} dx = \frac{1}{2} + 3\zeta^2 + 4\zeta^3 Z - 2\zeta^4 - 2\zeta^5 Z. \quad (159)$$

Another useful integral involves the Bessel functions,

$$\int_0^{\infty} y J_0^2(ay) \exp(-by^2) dy = \frac{1}{2b} \Gamma_0\left(\frac{a^2}{2b}\right), \quad (160)$$

its cubic moment,

$$\int_0^\infty y^3 J_0^2(ay) \exp(-by^2) dy = \frac{(2b - a^2) \Gamma_0 \left( \frac{a^2}{2b} \right) + a^2 \Gamma_1 \left( \frac{a^2}{2b} \right)}{4b^3}, \quad (161)$$

and its quintic moment,

$$\int_0^\infty y^5 J_0^2(ay) \exp(-by^2) dy = \frac{(2b - a^2)^2 \Gamma_0 \left( \frac{a^2}{2b} \right) + a^2 (3b - a^2) \Gamma_1 \left( \frac{a^2}{2b} \right)}{4b^5}. \quad (162)$$

### A.0.2 Dispersion Relation

Using the integral expressions in Appendix A.0.1, the first integral term in Equation (148) is

$$\begin{aligned} & \frac{1}{n_e} \frac{T_e}{e\delta\phi} \int T_1 d^3v = \\ & - Z(\zeta_i) \Gamma_0 \left( \tau \zeta_i + \frac{\omega_{*e}}{k_{\parallel} v_{ti}} \left( 1 - \frac{3}{2} \eta_i \right) \right) \\ & - \Gamma_0 \frac{\omega_{*e}}{k_{\parallel} v_{ti}} \eta_i (\zeta_i + \zeta_i^2 Z(\zeta_i)) \\ & - \frac{\omega_{*e}}{k_{\parallel} v_{ti}} \eta_i Z(\zeta_i) (\Gamma_0 + b_i (\Gamma_1 - \Gamma_0)). \end{aligned} \quad (163)$$

The second integral is  $Z(\zeta_i) \rightarrow 1 + 2\zeta_i Z + 2\zeta_i^2 + 2\zeta_i^3 Z(\zeta_i)$  or  $Z(\zeta_i) \rightarrow 1 + 6\zeta_i^2 + 4\zeta_i^3 Z(\zeta_i) + 2\zeta_i^4 + 2\zeta_i^5 Z(\zeta_i)$

$$\begin{aligned} & \frac{1}{n_e} \frac{T_e}{e\delta\phi} \int T_1 \frac{\omega_{\kappa i}}{\omega - k_{\parallel} v_{\parallel}} \hat{v}_{\parallel}^2 d^3v = \\ & - [1 + 2\zeta_i Z - 2\zeta_i^2 - 2\zeta_i^3 Z(\zeta_i)] \Gamma_0 \left( \tau \zeta_i + \frac{\omega_{*e}}{k_{\parallel} v_{ti}} \left( 1 - \frac{3}{2} \eta_i \right) \right) \frac{\omega_{\kappa i}}{k_{\parallel} v_{ti}} \\ & - \Gamma_0 \frac{\omega_{*e}}{k_{\parallel} v_{ti}} \eta_i \left( \frac{1}{2} + 3\zeta_i^2 + 4\zeta_i^3 Z - 2\zeta_i^4 - 2\zeta_i^5 Z \right) \frac{\omega_{\kappa i}}{k_{\parallel} v_{ti}} \\ & - \frac{\omega_{*e}}{k_{\parallel} v_{ti}} \eta_i [1 + 2\zeta_i Z - 2\zeta_i^2 - 2\zeta_i^3 Z(\zeta_i)] (\Gamma_0 + b_i (\Gamma_1 - \Gamma_0)) \frac{\omega_{\kappa i}}{k_{\parallel} v_{ti}}. \end{aligned} \quad (164)$$

The third integral is  $\Gamma_0 \rightarrow \Gamma_0 + b_i (\Gamma_1 - \Gamma_0)$ ,  $Z(\zeta_i) \rightarrow 2(1 + \zeta_i Z(\zeta_i))$ ,  $Z(\zeta_i) \rightarrow 1 + 2\zeta_i Z + 2\zeta_i^2 + 2\zeta_i^3 Z(\zeta_i)$ , and

$$\Gamma_0 + b_i (\Gamma_1 - \Gamma_0) \rightarrow 4 \left[ \Gamma_0 + b_i \left( \frac{3}{2} \Gamma_1 - 2\Gamma_0 \right) + b_i^2 (\Gamma_0 - \Gamma_1) \right], \quad (165)$$

giving

$$\begin{aligned} & \frac{1}{n_e} \frac{T_e}{e\delta\phi} \int T_1 \frac{1}{2} \frac{\omega_{\nabla Bi}}{\omega - k_{\parallel} v_{\parallel}} \hat{v}_{\perp}^2 d^3v = \\ & - 2(1 + \zeta_i Z(\zeta_i)) (\Gamma_0 + b_i (\Gamma_1 - \Gamma_0)) \left( \tau \zeta_i + \frac{\omega_{*e}}{k_{\parallel} v_{ti}} \left( 1 - \frac{3}{2} \eta_i \right) \right) \frac{\omega_{\nabla Bi}}{2k_{\parallel} v_{ti}} \\ & - 4 \left[ \Gamma_0 + b_i \left( \frac{3}{2} \Gamma_1 - 2\Gamma_0 \right) + b_i^2 (\Gamma_0 - \Gamma_1) \right] \frac{\omega_{*e}}{k_{\parallel} v_{ti}} \eta_i (1 + 2\zeta_i Z - 2\zeta_i^2 - 2\zeta_i^3 Z(\zeta_i)) \frac{\omega_{\nabla Bi}}{2k_{\parallel} v_{ti}} \\ & - \frac{\omega_{*e}}{k_{\parallel} v_{ti}} \eta_i 2(1 + \zeta_i Z(\zeta_i)) (\Gamma_0 + b_i (\Gamma_1 - \Gamma_0)) \frac{\omega_{\nabla Bi}}{2k_{\parallel} v_{ti}}. \end{aligned} \quad (166)$$

Putting it all together, the dispersion relation from Equation (147) is

$$\begin{aligned}
& 1 + \tau (1 + \Gamma_0 \zeta_i Z(\zeta_i)) \\
& + \frac{\omega_{*e}}{k_{\parallel} v_{ti}} \Gamma_0 Z(\zeta_i) \left(1 - \frac{3}{2} \eta_i\right) \\
& + \frac{\omega_{*e}}{k_{\parallel} v_{ti}} \eta_i \Gamma_0 (\zeta_i + \zeta_i^2 Z(\zeta_i)) \\
& + \frac{\omega_{*e}}{k_{\parallel} v_{ti}} \eta_i (\Gamma_0 + b_i (\Gamma_1 - \Gamma_0)) Z(\zeta_i) \\
& + \frac{\omega_{\kappa i}}{k_{\parallel} v_{ti}} \Gamma_0 [1 + 2\zeta_i Z - 2\zeta_i^2 - 2\zeta_i^3 Z(\zeta_i)] \left(\tau \zeta_i + \frac{\omega_{*e}}{k_{\parallel} v_{ti}} \left(1 - \frac{3}{2} \eta_i\right)\right) \\
& + \frac{\omega_{\kappa i}}{k_{\parallel} v_{ti}} \frac{\omega_{*e}}{k_{\parallel} v_{ti}} \eta_i \Gamma_0 \left(\frac{1}{2} + 3\zeta_i^2 + 4\zeta_i^3 Z - 2\zeta_i^4 - 2\zeta_i^5 Z\right) \\
& + \frac{\omega_{\kappa i}}{k_{\parallel} v_{ti}} \frac{\omega_{*e}}{k_{\parallel} v_{ti}} \eta_i (\Gamma_0 + b_i (\Gamma_1 - \Gamma_0)) [1 + 2\zeta_i Z - 2\zeta_i^2 - 2\zeta_i^3 Z(\zeta_i)] \\
& + \frac{\omega_{\nabla B i}}{k_{\parallel} v_{ti}} (\Gamma_0 + b_i (\Gamma_1 - \Gamma_0)) (1 + \zeta_i Z(\zeta_i)) \left(\tau \zeta_i + \frac{\omega_{*e}}{k_{\parallel} v_{ti}} \left(1 - \frac{3}{2} \eta_i\right)\right) \\
& + 2 \frac{\omega_{\nabla B i}}{k_{\parallel} v_{ti}} \frac{\omega_{*e}}{k_{\parallel} v_{ti}} \eta_i \left[\Gamma_0 + b_i \left(\frac{3}{2} \Gamma_1 - 2\Gamma_0\right) + b_i^2 (\Gamma_0 - \Gamma_1)\right] (1 + 2\zeta_i Z - 2\zeta_i^2 - 2\zeta_i^3 Z(\zeta_i)) \\
& + \frac{\omega_{\nabla B i}}{k_{\parallel} v_{ti}} \frac{\omega_{*e}}{k_{\parallel} v_{ti}} \eta_i (\Gamma_0 + b_i (\Gamma_1 - \Gamma_0)) (1 + \zeta_i Z(\zeta_i)) = 0.
\end{aligned} \tag{167}$$

## A.1 Toroidal ITG Instability

We now calculate the toroidal ITG instability by taking the limit

$$|\zeta_i| \gg 1, \tag{168}$$

and by ordering

$$\omega_{*e} \sim \zeta_i. \tag{169}$$

In the  $|\zeta_i| \gg 1$  limit, the plasma dispersion function can be expanded as

$$Z(\zeta_i) \sim -\frac{1}{\zeta_i} - \frac{1}{2\zeta_i^3} - \frac{3}{4\zeta_i^5} - \frac{15}{8\zeta_i^7} + \dots \tag{170}$$

In this limit, we will expand the frequently occurring expressions with  $Z(\zeta_i)$ .

$$1 + \zeta_i Z(\zeta_i) \sim -\frac{1}{2\zeta_i^2} - \frac{3}{4\zeta_i^3} + \dots, \tag{171}$$

$$\zeta_i + \zeta_i^2 Z(\zeta_i) \sim -\frac{1}{2\zeta_i} - \frac{3}{4\zeta_i^2} + \dots, \tag{172}$$

$$1 + 2\zeta_i Z(\zeta_i) - 2\zeta_i^2 - 2\zeta_i^3 Z(\zeta_i) \sim \frac{1}{2\zeta_i^2} + \dots, \tag{173}$$

$$\frac{1}{2} + 3\zeta_i^2 + 4\zeta_i^3 Z - 2\zeta_i^4 - 2\zeta_i^5 Z \sim \frac{3}{4\zeta_i^2} + \dots \tag{174}$$

Substituting these expressions into quasineutrality (Equation (167)), and for further simplification taking the long-wavelength limit  $b_i \rightarrow 0$ ,  $\Gamma_0 \rightarrow 1$ ,  $\Gamma_1 \rightarrow 0$ , gives

$$\omega^2 - \omega\omega_{*e} + \frac{\omega_{\kappa i}\omega_{*e}}{2}(\eta_i + 1) + \frac{\omega_{\nabla B i}\omega_{*e}}{2}(\eta_i - 1) = 0. \quad (175)$$

Finally, it is often assumed that the grad-B and curvature drift frequencies are equal,  $\omega_{\nabla B i} = \omega_{\kappa i}$ . In this limit, Equation (175) becomes

$$\omega^2 - \omega\omega_{*e} + \omega_{\kappa i}\omega_{*e}\eta_i = 0. \quad (176)$$

The frequency in Equation (176) has the solution

$$\omega = \frac{\omega_{*e} \pm \sqrt{(\omega_{*e})^2 - 4\omega_{\kappa i}\omega_{*e}\eta_i}}{2}, \quad (177)$$

with instability arising when

$$4\omega_{\kappa i}\eta_i > \omega_{*e}, \quad (178)$$

with a growth rate

$$\gamma = \frac{\sqrt{4\omega_{\kappa i}\omega_{*e}\eta_i - (\omega_{*e})^2}}{2}. \quad (179)$$

The growth rate in Equation (179) has some curious features. In the limit where  $\eta_i \gg 1$ , the ion temperature gradient is much steeper than density gradient. Assuming

$$\omega_{*e} \sim \omega_{\kappa i}, \quad \eta_i \gg 1, \quad (180)$$

and approximating the magnetic drift frequency as

$$\omega_{\kappa i} \approx k_y \rho_i \frac{v_{ti}}{R}, \quad (181)$$

the growth rate is approximately

$$\gamma \approx \sqrt{\omega_{\kappa i}\omega_{*e}\eta_i} \simeq k_y \rho_i \sqrt{\frac{v_{ti}^2}{RL_{T_i}}}. \quad (182)$$

Also note that a necessary condition for instability is

$$\omega_{\kappa i}\omega_{*e}\eta_i > 0, \quad (183)$$

which is the condition that the magnetic curvature and ion temperature gradient have the same sign. The region where  $\omega_{\kappa i}\omega_{*e} > 0$  is known as ‘bad curvature’ and  $\omega_{\kappa i}\omega_{*e} < 0$  is ‘good curvature.’ Generally, ITG is driven in bad-curvature regions, although electromagnetic effects (neglected above) can destabilize ITG in good-curvature regions [199].

The toroidal ITG mode is analytically complicated, and an in-depth treatment is beyond the scope of this tutorial. There are many excellent resources on the ITG instability including [350, 28, 328, 346].

## A.2 Slab ITG Instability

We can also take the ‘slab’ ITG limit, which is found when setting the magnetic drift frequencies in Equation (167) to zero. This gives the dispersion relation

$$\begin{aligned} 1 + \tau(1 + \zeta_i Z(\zeta_i)\Gamma_0) + \frac{\omega_{*e}}{k_{\parallel} v_{ti}} Z(\zeta_i)\Gamma_0 \left(1 - \frac{3}{2}\eta_i\right) \\ + \frac{\omega_{*e}}{k_{\parallel} v_{ti}} \eta_i \Gamma_0 (\zeta_i + \zeta_i^2 Z(\zeta_i)) + \frac{\omega_{*e}}{k_{\parallel} v_{ti}} \eta_i Z(\zeta_i) (\Gamma_0 + b_i (\Gamma_1 - \Gamma_0)) = 0. \end{aligned} \quad (184)$$

### A.2.1 Drift Wave

We recover the ‘drift-wave’ limit, which is when  $b_i \ll 1$ ,  $\zeta_i \gg 1$ ,  $\eta_i = 0$ , and  $\tau \ll 2\zeta_i^2$  we obtain,

$$1 - \frac{\omega_{*e}}{k_{\parallel} v_{ti}} \frac{1}{\zeta_i} \approx 0, \quad (185)$$

and so we obtain the drift-wave relation

$$\omega \approx \omega_{*e}. \quad (186)$$

This is a stable wave known as a drift wave.

### A.2.2 Instability

Next, we consider a mode that has a positive growth rate. In order to obtain analytic results, we follow the treatment in [316] using the limits

$$\eta_i \gg 1, \zeta_i \gg 1, b_i \ll 1, \Gamma_0 \rightarrow 1, \Gamma_1 \rightarrow 0, \omega \sim \omega_{*e}, \quad (187)$$

and the dispersion relation becomes cubic in  $\omega$

$$\omega^3 - \omega_{*e}\omega^2 - \omega_{*e}\eta_i \frac{k_{\parallel}^2 T_i}{m_i} = 0, \quad (188)$$

where to make all of the terms of the same order for  $\omega \sim \omega_{*e}$ , we had to assume

$$\zeta_i \sim \sqrt{\eta_i} \gg 1. \quad (189)$$

Next, we take the limit  $\eta_i \rightarrow \infty$ , and assuming that  $\omega > \omega_{*e}$ . This gives  $(\omega/\omega_{*e})^3 > (\omega/\omega_{*e})^2$ , so Equation (188) becomes

$$\omega^3 = \eta_i \frac{k_{\parallel}^2 T_i}{m_i} \omega_{*e}, \quad (190)$$

which has three roots,

$$\omega = \left( \eta_i \frac{k_{\parallel}^2 T_i}{m_i} \omega_{*e} \right)^{1/3} e^{\frac{2\pi i}{3}}, \quad \left( \eta_i \frac{k_{\parallel}^2 T_i}{m_i} \omega_{*e} \right)^{1/3} e^{\frac{4\pi i}{3}}, \quad \left( \eta_i \frac{k_{\parallel}^2 T_i}{m_i} \omega_{*e} \right)^{1/3}. \quad (191)$$

The first root is unstable, since  $\text{Im}(\omega) > 0$ ,

$$\omega = \left( \eta_i \frac{k_{\parallel}^2 T_i}{m_i} \omega_{*e} \right)^{1/3} e^{\frac{2\pi i}{3}} = \left( \eta_i \frac{k_{\parallel}^2 T_i}{m_i} \omega_{*e} \right)^{1/3} \left( -\frac{1}{2} + i\frac{\sqrt{3}}{2} \right). \quad (192)$$

Writing the complex frequency as a sum of a real frequency  $\omega_R$  and growth rate  $\gamma$ ,

$$\omega = \omega_R + i\gamma, \quad (193)$$

Equation (192) gives that the growth rate increases with increasing  $k_{\parallel}$ ,

$$\gamma = \frac{\sqrt{3}}{2} \left( \eta_i \frac{k_{\parallel}^2 T_i}{m_i} \omega_{*e} \right)^{1/3} \sim k_{\parallel}^{2/3}. \quad (194)$$

### A.2.3 Landau Damping

However,  $\gamma \sim k_{\parallel}^{2/3}$  cannot hold for all values of  $k_{\parallel}$ , because another kinetic effect called Landau damping [233] decreasing the growth rate of modes at sufficiently high  $k_{\parallel}$  values. Therefore, we want to obtain the  $k_{\parallel}$  at which the growth rate goes to zero ( $\gamma = 0$ ). First, for Landau damping to occur the frequency is set to

$$\omega \sim k_{\parallel} v_{ti} \sim \eta_i \omega_{*e}. \quad (195)$$

Using this ordering for the dispersion relation, we obtain in the limit  $\eta_i \gg 1$ ,

$$1 + \tau \left( 1 + \zeta_i Z(\zeta_i) \Gamma_0 \right) + \frac{w_{*e} \eta_i}{k_{\parallel} v_{ti}} \left( \zeta_i (1 + \zeta_i Z(\zeta_i)) \Gamma_0 + b_i Z(\zeta_i) (\Gamma_1 - \Gamma_0) - \frac{1}{2} Z(\zeta_i) \Gamma_0 \right) = 0. \quad (196)$$

To obtain the  $k_{\parallel}$  for which  $\gamma = 0$ , we require  $\omega$  is real. When  $\omega$  real, the dispersion function becomes

$$Z(\zeta) = \frac{1}{\sqrt{\pi}} \int_{-\infty}^{\infty} \frac{dp e^{-p^2}}{p - \zeta}, \quad (197)$$

which we can evaluate using contour integration. First, let  $f(p)$  equal

$$f(p) = \frac{1}{\sqrt{\pi}} \frac{e^{-p^2}}{p - \zeta}. \quad (198)$$

Next, choosing the standard upper hemisphere contour, with a pole at  $p = \zeta$  on the real axis (refer to Figure 18) <sup>1</sup>,

$$Z(\zeta) = \mathcal{P} \oint f(p) dp = 2\pi i \sum_k \text{Res}(f(p), \zeta_k) = \pi i \lim_{p \rightarrow \zeta} \left( (p - \zeta) f(p) \right) = \sqrt{\pi} i e^{-\zeta_i^2}. \quad (199)$$

---

<sup>1</sup>There is a pole on the real axis, so

$$Z(\zeta) = \mathcal{P} \int_{-\infty}^{\infty} f(p)$$

$$\oint f(p) dp = \int_{-\infty}^{\infty} f(p) + \int_{\text{hemisphere}} f(p)$$

but

$$\int_{\text{hemisphere}} f(p) = 0,$$

so

$$\oint f(p) dp = \mathcal{P} \int_{-\infty}^{\infty} f(p) + \int_{H_r} f(p).$$

Now, letting  $z - \zeta = \epsilon e^{i\theta}$ ,

$$\int_{H_r} f(p) = \frac{1}{\sqrt{\pi}} \lim_{\epsilon \rightarrow 0} \int_{\zeta - \epsilon}^{\zeta + \epsilon} \frac{e^{-z^2}}{z - \zeta} dz = \frac{1}{\sqrt{\pi}} \lim_{\epsilon \rightarrow 0} \int_{-\pi}^0 \frac{e^{-z^2}}{\epsilon e^{i\theta}} \epsilon i \theta e^{i\theta} d\theta = \frac{1}{\sqrt{\pi}} \lim_{\epsilon \rightarrow 0} \int_{-\pi}^0 e^{-(\epsilon e^{i\theta} - \zeta)^2} i \theta e^{i\theta} d\theta = i \sqrt{\pi} e^{-\zeta_i^2}.$$

Next, using the residue theorem,

$$\oint f(p) dp = 2\pi i \sum_k \text{Res}(f(p), \zeta_k) = \pi i \lim_{p \rightarrow \zeta} \left( (p - \zeta) f(p) \right) = 2i \sqrt{\pi} e^{-\zeta_i^2} = \int_{-\infty}^{\infty} f(p) + i \sqrt{\pi} e^{-\zeta_i^2}.$$

Therefore

$$\int_{-\infty}^{\infty} f(p) = i \sqrt{\pi} e^{-\zeta_i^2}.$$

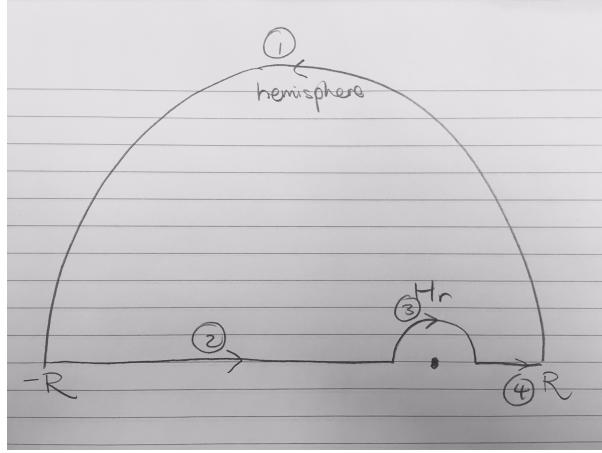


Figure 18: Contour for  $Z(\zeta)$  integral, with the pole at  $p = \zeta$ .

$$Z(\zeta) = i\sqrt{\pi}e^{-\zeta^2} \quad (200)$$

However, all remaining terms in the dispersion relation are real if  $\omega$  is real. So, we just find the coefficients to  $Z(\zeta)$ , and set them equal to zero. So, we have

$$\left[ \tau \zeta_i \Gamma_0 + \frac{w_{*e} \eta_i}{k_{\parallel} v_{ti}} \left( \zeta_i^2 \Gamma_0 + b_i (\Gamma_1 - \Gamma_0) - \frac{1}{2} \Gamma_0 \right) \right] \sqrt{\pi} i e^{-\zeta_i^2} = 0. \quad (201)$$

Thus, we require that the real and imaginary parts of the dispersion relation are individually equal to zero. For the real part,

$$1 + \tau + \frac{w_{*e} \eta_i}{k_{\parallel} v_{ti}} \zeta_i \Gamma_0 = 0, \quad (202)$$

which gives a relation for  $\zeta_i$ :

$$\zeta_i = -(1 + \tau) \frac{1}{\Gamma_0} \frac{k_{\parallel} v_{ti}}{\eta_i \omega_{*e}}. \quad (203)$$

Next, substituting Equation (203) into the imaginary component of the dispersion relation (Equation (201)),

$$\left( \frac{k_{\parallel} v_{ti}}{\eta_i \omega_{*e}} \right)^2 \left( -\tau(1 + \tau) + (1 + \tau)^2 \frac{1}{\Gamma_0} \right) + b_i (\Gamma_1 - \Gamma_0) - \frac{\Gamma_0}{2} = 0. \quad (204)$$

This gives the  $k_{\parallel}$  at which the growth rate goes to zero,

$$\frac{k_{\parallel} v_{ti}}{\eta_i \omega_{*e}} = \pm \left( \Gamma_0 \frac{b_i (\Gamma_1 - \Gamma_0) + \frac{\Gamma_0}{2}}{(1 + \tau)(1 + \tau(1 - \Gamma_0))} \right)^{1/2}. \quad (205)$$

Letting  $b_i \ll 1$ ,

$$\frac{k_{\parallel} v_{ti}}{\eta_i \omega_{*e}} \approx \left( \frac{1}{2(1 + \tau)} \right)^{1/2}. \quad (206)$$

Finally, plugging this into the equation for  $\zeta_i$ , Equation 203 we obtain, when assuming that the frequency is only real (i.e. no damping/instability), we obtain the frequency at which the growth rate goes to zero:

$$\omega = -\frac{b_i (\Gamma_1 - \Gamma_0) + \frac{\Gamma_0}{2}}{1 + \tau(1 - \Gamma_0)} \eta_i \omega_{*e} \Big|_{b_i \ll 1} = -\frac{1}{2} \eta_i \omega_{*e}. \quad (207)$$

### A.2.4 Low $k_{\parallel}$ Growth Rate

Next, we calculate the mode at  $k_{\parallel} \rightarrow 0$ , with  $\eta \gg 1$ , and we drop the restriction of  $\gamma = 0$ . Recall that for  $b_i = 0$ , we found  $\gamma \sim k_{\parallel}^{2/3}$ . Here, we take  $\zeta_i \gg 1$ . For the dispersion relation in Equation (196), we use the limits  $|\text{Re}(\zeta_i)| \gg 1$ ,  $|\text{Re}(\zeta_i)||\text{Im}(\zeta_i)| \ll 1$  to expand the dispersion function,

$$Z(\zeta_i) = -\frac{1}{\zeta_i} - \frac{1}{2\zeta_i^3} + \dots + i\sqrt{\pi}e^{-\zeta_i^2}. \quad (208)$$

The dispersion relation is

$$\begin{aligned} 1 + \tau \left( 1 + \zeta_i Z(\zeta_i) \Gamma_0 \right) + \frac{w_{*e} \eta_i}{k_{\parallel} v_{ti}} \left( \zeta_i (1 + \zeta_i Z(\zeta_i)) \Gamma_0 + b_i Z(\zeta_i) (\Gamma_1 - \Gamma_0) - \frac{1}{2} Z(\zeta_i) \Gamma_0 \right) &= 0 \\ 1 + \tau + \frac{w_{*e} \eta_i}{k_{\parallel} v_{ti}} \zeta_i \Gamma_0 + Z(\zeta_i) \left[ \tau \zeta_i \Gamma_0 + \frac{w_{*e} \eta_i}{k_{\parallel} v_{ti}} \left( \zeta_i^2 \Gamma_0 + b_i (\Gamma_1 - \Gamma_0) - \frac{1}{2} \Gamma_0 \right) \right] &= 0. \end{aligned} \quad (209)$$

Inserting the plasma dispersion function in Equation 208, we find<sup>2</sup>

$$\begin{aligned} 0 &= 1 + \tau + \frac{w_{*e} \eta_i}{k_{\parallel} v_{ti}} \zeta_i \Gamma_0 \\ &+ \left( -\frac{1}{\zeta_i} - \frac{1}{2\zeta_i^3} + i\sqrt{\pi}e^{-\zeta_i^2} \right) \left[ \tau \zeta_i \Gamma_0 + \frac{w_{*e} \eta_i}{k_{\parallel} v_{ti}} \left( \zeta_i^2 \Gamma_0 + b_i (\Gamma_1 - \Gamma_0) - \frac{1}{2} \Gamma_0 \right) \right] = 0 \\ &\approx 1 + \tau(1 - \Gamma_0) \\ &- \frac{w_{*e} \eta_i}{k_{\parallel} v_{ti}} \frac{1}{\zeta_i} \left( b_i (\Gamma_1 - \Gamma_0) - \frac{\Gamma_0}{2} \right) + i\sqrt{\pi}e^{-\zeta_i^2} \left[ \tau \zeta_i \Gamma_0 + \frac{w_{*e} \eta_i}{k_{\parallel} v_{ti}} \left( \zeta_i^2 \Gamma_0 + b_i (\Gamma_1 - \Gamma_0) - \frac{1}{2} \Gamma_0 \right) \right]. \end{aligned} \quad (211)$$

Next, assuming that  $\omega_R \gg \gamma$ , the real part of Equation (211) is

$$1 + \tau(1 - \Gamma_0) + \eta_i \frac{\omega_{*e}}{\omega_R} \left( b_i (\Gamma_1 - \Gamma_0) \right) = 0. \quad (212)$$

This gives the real frequency

$$\omega_R = \frac{\eta_i}{\omega_{*e}} \frac{b_i (\Gamma_0 - \Gamma_1)}{1 + \tau(1 - \Gamma_0)}. \quad (213)$$

The imaginary part of the dispersion relation is

$$-\gamma \eta_i \frac{\omega_{*e}}{\omega_R^2} b_i (\Gamma_1 - \Gamma_0) + \eta_i \sqrt{\pi} e^{-\frac{\omega_R^2}{k_{\parallel}^2 v_{ti}^2}} \frac{\omega_R^2 \omega_{*e}}{k_{\parallel}^3 v_{ti}^3} \Gamma_0 = 0. \quad (214)$$

Rearranging for the growth rate gives

$$\gamma = \frac{\omega_R^4}{k_{\parallel}^3 v_{ti}^3} \frac{\sqrt{\pi} e^{-\frac{\omega_R^2}{k_{\parallel}^2 v_{ti}^2}}}{b_i (\Gamma_1 - \Gamma_0)} \Gamma_0, \quad (215)$$

---

<sup>2</sup>Note that

$$\begin{aligned} \text{Re} \left( Z(\zeta_i) \left( \zeta_i^2 \Gamma_0 + b_i (\Gamma_1 - \Gamma_0) - \frac{1}{2} \Gamma_0 \right) \right) &\approx \left( -\frac{1}{\zeta_i} - \frac{1}{2\zeta_i^3} \right) \left( \zeta_i^2 \Gamma_0 + b_i (\Gamma_1 - \Gamma_0) \right) \\ &\approx -\zeta_i \Gamma_0 - \frac{1}{\zeta_i} b_i (\Gamma_1 - \Gamma_0) \end{aligned} \quad (210)$$



where we used  $w_R \gg \gamma$  and  $\zeta_i \gg 1$ . Therefore Equation (215) gives the ITG growth in the  $k_{\parallel} \rightarrow 0$  limit.

### A.2.5 Critical $\eta_i$

In this section, we find an expression for the critical value of  $\eta_i$ , which occurs when  $\gamma = 0$ . We no longer assume that  $\eta_i$  is large, instead ordering  $\eta_i \sim 1$ .

When  $\gamma = 0$ , the only imaginary components in the dispersion relation (Equation (209)) come from coefficients of  $Z(\zeta_i)$ ,

$$\tau \zeta_i \Gamma_0 + \frac{\omega_{*e}}{k_{\parallel} v_{ti}} \left( \Gamma_0 + \eta_i (\zeta_i^2 \Gamma_0 + b_i (\Gamma_1 - \Gamma_0) - \frac{1}{2} \Gamma_0) \right) = 0. \quad (216)$$

Therefore for  $\gamma = 0$  the real components of the dispersion relation are

$$1 + \tau + \eta_i \frac{\omega_{*e}}{k_{\parallel} v_{ti}} \zeta_i \Gamma_0 = 0, \quad (217)$$

giving the  $\zeta_i$  for which  $\gamma = 0$

$$\zeta_i = -\frac{k_{\parallel} v_{ti}}{\eta_i \omega_{*e}} \frac{1}{\Gamma_0} (1 + \tau). \quad (218)$$

Substituting  $\zeta_i$  into Equation (216) gives the zero growth rate dispersion relation

$$-\tau \frac{k_{\parallel} v_{ti}}{\eta_i \omega_{*e}} \frac{1}{\Gamma_0} (1 + \tau) \Gamma_0 + \frac{\omega_{*e}}{k_{\parallel} v_{ti}} \left( \Gamma_0 + \eta_i \left( \left[ \frac{k_{\parallel} v_{ti}}{\eta_i \omega_{*e}} \frac{1}{\Gamma_0} (1 + \tau) \right]^2 \Gamma_0 + b_i (\Gamma_1 - \Gamma_0) - \frac{1}{2} \Gamma_0 \right) \right) = 0. \quad (219)$$

The growth rate vanishes when the frequency satisfies

$$\omega = -\eta_i \omega_{*e} \Gamma_0 \frac{b_i (1 - \Gamma_1/\Gamma_0) - 1/\eta_i + 1/2}{1 + \tau (1 - \Gamma_0)}. \quad (220)$$

and  $k_{\parallel} v_{ti}$  is

$$k_{\parallel} v_{ti} = \pm \eta_i \omega_{*e} \Gamma_0 \left[ \frac{b_i (1 - \Gamma_1/\Gamma_0) - 1/\eta_i + 1/2}{(1 + \tau) (1 + \tau (1 - \Gamma_0))} \right]^{1/2}. \quad (221)$$

To find the critical value of  $\eta_i$  where the growth rate is zero for all  $k_{\parallel}$  values, we set  $k_{\parallel} = 0$  in Equation (221). This gives the critical  $\eta_i$  value for which the slab ITG mode is stabilized

$$\eta_{i,\text{crit}} = \frac{1}{b_i (1 - \Gamma_1/\Gamma_0) + 1/2}. \quad (222)$$

In the long-wavelength limit where  $b_i \rightarrow 0$ , this gives the well-known result that  $\eta_{i,\text{crit}} = 2$ .

## References

- [1] J. Abbate, R. Conlin, and E. Kolemen. Data-driven profile prediction for diii-d. *Nuclear Fusion*, 61(4):046027, 2021.
- [2] M. Abdou, M. Riva, A. Ying, C. Day, A. Loarte, L. R. Baylor, P. Humrickhouse, T. F. Fuerst, and S. Cho. Physics and technology considerations for the deuterium-tritium fuel cycle and conditions for tritium fuel self sufficiency. *Nuclear Fusion*, 61, 2021.

- [3] M. A. Abdou, E. L. Vold, C. Y. Gung, M. Z. Youssef, and K. Shin. Deuterium-tritium fuel self-sufficiency in fusion reactors. *Fusion Technology*, 9, 1986.
- [4] I. G. Abel, G. G. Plunk, E. Wang, M. Barnes, S. C. Cowley, W. Dorland, and A. A. Schekochihin. Multiscale gyrokinetics for rotating tokamak plasmas: fluctuations, transport and energy flows. *Reports on Progress in Physics*, 76(11):116201, 2013.
- [5] T. Adkins, A. A. Schekochihin, P. G. Ivanov, and C. M. Roach. Electromagnetic instabilities and plasma turbulence driven by electron-temperature gradient. *Journal of Plasma Physics*, 88, 2022.
- [6] K. Aleynikova, A. Zocco, P. Xanthopoulos, P. Helander, and C. Nührenberg. Kinetic ballooning modes in tokamaks and stellarators. *Journal of Plasma Physics*, 84, 2018.
- [7] C. Angioni. Impurity transport in tokamak plasmas, theory, modelling and comparison with experiments. *Plasma Physics and Controlled Fusion*, 63(7):073001, 2021.
- [8] C. Angioni, Y. Camenen, F. J. Casson, E. Fable, R. M. McDermott, A. G. Peeters, and J. E. Rice. Off-diagonal particle and toroidal momentum transport: A survey of experimental, theoretical and modelling aspects. *Nuclear Fusion*, 52(11), 2012.
- [9] D. Applegate, C. Roach, J. Connor, S. Cowley, W. Dorland, R. Hastie, and N. Joiner. Micro-tearing modes in the mega ampere spherical tokamak. *Plasma Physics and Controlled Fusion*, 49(8):1113, 2007.
- [10] M. E. Austin, A. Marinoni, M. L. Walker, M. W. Brookman, J. S. Degraessie, A. W. Hyatt, G. R. McKee, C. C. Petty, T. L. Rhodes, S. P. Smith, C. Sung, K. E. Thome, and A. D. Turnbull. Achievement of Reactor-Relevant Performance in Negative Triangularity Shape in the DIII-D Tokamak. *Physical Review Letters*, 122(11):115001, 2019.
- [11] D. R. Baker, C. M. Greenfield, K. H. Burrell, J. C. DeBoo, E. J. Doyle, R. J. Groebner, T. C. Luce, C. C. Petty, B. W. Stallard, D. M. Thomas, M. R. Wade, and D. Team. Thermal diffusivities in diii-d show evidence of critical gradients. *Physics of Plasmas*, 8(9):4128–4137, 09 2001.
- [12] R. Balescu. Irreversible processes in ionized gases. *The Physics of Fluids*, 3(1):52–63, 1960.
- [13] R. Balescu. Transport processes in plasmas. neoclassical transport theory. vol. 2, Jan 1988.
- [14] A. Balestri, J. Ball, S. Coda, D. J. Cruz-Zabala, M. Garcia-Munoz, and E. Viezzer. Physical insights from the aspect ratio dependence of turbulence in negative triangularity plasmas. *Plasma Physics and Controlled Fusion*, 66(7):075012, may 2024.
- [15] J. Ball and F. I. Parra. Intuition for the radial penetration of flux surface shaping in tokamaks. *Plasma Physics and Controlled Fusion*, 57(3):035006, 2015.
- [16] M. Barnes, I. G. Abel, W. Dorland, Gö, T.rler, G. W. Hammett, and F. Jenko. Direct multiscale coupling of a transport code to gyrokinetic turbulence codes. *Physics of Plasmas*, 17, 2010.

- [17] M. Barnes, F. I. Parra, E. G. Highcock, A. A. Schekochihin, S. C. Cowley, and C. M. Roach. Turbulent transport in tokamak plasmas with rotational shear. *Physical Review Letters*, 106(17):175004, 2011.
- [18] M. Barnes, F. I. Parra, and M. Landreman. stella: An operator-split, implicit–explicit  $\delta f$ -gyrokinetic code for general magnetic field configurations. *Journal of Computational Physics*, 391:365, 2019.
- [19] M. Barnes, F. I. Parra, and A. A. Schekochihin. Critically balanced ion temperature gradient turbulence in fusion plasmas. *Physical Review Letters*, 107(11):115003, 2011.
- [20] M. A. Barnes. *Trinity: A unified treatment of turbulence, transport, and heating in magnetized plasmas*. University of Maryland, College Park, 2009.
- [21] L. R. Baylor, P. Parks, T. C. Jernigan, J. B. Caughman, S. K. Combs, C. R. Foust, W. A. Houlberg, S. Maruyama, and D. A. Rasmussen. Pellet fuelling and control of burning plasmas in iter. *Nuclear fusion*, 47(5):443, 2007.
- [22] M. A. Beer, S. C. Cowley, and G. W. Hammett. Field aligned coordinates for nonlinear simulations of tokamak turbulence. *Physics of Plasmas*, 2(7):2687, 1995.
- [23] E. Belli and J. Candy. Kinetic calculation of neoclassical transport including self-consistent electron and impurity dynamics. *Plasma Physics and Controlled Fusion*, 50(9):095010, 2008.
- [24] E. Belli, J. Candy, and I. Sfiligoi. Spectral transition of multiscale turbulence in the tokamak pedestal. *Plasma Physics and Controlled Fusion*, 65(2):024001, 2022.
- [25] E. A. Belli, G. W. Hammett, and W. Dorland. Effects of plasma shaping on nonlinear gyrokinetic turbulence. *Physics of Plasmas*, 15(9):092303, 2008.
- [26] J. W. Berkery. Nstx-u research advancing the physics of spherical tokamaks (in review). *Nuclear Fusion*, 2024.
- [27] R. Betti, P. Chang, B. Spears, K. Anderson, J. Edwards, M. Fatenejad, J. Lindl, R. McCrory, R. Nora, and D. Shvarts. Thermonuclear ignition in inertial confinement fusion and comparison with magnetic confinement. *Physics of Plasmas*, 17(5), 2010.
- [28] H. Biglari, P. H. Diamond, and M. N. Rosenbluth. Toroidal ion-pressure-gradient-driven drift instabilities and transport revisited. *Physics of Fluids B: Plasma Physics*, 1(1):109, 1989.
- [29] J. Boedo. Edge turbulence and sol transport in tokamaks. *Journal of nuclear materials*, 390:29–37, 2009.
- [30] A. H. Boozer. Theory of tokamak disruptions. *Physics of plasmas*, 19(5), 2012.
- [31] A. H. Boozer. Stellarators as a fast path to fusion. *Nuclear Fusion*, 61, 2021.
- [32] A. H. Boozer. The tritium burn-fraction in dt fusion. *arXiv preprint arXiv:2106.01304*, 2021.

- [33] C. Bourdelle, J. Citrin, B. Baiocchi, A. Casati, P. Cottier, X. Garbet, and F. Imbeaux. Core turbulent transport in tokamak plasmas: Bridging theory and experiment with QuaLiKiz. *Plasma Physics and Controlled Fusion*, 58(1):014036, 2015.
- [34] C. Bourdelle, C. Maggi, L. Chôné, P. Beyer, J. Citrin, N. Fedorczak, X. Garbet, A. Loarte, F. Millitello, M. Romanelli, et al. L to h mode transition: on the role of zeff. *Nuclear Fusion*, 54(2):022001, 2014.
- [35] M. D. Boyer and J. Chadwick. Prediction of electron density and pressure profile shapes on nstx-u using neural networks. *Nuclear Fusion*, 61(4):046024, 2021.
- [36] S. Braginskii. Transport phenomena in a completely ionized two-temperature plasma. *Sov. Phys. JETP*, 6(33):358–369, 1958.
- [37] K. Brau, M. Bitter, R. J. Goldston, D. Manos, K. McGuire, and S. Suckewer. Plasma rotation in the pdx tokamak. *Nuclear fusion*, 23(12):1643, 1983.
- [38] A. J. Brizard and T. S. Hahm. Foundations of nonlinear gyrokinetic theory. *Rev. Mod. Phys.*, 79:421–468, Apr 2007.
- [39] D. Brunner, B. LaBombard, A. Kuang, and J. Terry. High-resolution heat flux width measurements at reactor-level magnetic fields and observation of a unified width scaling across confinement regimes in the alcator c-mod tokamak. *Nuclear Fusion*, 58(9):094002, 2018.
- [40] J. M. Burgers. A mathematical model illustrating the theory of turbulence. *Advances in applied mechanics*, 1:171–199, 1948.
- [41] R. Burhenn, Y. Feng, K. Ida, H. Maassberg, K. McCarthy, D. Kalinina, M. Kobayashi, S. Morita, Y. Nakamura, H. Nozato, et al. On impurity handling in high performance stellarator/heliotron plasmas. *Nuclear fusion*, 49(6):065005, 2009.
- [42] K. H. Burrell. Effects of ExB velocity shear and magnetic shear on turbulence and transport in magnetic confinement devices. *Physics of Plasmas*, 4(5), 1997.
- [43] K. H. Burrell, M. E. Austin, D. P. Brennan, J. C. DeBoo, E. J. Doyle, C. Fenzi, C. Fuchs, P. Gohil, C. M. Greenfield, R. J. Groebner, L. L. Lao, T. C. Luce, M. A. Makowski, G. R. McKee, R. A. Moyer, C. C. Petty, M. Porkolab, C. L. Rettig, T. L. Rhodes, J. C. Rost, B. W. Stallard, E. J. Strait, E. J. Synakowski, M. R. Wade, J. G. Watkins, and W. P. West. Quiescent double barrier high-confinement mode plasmas in the DIII-D tokamak. *Physics of Plasmas*, 8(5):2153–2162, 05 2001.
- [44] K. H. Burrell, K. Barada, X. Chen, A. M. Garofalo, R. J. Groebner, C. M. Muscatello, T. H. Osborne, C. C. Petty, T. L. Rhodes, P. B. Snyder, W. M. Solomon, Z. Yan, and L. Zeng. Discovery of stationary operation of quiescent h-mode plasmas with net-zero neutral beam injection torque and high energy confinement on diii-d. *Physics of Plasmas*, 23(5):056103, 03 2016.
- [45] K. H. Burrell, T. N. Carlstrom, E. J. Doyle, D. Finkenthal, P. Gohil, R. J. Groebner, D. L. Hillis, J. Kim, H. Matsumoto, R. A. Moyer, T. H. Osborne, C. L. Rettig, W. A. Peebles, T. L. Rhodes, H. StJohn, R. D. Stambaugh, M. R. Wade, and J. G.

- Watkins. Physics of the L-mode to H-mode transition in tokamaks. *Plasma Physics and Controlled Fusion*, 34(13):1859, 1992.
- [46] Y. Camenen, A. Pochelon, A. Bottino, S. Coda, F. Ryter, O. Sauter, R. Behn, T. P. Goodman, M. A. Henderson, A. Karpushov, L. Porte, and G. Zhuang. Electron heat transport in shaped tcv l-mode plasmas. *Plasma Physics and Controlled Fusion*, 47(11):1971, oct 2005.
  - [47] João Cândido and Rogério Jorge. Design of quasisymmetric fusion devices using novel machine learning methods. Master’s thesis, Instituto Superior Técnico, Universidade De Lisboa, 2023.
  - [48] J. Candy, E. Belli, and R. Bravenec. A high-accuracy eulerian gyrokinetic solver for collisional plasmas. *Journal of Computational Physics*, 324:73–93, 2016.
  - [49] J. Candy, C. Holland, R. E. Waltz, M. R. Fahey, and E. Belli. Tokamak profile prediction using direct gyrokinetic and neoclassical simulation. *Physics of Plasmas*, 16, 2009.
  - [50] J. Candy and R. Waltz. Anomalous transport scaling in the diii-d tokamak matched by supercomputer simulation. *Physical review letters*, 91(4):045001, 2003.
  - [51] J. Candy and R. Waltz. An eulerian gyrokinetic-maxwell solver. *Journal of Computational Physics*, 186(2):545–581, 2003.
  - [52] J. M. Canik, W. Guttenfelder, R. Maingi, T. H. Osborne, S. Kubota, Y. Ren, R. E. Bell, H. W. Kugel, B. P. Leblanc, and V. A. Souhkanovskii. Edge microstability of NSTX plasmas without and with lithium-coated plasma-facing components. *Nuclear Fusion*, 53(11), 2013.
  - [53] N. M. Cao and D. Qi. Nearly integrable flows and chaotic tangles in the dimits shift regime of plasma edge turbulence. *Physics of Plasmas*, 30(9), 2023.
  - [54] F. J. Casson, A. Peeters, Y. Camenen, W. Hornsby, A. Snodin, D. Strintzi, and G. Szepesi. Anomalous parallel momentum transport due to  $e \times b$  flow shear in a tokamak plasma. *Physics of Plasmas*, 16(9), 2009.
  - [55] P. J. Catto. Linearized gyro-kinetics. *Plasma Physics*, 20(7):719, 1978.
  - [56] P. J. Catto, M. N. Rosenbluth, and C. S. Liu. Parallel velocity shear instabilities in an inhomogeneous plasma with a sheared magnetic field. *The Physics of Fluids*, 16(10):1719, 1973.
  - [57] C. Chang, S. Ku, P. Diamond, Z. Lin, S. Parker, T. S. Hahm, and N. Samatova. Compressed ion temperature gradient turbulence in diverted tokamak edge. *Physics of Plasmas*, 16(5), 2009.
  - [58] A. Chankin and G. McCracken. Loss ion orbits at the tokamak edge. *Nuclear fusion*, 33(10):1459, 1993.
  - [59] I. Chapman, S. Sharapov, G. Huysmans, and A. Mikhailovskii. Modeling the effect of toroidal plasma rotation on drift-magnetohydrodynamic modes in tokamaks. *Physics of plasmas*, 13(6), 2006.

- [60] B. Chapman-Oplopoiou, D. Hatch, A. Field, L. Frassinetti, J. Hillesheim, L. Horvath, C. Maggi, J. Parisi, C. Roach, S. Saarelma, J. Walker, and J. Contributors. The role of etg modes in jet-ilw pedestals with varying levels of power and fuelling. *Nuclear Fusion*, 62(8):086028, jun 2022.
- [61] X. Chen, K. H. Burrell, T. H. Osborne, K. Barada, N. M. Ferraro, A. M. Garofalo, R. J. Groebner, G. R. McKee, C. C. Petty, M. Porkolab, T. L. Rhodes, J. C. Rost, P. B. Snyder, W. M. Solomon, and Z. Yan. Bifurcation of quiescent h-mode to a wide pedestal regime in diii-d and advances in the understanding of edge harmonic oscillations. *Nuclear Fusion*, 57, 2017.
- [62] M. Choi, J. Kim, J. Kwon, H. Park, Y. In, W. Lee, K. Lee, G. Yun, J. Lee, M. Kim, et al. Multiscale interaction between a large scale magnetic island and small scale turbulence. *Nuclear Fusion*, 57(12):126058, 2017.
- [63] J. Citrin, J. Garcia, T Görlner, F Jenko, P Mantica, D Told, C Bourdelle, DR Hatch, GMD Hogeweyj, Thomas Johnson, et al. Electromagnetic stabilization of tokamak microturbulence in a high- $\beta$  regime. *Plasma Physics and Controlled Fusion*, 57(1):014032, 2014.
- [64] J. Citrin, F. Jenko, P. Mantica, D. Told, C. Bourdelle, R. Dumont, J. Garcia, J. Haverkort, G. Hogeweyj, T. Johnson, et al. Ion temperature profile stiffness: non-linear gyrokinetic simulations and comparison with experiment. *Nuclear Fusion*, 54(2):023008, 2014.
- [65] C. F. Clauser, W. Guttenfelder, T. Rafiq, and E. Schuster. Linear ion-scale microstability analysis of high and low-collisionality nstx discharges and nstx-u projections. *Physics of Plasmas*, 29, 2022.
- [66] T. M. Collaboration, G. Rutherford, H. S. Wilson, A. Saltzman, D. Arnold, J. L. Ball, S. Benjamin, R. Bielajew, N. de Boucaud, M. Calvo-Carrera, R. Chandra, H. Choudhury, C. Cummings, L. Corsaro, N. DaSilva, R. Diab, A. R. Devitre, S. Ferry, S. J. Frank, C. J. Hansen, J. Jerkins, J. D. Johnson, P. Lunia, J. van de Lindt, S. Mackie, A. D. Maris, N. R. Mandell, M. A. Miller, T. Mouratidis, A. O. Nelson, M. Pharr, E. E. Peterson, P. Rodriguez-Fernandez, S. Segantin, M. Tobin, A. Velberg, A. M. Wang, M. Wigram, J. Witham, C. Paz-Soldan, and D. G. Whyte. Manta: a negative-triangularity nasem-compliant fusion pilot plant. *Plasma Physics and Controlled Fusion*, 66(10):105006, aug 2024.
- [67] G. J. Colyer, A. A. Schekochihin, F. I. Parra, C. M. Roach, M. A. Barnes, Y. C. Ghim, and W. Dorland. Collisionality scaling of the electron heat flux in ETG turbulence. *Plasma Physics and Controlled Fusion*, 2017.
- [68] S. Combs. Pellet injection technology. *Review of scientific instruments*, 64(7):1679–1698, 1993.
- [69] J. Connor. Transport in tokamaks: Theoretical models and comparison with experimental results. *Plasma Physics and Controlled Fusion*, 37(11A):A119, 1995.
- [70] J. W. Connor, S. C. Cowley, and R. J. Hastie. Micro-tearing stability in tokamaks. *Plasma Physics and Controlled Fusion*, 32(10):799, 1990.

- [71] J. W. Connor, R. J. Hastie, and J. B. Taylor. High mode number stability of an axisymmetric toroidal plasma. *Proc R Soc London Ser A*, 365(1720):3651–17, 1979.
- [72] J. W. Connor, R. J. Hastie, H. R. Wilson, and R. L. Miller. Magnetohydrodynamic stability of tokamak edge plasmas. *Physics of Plasmas*, 5(7):2687, 1998.
- [73] J. G. Cordey, K. Thomsen, A. Chudnovskiy, O. J. W. F. Kardaun, T. Takizuka, J. A. Snipes, M. Greenwald, L. Sugiyama, F. Ryter, A. Kus, J. Stober, J. C. DeBoo, C. C. Petty, G. Bracco, M. Romanelli, Z. Cui, Y. Liu, D. C. McDonald, A. Meakins, Y. Miura, K. Shinohara, K. Tsuzuki, Y. Kamada, H. Urano, M. Valovic, R. Akers, C. Brickley, A. Sykes, M. J. Walsh, S. M. Kaye, C. Bush, D. Hogewei, Y. Martin, A. Cote, G. Pacher, J. Ongena, F. Imbeaux, G. T. Hoang, S. Lebedev, and V. Leonov. Scaling of the energy confinement time with beta and collisionality approaching iter conditions. *Nuclear Fusion*, 45(9):1078, aug 2005.
- [74] P. Costello, J. Proll, G. Plunk, M. Pueschel, and JA Alcusó,n. The universal instability in optimised stellarators. *Journal of Plasma Physics*, 89(4):905890402, 2023.
- [75] A. Costley, J. Hugill, and P. Buxton. On the power and size of tokamak fusion pilot plants and reactors. *Nuclear Fusion*, 55(3):033001, 2015.
- [76] S. C. Cowley, R. M. Kulsrud, and R. Sudan. Considerations of ion temperature gradient driven turbulence. *Physics of Fluids B: Plasma Physics*, 3(10):2767, 1991.
- [77] A. J. Creely, M. J. Greenwald, S. B. Ballinger, D. Brunner, J. Canik, J. Doody, F. F. F. T. T. Garnier, R. Granetz, T. K. Gray, C. Holland, N. T. Howard, J. W. Hughes, J. H. Irby, V. A. Izzo, G. J. Kramer, A. Q. Kuang, B. LaBom-bard, Y. Lin, B. Lipschultz, N. C. Logan, J. D. Lore, E. S. Marmar, K. Montes, R. T. Mumgaard, C. Paz-Soldan, C. Rea, M. L. Reinke, P. Rodriguez-Fernandez, K. Särkimäki, F. Sciortino, S. D. Scott, A. Snicker, P. B. Snyder, B. N. Sorbom, R. Sweeney, R. A. Tinguely, E. A. Tolman, M. Umansky, O. Vallhagen, J. Varje, D. G. Whyte, J. C. Wright, S. J. Wukitch, and J. Zhu. Overview of the sparc tokamak. *Journal of Plasma Physics*, 86, 2020.
- [78] T. Dannert and F. Jenko. Gyrokinetic simulation of collisionless trapped-electron mode turbulence. *Physics of Plasmas*, 12(7):072309, 2005.
- [79] D. Darrow, S. Zweben, S. Batha, R. Budny, C. Bush, Z. Chang, C. Cheng, H. Duong, J. Fang, N. Fisch, et al. Alpha particle losses from tokamak fusion test reactor deuterium–tritium plasmas. *Physics of Plasmas*, 3(5):1875–1880, 1996.
- [80] A. W. Degeling, Y. R. Martin, J. B. Lister, L. Villard, V. N. Dokouka, V. E. Lukash, and R. R. Khayrutdinov. Magnetic triggering of elms in tcv. *Plasma Physics and Controlled Fusion*, 45(9):1637, aug 2003.
- [81] D. del Castillo-Negrete. Chaotic transport in zonal flows in analogous geophysical and plasma systems. *Physics of Plasmas*, 7(5):1702–1711, 2000.
- [82] B. Deng, C. Domier, N. Luhmann Jr, D. Brower, AJH Donné,, T Oyevaar, and MJ van de Pol. Electron cyclotron emission imaging diagnostic of the profiles and fluctuations. *Physics of Plasmas*, 8(5):2163–2169, 2001.

- [83] L. E. di Grazia, E. Fable, M. Mattei, M. Siccino, F. Maviglia, and H. Zohm. Burn control strategies using plasma elongation in demo. *Fusion Engineering and Design*, 215:114976, 2025.
- [84] A. Di Siena, T Görlner, H Doerk, E Poli, and R Bilato. Fast-ion stabilization of tokamak plasma turbulence. *Nuclear Fusion*, 58(5):054002, 2018.
- [85] A. Di Siena, A. B. Navarro, G. Luda, T. and Merlo, L. Bergmann, M. and Leppin, T. Görler, J. B. Parker, L. LoDestro, T. Dannert, et al. Global gyrokinetic simulations of asdex upgrade up to the transport timescale with gene-tango. *Nuclear Fusion*, 62(10):106025, 2022.
- [86] P. Diamond, C. McDevitt, Özgür D Gürcan, TS Hahm, WX Wang, ES Yoon, I Holod, Z Lin, Volker Naulin, and R Singh. Physics of non-diffusive turbulent transport of momentum and the origins of spontaneous rotation in tokamaks. *Nuclear Fusion*, 49(4):045002, 2009.
- [87] P. H. Diamond, S. Itoh, K. Itoh, and T. Hahm. Zonal flows in plasma—a review. *Plasma Physics and Controlled Fusion*, 47(5):R35, 2005.
- [88] D. Dickinson, C. M. Roach, S. Saarelma, R. Scannell, A. Kirk, and H. R. Wilson. Microtearing modes at the top of the pedestal. *Plasma Physics and Controlled Fusion*, 55(7):074006, 2013.
- [89] A. M. Dimits, G. Bateman, M. A. Beer, B. I. Cohen, W. Dorland, G. W. Hammett, C. Kim, J. E. Kinsey, M. Kotschenreuther, A. H. Kritz, L. L. Lao, J. Mandrekas, W. M. Nevins, S. E. Parker, A. J. Redd, D. E. Shumaker, R. Sydora, and J. Weiland. Comparisons and physics basis of tokamak transport models and turbulence simulations. *Physics of Plasmas*, 7(3):969, 2000.
- [90] H. Doerk, F. Jenko, T Görlner, D Told, MJ Pueschel, and DR Hatch. Gyrokinetic prediction of microtearing turbulence in standard tokamaks. *Physics of Plasmas*, 19(5), 2012.
- [91] H. Doerk, F. Jenko, M. Pueschel, and D. Hatch. Gyrokinetic microtearing turbulence. *Physical review letters*, 106(15):155003, 2011.
- [92] J. Dominski, W. Guttenfelder, D. Hatch, T. Goerler, F. Jenko, S. Munaretto, and S. Kaye. Global micro-tearing modes in the wide pedestal of an nstx plasma. *Physics of Plasmas*, 31(4), 2024.
- [93] W. Dorland, F. Jenko, M. Kotschenreuther, and B. N. Rogers. Electron temperature gradient turbulence. *Physical Review Letters*, 85(26):5579, 2000.
- [94] J. F. Drake, N. T. Gladd, C. S. Liu, and C. L. Chang. Microtearing modes and anomalous transport in tokamaks. *Physical Review Letters*, 44(15):994, 1980.
- [95] S. Dubbioso, G. De Tommasi, A. Mele, G. Tartaglione, M. Ariola, and A. Pironti. A deep reinforcement learning approach for vertical stabilization of tokamak plasmas. *Fusion Engineering and Design*, 194:113725, 2023.



- [96] G. Duesing, H. Altmann, H. Falter, A. Goede, R. Haange, R. Hemsworth, P. Kupschus, D. Stork, and E. Thompson. Neutral beam injection system. *Fusion Technology*, 11(1):163–202, 1987.
- [97] M. G. Dunne, M. Faitsch, L. Radovanović,, and E. Wolfrum. Quasi-continuous exhaust operational space. *Nuclear Fusion*, 2024.
- [98] R. Durst, R. Fonck, G. Cosby, H. Evensen, and S. Paul. Density fluctuation measurements via beam emission spectroscopy. *Review of scientific instruments*, 63(10):4907–4912, 1992.
- [99] R. Dux and A. Peeters. Neoclassical impurity transport in the core of an ignited tokamak plasma. *Nuclear fusion*, 40(10):1721, 2000.
- [100] M. Eder, C. Albert, L. Bauer, S. Kasilov, and W. Kernbichler. Quasi-geometric integration of guiding-center orbits in piecewise linear toroidal fields. *Physics of Plasmas*, 27(12), 2020.
- [101] M. Eder, D. Forstenlechner, Georg S Graßler, Sergei V Kasilov, Winfried Kernbichler, Markus Meisterhofer, Michael Scheidt, Christopher G Albert, et al. Gorilla: Guiding-center orbit integration with local linearization approach. *Journal of Open Source Software*, 8(86):4890, 2023.
- [102] T. Eich, A. Leonard, R. Pitts, W. Fundamenski, R. J. Goldston, T. Gray, A. Herrmann, A. Kirk, A. Kallenbach, O. Kardaun, et al. Scaling of the tokamak near the scrape-off layer h-mode power width and implications for iter. *Nuclear fusion*, 53(9):093031, 2013.
- [103] L. A. El-Guebaly and S. Malang. Toward the ultimate goal of tritium self-sufficiency: Technical issues and requirements imposed on aries advanced power plants. *Fusion Engineering and Design*, 84, 2009.
- [104] D. Eldon, L. Casali, I. Bykov, C. Chrystal, K. Erickson, A. Hyatt, A. Leonard, A. Moser, A. Nelson, T Odstrčil, et al. Characterization and controllability of radiated power via extrinsic impurity seeding in strongly negative triangularity plasmas in diiii-d. *Plasma Physics and Controlled Fusion*, 67(1):015018, 2024.
- [105] D. R. Ernst, P. T. Bonoli, P. J. Catto, W. Dorland, C. L. Fiore, R. S. Granetz, M. Greenwald, A. E. Hubbard, M. Porkolab, M. H. Redi, J. E. Rice, and K. Zhurovich. Role of trapped electron mode turbulence in internal transport barrier control in the Alcator C-Mod Tokamak. *Physics of Plasmas*, 11:2637, 2004.
- [106] D. R. Ernst, A. Bortolon, C. S. Chang, S. Ku, F. Scotti, H. Q. Wang, Z. Yan, J. Chen, C. Chrystal, F. Glass, S. Haskey, R. Hood, F. Khabanov, F. Laggner, C. Lasnier, G. R. McKee, T. L. Rhodes, D. Truong, and J. Watkins. Broadening of the divertor heat flux profile in high confinement tokamak fusion plasmas with edge pedestals limited by turbulence in diiii-d. *Phys. Rev. Lett.*, 132:235102, Jun 2024.
- [107] T. E. Evans, R. A. Moyer, P. R. Thomas, J. G. Watkins, T. H. Osborne, J. A. Boedo, E. J. Doyle, M. E. Fenstermacher, K. H. Finken, R. J. Groebner, M. Groth, J. H. Harris, R. J. La Haye, C. J. Lasnier, S. Masuzaki, N. Ohyabu, D. G. Pretty,

- T. L. Rhodes, H. Reimerdes, D. L. Rudakov, M. J. Schaffer, G. Wang, and L. Zeng. Suppression of large edge-localized modes in high-confinement dIII-d plasmas with a stochastic magnetic boundary. *Phys. Rev. Lett.*, 92:235003, Jun 2004.
- [108] H. T. Evensen, R. J. Fonck, S. F. Paul, G. Rewoldt, S. D. Scott, W. M. Tang, and M. C. Zarnstorff. Measurements of ion temperature fluctuations in the tokamak fusion test reactor. *Nuclear Fusion*, 38(2), 1998.
- [109] E. Fable, A. Kallenbach, R. M. McDermott, M. Bernert, C. Angioni, and T. A. U. Team. High-confinement radiative l-modes in asdex upgrade. *Nuclear Fusion*, 62(2):024001, dec 2021.
- [110] V. N. Faddeeva and N. Terent'ev. *Tables of Values of the Function  $w(z) = \exp(-z^2)(1+2i/\sqrt{\pi} \int_0^z \exp(t^2)dt)$  for Complex Argument*. English Translation: New York Pergamon Press, 1961, 1954.
- [111] M. Faitsch, T. Eich, G. Harrer, E. Wolfrum, D. Brida, P. David, M. Griener, U. Stroth, A. U. Team, E. M. Team, et al. Broadening of the power fall-off length in a high density, high confinement h-mode regime in asdex upgrade. *Nuclear Materials and Energy*, 26:100890, 2021.
- [112] M. Faitsch, T. Eich, G.F. Harrer, E. Wolfrum, D. Brida, P. David, M. Dunne, L. Gil, B. Labit, U. Stroth, et al. Analysis and expansion of the quasi-continuous exhaust (qce) regime in asdex upgrade. *Nuclear Fusion*, 63(7):076013, 2023.
- [113] A. Fasoli. Essay: Overcoming the obstacles to a magnetic fusion power plant. *Physical Review Letters*, 130(22):220001, 2023.
- [114] G. Federici, C. Bachmann, L. Barucca, C. Baylard, W. Biel, L. Boccaccini, C. Bustrero, S. Ciattaglia, F. Cismonti, V. Corato, C. Day, E. Diegele, T. Franke, E. Gaio, C. Gliss, T. Haertl, A. Ibarra, J. Holden, G. Keech, R. Kembleton, A. Loving, F. Maviglia, J. Morris, B. Meszaros, I. Moscato, G. Pintsuk, M. Siccini, N. Taylor, M. Tran, C. Vorpahl, H. Walden, and J. You. Overview of the demo staged design approach in europe. *Nuclear Fusion*, 59(6):066013, apr 2019.
- [115] F. Felici et al. Real-time physics-model-based simulation of the current density profile in tokamak plasmas. *Nuclear Fusion*, 51(8):083052, 2011.
- [116] A. Field, D. Dunai, R. Gaffka, Y. Ghim, I. Kiss, B. Meszaros, T. Krizsanoczi, S. Shibaev, and S. Zoletnik. Beam emission spectroscopy turbulence imaging system for the mst spherical tokamak. *Review of Scientific Instruments*, 83(1), 2012.
- [117] S. Freethy, G. Conway, I. Classen, A. Creely, T. Happel, A. Köhn, B. Vanovac, and AE White. Measurement of turbulent electron temperature fluctuations on the asdex upgrade tokamak using correlated electron cyclotron emission. *Review of Scientific Instruments*, 87(11), 2016.
- [118] E. A. Frieman and L. Chen. Nonlinear gyrokinetic equations for low-frequency electromagnetic waves in general plasma equilibria. *The Physics of Fluids*, 25(3):502, 1982.
- [119] U. Frisch and A. N. Kolmogorov. *Turbulence: the legacy of AN Kolmogorov*. Cambridge university press, 1995.

- [120] A. Fujisawa, T. Ido, A. Shimizu, S. Okamura, K. Matsuoka, H. Iguchi, Y. Hamada, H. Nakano, S. Ohshima, K. Itoh, et al. Experimental progress on zonal flow physics in toroidal plasmas. *Nuclear fusion*, 47(10):S718, 2007.
- [121] W. Fundamenski, O. E. Garcia, V. Naulin, R. A. Pitts, A. H. Nielsen, J. Juul Rasmussen, J. Horacek, J. P. Graves, and J. E. contributors. Dissipative processes in interchange driven scrape-off layer turbulence. *Nuclear Fusion*, 47(5):417, apr 2007.
- [122] H. Furth, R. J. Goldston, S. Zweben, and D. Sigmar. Burning plasmas. *Nuclear fusion*, 30(9):1799, 1990.
- [123] X. Garbet, P. Mantica, C. Angioni, E. Asp, Y. Baranov, C. Bourdelle, R. Budny, F. Crisanti, G. Cordey, L. Garzotti, N. Kirneva, D. Hogeweyj, T. Hoang, F. Imbeaux, E. Joffrin, X. Litaudon, A. Manini, D. C. McDonald, H. Nordman, V. Parail, A. Peeters, F. Ryter, C. Sozzi, M. Valovic, T. Tala, A. Thyagaraja, I. Voitskhovitch, J. Weiland, H. Weisen, and A. Zabolotsky. Physics of transport in tokamaks. *Plasma Physics and Controlled Fusion*, 46(12B):B557, 2004.
- [124] X. Garbet, P. Mantica, F. Ryter, G. Cordey, F. Imbeaux, C. Sozzi, A. Manini, E. Asp, V. Parail, R. Wolf, et al. Profile stiffness and global confinement. *Plasma physics and controlled fusion*, 46(9):1351, 2004.
- [125] J. Garcia and J. Contributors. Electromagnetic and fast ions effects as a key mechanism for turbulent transport suppression at jet. *Plasma Physics and Controlled Fusion*, 64(10):104002, 2022.
- [126] A. Garofalo, W. Solomon, J. Park, K. Burrell, J. DeBoo, M. Lanctot, G. McKee, H. Reimerdes, L. Schmitz, M. Schaffer, and P. Snyder. Advances towards qh-mode viability for elm-stable operation in iter. *Nuclear Fusion*, 51(8):083018, jul 2011.
- [127] S. Gerhardt, J. Canik, R. Maingi, D. Battaglia, R. Bell, W. Guttenfelder, B. LeBlanc, D. Smith, H. Yuh, and S. Sabbagh. Progress in understanding the enhanced pedestal h-mode in nstx. *Nuclear Fusion*, 54(8):083021, jun 2014.
- [128] M. Giacomini, D. Dickinson, W. Dorland, N. Mandell, A. Bokshi, F. Casson, H. Dudding, D. Kennedy, B. Patel, and C. Roach. A quasi-linear model of electromagnetic turbulent transport and its application to flux-driven transport predictions for step. *Journal of Plasma Physics*, 91(1):E16, 2025.
- [129] L. Giannone, J. Baldzuhn, R. Burhenn, P. Grigull, U. Stroth, F. Wagner, R. Brakel, C. Fuchs, H. Hartfuss, K. McCormick, et al. Physics of the density limit in the w7-as stellarator. *Plasma physics and controlled fusion*, 42(6):603, 2000.
- [130] L. Gil, C. Silva, T. Happel, G. Birkenmeier, G. Conway, L. Guimaraes, A. Kallenbach, P. T. Tterich, J. Santos, P.A. Schneider, M. Schubert, E. Seliunin, A. Silva, J. Stober, U. Stroth, E. Trier, E. Wolfrum, the ASDEX Upgrade team, and the EUROfusion MST1 team. Stationary elm-free h-mode in asdex upgrade. *Nuclear Fusion*, 60(5):054003, apr 2020.
- [131] N. Gladd, J. Drake, C. Chang, and C. Liu. Electron temperature gradient driven microtearing mode. *The Physics of Fluids*, 23(6):1182–1192, 1980.

- [132] T. Goerler, X. Lapillonne, S. Brunner, T. Dannert, F. Jenko, F. Merz, and D. Told. The global version of the gyrokinetic turbulence code gene. *Journal of Computational Physics*, 230(18):7053–7071, 2011.
- [133] R. J. Goldston. Energy confinement scaling in tokamaks: some implications of recent experiments with ohmic and strong auxiliary heating. *Plasma Physics and Controlled Fusion*, 26:87–103, 1 1984.
- [134] N. N. Gorelenkov, S. Pinches, and K. Toi. Energetic particle physics in fusion research in preparation for burning plasma experiments. *Nuclear Fusion*, 54(12):125001, 2014.
- [135] V. Grandgirard, Y. Sarazin, P. Angelino, A. Bottino, N. Crouseilles, G. Darmet, G. Dif-Pradalier, X. Garbet, P. Ghendrih, S. Jolliet, et al. Global full-f gyrokinetic simulations of plasma turbulence. *Plasma Physics and Controlled Fusion*, 49(12B):B173, 2007.
- [136] R. Greaves, J. Chen, and A. Sen. Experimental study of an ion-temperature-gradient driven instability in a linear machine. *Plasma physics and controlled fusion*, 34(7):1253, 1992.
- [137] B. Green et al. Iter: burning plasma physics experiment. *Plasma physics and controlled fusion*, 45(5):687, 2003.
- [138] M. Greenwald, J. Schachter, W. Dorland, R. Granetz, A. Hubbard, J. Rice, J. Snipes, P. Stek, and S. Wolfe. Transport phenomena in alcator c-mod h-modes. *Plasma physics and controlled fusion*, 40(5):789, 1998.
- [139] M. Greenwald, J. L. Terry, S. M. Wolfe, S. Ejima, M. G. Bell, S. M. Kaye, and G. H. Neilson. A new look at density limits in tokamaks. *Nuclear Fusion*, 28(12):2199, 1988.
- [140] L. Guazzotto, R. Betti, J. Manickam, and S. Kaye. Numerical study of tokamak equilibria with arbitrary flow. *Physics of Plasmas*, 11(2):604–614, 2004.
- [141] W. Guttenfelder, J. Candy, S. M. Kaye, W. M. Nevins, E. Wang, R. E. Bell, G. W. Hammett, B. P. Leblanc, D. R. Mikkelsen, and H. Yuh. Electromagnetic transport from microtearing mode turbulence. *Physical Review Letters*, 106(15):155004, 2011.
- [142] T. Hahm and W. Tang. Weak turbulence theory of collisionless trapped electron driven drift instability in tokamaks. *Physics of Fluids B: Plasma Physics*, 3(4):989–999, 1991.
- [143] T. S. Hahm and K. H. Burrell. Flow shear induced fluctuation suppression in finite aspect ratio shaped tokamak plasma. *Physics of Plasmas*, 2(5):1648, 1995.
- [144] A. H. Hakim, N. R. Mandell, T. Bernard, M. Francisquez, G. Hammett, and E. Shi. Continuum electromagnetic gyrokinetic simulations of turbulence in the tokamak scrape-off layer and laboratory devices. *Physics of Plasmas*, 27(4), 2020.
- [145] V. H. Hall-Chen, F. I. Parra, and J. C. Hillesheim. Beam model of doppler backscattering. *Plasma Physics and Controlled Fusion*, 64(9):095002, 2022.

- [146] A. Hallenbert and G. G. Plunk. Predicting the dimits shift through reduced mode tertiary instability analysis in a strongly driven gyrokinetic fluid limit. *Journal of Plasma Physics*, 87(5):905870508, 2021.
- [147] G. W. Hammett and F. I. Parra. Turbulence and nonlinear processes in fluids and plasmas (lecture notes forthcoming). 2025.
- [148] G. W. Hammett and F. W. Perkins. Fluid moment models for landau damping with application to the ion-temperature-gradient instability. *Physical Review Letters*, 64, 1990.
- [149] C. Hansen, I. Stewart, D. Burgess, M. Pharr, S. Guizzo, F. Logak, A. Nelson, and C. Paz-Soldan. Tokamaker: An open-source time-dependent grad-shafranov tool for the design and modeling of axisymmetric fusion devices. *Computer Physics Communications*, 298:109111, 2024.
- [150] M. R. Hardman, M. Barnes, C. M. Roach, and F. I. Parra. A scale-separated approach for studying coupled ion and electron scale turbulence. *Plasma Physics and Controlled Fusion*, 61(6):065025, 2019.
- [151] M. R. Hardman, F. I. Parra, C. Chong, T. Adkins, M. S. Anastopoulos-Tzanis, M. Barnes, D. Dickinson, J. F. Parisi, and H. Wilson. Extended electron tails in electrostatic microinstabilities and the nonadiabatic response of passing electrons. *Plasma Physics and Controlled Fusion*, 64, 2022.
- [152] M. R. Hardman, F. I. Parra, B. S. Patel, C. M. Roach, J. R. Ruiz, M. Barnes, D. Dickinson, W. Dorland, J. F. Parisi, D. St-Onge, and H. Wilson. New linear stability parameter to describe low-beta electromagnetic microinstabilities driven by passing electrons in axisymmetric toroidal geometry. *Plasma Physics and Controlled Fusion*, 65(4):045011, 2023.
- [153] G. F. Harrer, M. Faitsch, L. Radovanovic, E. Wolfrum, C. Albert, A. Cathey, M. Cavedon, M. Dunne, T. Eich, R. Fischer, M. Griener, M. Hoelzl, B. Labit, H. Meyer, F. Aumayr, T. A. U. Team, and T. E. M. Team. Quasicontinuous exhaust scenario for a fusion reactor: The renaissance of small edge localized modes. *Phys. Rev. Lett.*, 129:165001, Oct 2022.
- [154] M Häse, M Hirsch, and HJ Hartfuss. Temperature fluctuations and their correlation with density fluctuations in w7-as. *Review of scientific instruments*, 70(1):1014–1017, 1999.
- [155] E. Hassan, D. Hatch, M. Halfmoon, M. Curie, M. Kotchenreuther, S. Mahajan, G. Merlo, R. Groebner, A. Nelson, and A. Diallo. Identifying the microtearing modes in the pedestal of diii-d h-modes using gyrokinetic simulations. *Nuclear Fusion*, 62(2):026008, 2021.
- [156] D. Hatch, M. Kotschenreuther, P. Li, B. Chapman-Oplopoiou, J. Parisi, S. Mahajan, and R. Groebner. Modeling electron temperature profiles in the pedestal with simple formulas for etg transport. *Nuclear Fusion*, 64(6):066007, apr 2024.
- [157] D. R. Hatch, M. Kotschenreuther, S. Mahajan, P. Valanju, F. Jenko, D. Told, T. Görler, and S. Saarelma. Microtearing turbulence limiting the JET-ILW pedestal. *Nuclear Fusion*, 56(10):104003, 2016.

- [158] D. R. Hatch, M. Kotschenreuther, S. M. Mahajan, G. Merlo, A. R. Field, C. Giroud, and J. Hillesheim. Direct Gyrokinetic Comparison of Pedestal Transport in JET with Carbon and ITER-Like Walls. *Nuclear Fusion*, 59(8):086056, 2019.
- [159] D. R. Hatch, M. Kotschenreuther, S. M. Mahajan, M. J. Pueschel, C. Michoski, G. Merlo, E. Hassan, A. R. Field, L. Frassinetti, C. Giroud, J. C. Hillesheim, C. F. Maggi, C. Perez Von Thun, C. M. Roach, S. Saarelma, D. Jarema, and F. Jenko. Microtearing modes as the source of magnetic fluctuations in the JET pedestal. *Nuclear Fusion*, 61(3):036015, 2021.
- [160] D. R. Hatch, D. Told, F. Jenko, H. Doerk, M. G. Dunne, E. Wolfrum, E. Viezzer, and M. J. Pueschel. Gyrokinetic study of ASDEX Upgrade inter-ELM pedestal profile evolution. *Nuclear Fusion*, 55(6):063028, 2015.
- [161] R. Hawryluk, S. Suckewer, and S. Hirshman. Low-z impurity transport in tokamaks. *Nuclear Fusion*, 19(5):607, 1979.
- [162] R. J. Hawryluk and H. Zohm. The challenge and promise of studying burning plasmas. *Physics Today*, 72(12):34–40, 2019.
- [163] W. Heidbrink. Alpha particle physics in a tokamak burning plasma experiment. *Physics of Plasmas*, 9(5):2113–2119, 2002.
- [164] W. Heidbrink. Basic physics of alfvén instabilities driven by energetic particles in toroidally confined plasmas. *Physics of Plasmas*, 15(5), 2008.
- [165] J. A. Heikkinen, S. J. Janhunen, T. P. Kiviniemi, and F. Ogando. Full f gyrokinetic method for particle simulation of tokamak transport. *Journal of Computational Physics*, 227(11):5582–5609, 2008.
- [166] P. Helander, S. L. Newton, Albert Mollén, and Håkan M Smith. Impurity transport in a mixed-collisionality stellarator plasma. *Physical review letters*, 118(15):155002, 2017.
- [167] P. Helander and G. Plunk. The universal instability in general geometry. *Physics of Plasmas*, 22(9), 2015.
- [168] P. Helander and D. J. Sigmar. *Collisional transport in magnetized plasmas*. Cambridge University Press, 2002.
- [169] R. Hemsworth and D. Boilson. Considerations for the development of neutral beam injection for fusion reactors or demo. In *AIP Conference Proceedings*, volume 1869. AIP Publishing, 2017.
- [170] T. C. Hender, J. C. Wesley, J. Bialek, A. Bondeson, A. H. Boozer, R. J. Buttery, A. Garofalo, T. P. Goodman, R. S. Granetz, Y. Gribov, O. Gruber, M. Gryaznevich, G. Giruzzi, S. Günter, N. Hayashi, P. Helander, C. C. Hegna, D. F. Howell, D. A. Humphreys, G. T.A. Huysmans, A. W. Hyatt, A. Isayama, S. C. Jardin, Y. Kawano, A. Kellman, C. Kessel, H. R. Koslowski, R. J. La Haye, E. Lazzaro, Y. Q. Liu, V. Lukash, J. Manickam, S. Medvedev, V. Mertens, S. V. Mirnov, Y. Nakamura, G. Navratil, M. Okabayashi, T. Ozeki, R. Paccagnella, G. Pautasso, F. Porcelli, V. D. Pustovitov, V. Riccardo, M. Sato, O. Sauter, M. J. Schaffer, M. Shimada,

- P. Sonato, E. J. Strait, M. Sugihara, M. Takechi, A. D. Turnbull, E. Westerhof, D. G. Whyte, R. Yoshino, and H. Zohm. Chapter 3: MHD stability, operational limits and disruptions. *Nuclear Fusion*, 47(6):S128, 2007.
- [171] P. Hennequin, C Honoré, A Truc, A Quéméneur, C Fenzi-Bonizec, C Bourdelle, X Garbet, GT Hoang, Tore Supra team, et al. Fluctuation spectra and velocity profile from doppler backscattering on tore supra. *Nuclear fusion*, 46(9):S771, 2006.
- [172] M. F. Heyn, I. B. Ivanov, S. V. Kasilov, W. Kernbichler, P. Leitner, V. V. Nemov, W. Suttrop, A. U. Team, et al. Quasilinear modelling of rmp interaction with a tokamak plasma: application to asdex upgrade elm mitigation experiments. *Nuclear Fusion*, 54(6):064005, 2014.
- [173] J. Hillesheim, N. Crocker, W. Peebles, H. Meyer, A. Meakins, A. Field, D. Dunai, M. Carr, N. Hawkes, M. Team, et al. Doppler backscattering for spherical tokamaks and measurement of high-k density fluctuation wavenumber spectrum in mast. *Nuclear Fusion*, 55(7):073024, 2015.
- [174] J. Hillesheim, J. DeBoo, W. Peebles, T. Carter, G. Wang, T. Rhodes, L. Schmitz, G. McKee, Z. Yan, G. Staebler, et al. Experimental characterization of multiscale and multifield turbulence as a critical gradient threshold is surpassed in the diii-d tokamak. *Physics of Plasmas*, 20(5), 2013.
- [175] J. Hillesheim, J. DeBoo, W. Peebles, T. Carter, G. Wang, T. Rhodes, L. Schmitz, G. McKee, Z. Yan, G. Staebler, et al. Observation of a critical gradient threshold for electron temperature fluctuations in the diii-d tokamak. *Physical Review Letters*, 110(4):045003, 2013.
- [176] J. Hillesheim, E. Delabie, H. Meyer, C. Maggi, L. Meneses, E. Poli, J. Contributors, and J. C. S. C. A. O. O. 3. U. K. EUROfusion Consortium. Stationary zonal flows during the formation of the edge transport barrier in the jet tokamak. *Physical review letters*, 116(6):065002, 2016.
- [177] S. Hirshman and D. Sigmar. Neoclassical transport of impurities in tokamak plasmas. *Nuclear Fusion*, 21(9):1079, 1981.
- [178] S. P. Hirshman and J. C. Whitson. Steepest-descent moment method for three-dimensional magnetohydrodynamic equilibria. *The Physics of Fluids*, 26(12):3553–3568, 12 1983.
- [179] G. T. Hoang, C. Bourdelle, X. Garbet, G. Giruzzi, T. Aniel, M. Ottaviani, W. Horton, P. Zhu, and R. V. Budny. Experimental determination of critical threshold in electron transport on tore supra. *Phys. Rev. Lett.*, 87:125001, 2001.
- [180] A. C. D. Hoffmann, B. J. Frei, and P. Ricci. Gyrokinetic moment-based simulations of the dimits shift. *Journal of Plasma Physics*, 89(6):905890611, 2023.
- [181] C. Holland, J. Kinsey, J. DeBoo, K. Burrell, T. Luce, S. Smith, C. Petty, A. White, T. Rhodes, L. Schmitz, et al. Validation studies of gyrofluid and gyrokinetic predictions of transport and turbulence stiffness using the diii-d tokamak. *Nuclear Fusion*, 53(8):083027, 2013.

- [182] C. Holland, T. C. Luce, B. A. Grierson, S. P. Smith, A. Marinoni, K. H. Burrell, C. Petty, and E. Bass. Examination of stiff ion temperature gradient mode physics in simulations of diii-d h-mode transport. *Nuclear Fusion*, 61(6):066033, 2021.
- [183] C. Hopf, G. Starnella, N. Den Harder, and U. Fantz. Neutral beam injection for fusion reactors: technological constraints versus functional requirements. *Nuclear Fusion*, 61(10):106032, 2021.
- [184] W. Horton. Drift waves and transport. *Reviews of Modern Physics*, 71(3):735, 1999.
- [185] W. Horton. *Turbulent transport in magnetized plasmas*. World Scientific, 2012.
- [186] S. Houshmandyar, K. Burrell, B. Grierson, J. McClenaghan, G. Staebler, C. Chrystal, M. Halfmoon, D. Hatch, L. Zeng, and M. Austin. Explaining the lack of power degradation of energy confinement in wide pedestal quiescent h-modes via transport modeling. *Nuclear Fusion*, 62(5):056024, 2022.
- [187] N. Howard, C. Holland, A. White, M. Greenwald, and J. Candy. Synergistic cross-scale coupling of turbulence in a tokamak plasma. *Physics of Plasmas*, 21(11), 2014.
- [188] N. Howard, A. White, M. Greenwald, C. Holland, J. Candy, and J. Rice. Impurity transport, turbulence transitions and intrinsic rotation in alcator c-mod plasmas. *Plasma Physics and Controlled Fusion*, 56(12):124004, 2014.
- [189] N. T. Howard, C. Holland, A. E. White, M. Greenwald, and J. Candy. Multi-scale gyrokinetic simulation of tokamak plasmas: Enhanced heat loss due to cross-scale coupling of plasma turbulence. *Nuclear Fusion*, 56(1):014004, 2016.
- [190] G. G. Howes, S. C. Cowley, W. Dorland, G. W. Hammett, E. Quataert, and A. A. Schekochihin. Astrophysical gyrokinetics: Basic equations and linear theory. *The Astrophysical Journal*, 651(1):590, 2006.
- [191] A. Hubbard, S. Baek, D. Brunner, A. Creely, I. Cziegler, E. Edlund, J. Hughes, B. LaBombard, Y. Lin, Z. Liu, E. Marmor, M. Reinke, J. Rice, B. Sorbom, C. Sung, J. Terry, C. Theiler, E. Tolman, J. Walk, A. White, D. Whyte, S. Wolfe, S. Wukitch, X. Xu, and T. A. C. team. Physics and performance of the i-mode regime over an expanded operating space on alcator c-mod. *Nuclear Fusion*, 57(12):126039, oct 2017.
- [192] A. E. Hubbard, R. L. Boivin, R. S. Granetz, M. Greenwald, J. W. Hughes, I. H. Hutchinson, J. Irby, B. LaBombard, Y. Lin, E. S. Marmor, et al. Pedestal profiles and fluctuations in c-mod enhanced d-alpha h-modes. *Physics of Plasmas*, 8(5):2033–2040, 2001.
- [193] J. W. Hughes, N. T. Howard, P. Rodriguez-Fernandez, A. J. Creely, A. Q. Kuang, P. B. Snyder, T. M. Wilks, R. Sweeney, and M. Greenwald. Projections of H-mode access and edge pedestal in the SPARC tokamak. *Journal of Plasma Physics*, 86, 2020.
- [194] K. Ida and J. Rice. Rotation and momentum transport in tokamaks and helical systems. *Nuclear Fusion*, 54(4):045001, 2014.



- [195] Y. Idomura, H. Urano, N. Aiba, and S. Tokuda. Study of ion turbulent transport and profile formations using global gyrokinetic full-f vlasov simulation. *Nuclear Fusion*, 49(6):065029, 2009.
- [196] K. Ikeda. Progress in the iter physics basis. *Nuclear Fusion*, 47(6):E01, 2007.
- [197] A. Ishizawa, K. Imadera, Y. Nakamura, and Y. Kishimoto. Global gyrokinetic simulation of turbulence driven by kinetic ballooning mode. *Physics of Plasmas*, 26(8), 2019.
- [198] K. Itoh, S. Itoh, P. Diamond, T. Hahm, A. Fujisawa, G. Tynan, M. Yagi, and Y. Nagashima. Physics of zonal flows. *Physics of plasmas*, 13(5), 2006.
- [199] P. Ivanov, P. Luhadiya, T. Adkins, and A. Schekochihin. The gyrokinetic field invariant and electromagnetic temperature-gradient instabilities in good-curvature plasmas. *arXiv preprint arXiv:2501.11764*, 2025.
- [200] P. G. Ivanov and T. Adkins. An analytical form of the dispersion function for local linear gyrokinetics in a curved magnetic field. *Journal of Plasma Physics*, 89(2):905890213, 2023.
- [201] P. G. Ivanov, A. A. Schekochihin, and W. Dorland. Dimits transition in three-dimensional ion-temperature-gradient turbulence. *Journal of Plasma Physics*, 88(5):905880506, 2022.
- [202] G. L. Jackson, V. S. Chan, and R. D. Stambaugh. An analytic expression for the tritium burnup fraction in burning-plasma devices. *Fusion Science and Technology*, 64, 2013.
- [203] S. Jardin, C. Bathke, D. Ehst, S. Kaye, C. Kessel, B. Lee, T. Mau, J. Menard, R. Miller, and F. Najmabadi. Physics basis for a tokamak fusion power plant. *Fusion Engineering and Design*, 48(3):281–298, 2000.
- [204] F. Jenko, W. Dorland, and G. W. Hammett. Critical gradient formula for toroidal electron temperature gradient modes. *Physics of Plasmas*, 8(9):4096, 2001.
- [205] F. Jenko, W. Dorland, M. Kotschenreuther, and B. N. Rogers. Electron temperature gradient driven turbulence. *Physics of Plasmas*, 7(5):1904, 2000.
- [206] R. V. Jensen, D. Post, W. Grasberger, C. Tarter, and W. Lokke. Calculations of impurity radiation and its effects on tokamak experiments. *Nuclear Fusion*, 17(6):1187, 1977.
- [207] X. Jian, J. Chen, S. Ding, A. Garofalo, X. Gong, C. Holland, J. Huang, V. Chan, X. Qin, G. Yu, et al. Experimental validation of a kinetic ballooning mode in high-performance high-bootstrap current fraction fusion plasmas. *Physical Review Letters*, 131(14):145101, 2023.
- [208] X. Jian, C. Holland, J. Candy, E. Belli, V. Chan, A. M. Garofalo, and S. Ding. Role of microtearing turbulence in dIII-d high bootstrap current fraction plasmas. *Physical review letters*, 123(22):225002, 2019.

- [209] J. Jung. Tritium inventories and associated tritium-breeding requirement for fusion power reactors. *Transactions of the American Nuclear Society*, 46, 1984.
- [210] A. Kallenbach, M. Bernert, T. Eich, J. Fuchs, L. Giannone, A. Herrmann, J. Schweinzer, W. Treutterer, A. U. Team, et al. Optimized tokamak power exhaust with double radiative feedback in asdex upgrade. *Nuclear Fusion*, 52(12):122003, 2012.
- [211] J. Kates-Harbeck, A. Svyatkovskiy, and W. Tang. Predicting disruptive instabilities in controlled fusion plasmas through deep learning. *Nature*, 568(7753):526–531, 2019.
- [212] S. Kaye and R. Goldston. Global energy confinement scaling for neutral-beam-heated tokamaks. *Nuclear Fusion*, 25:65–69, 1 1985.
- [213] S. Kaye, M. Greenwald, U. Stroth, O. Kardaun, A. Kus, D. Schissel, J. DeBoo, G. Bracco, K. Thomsen, J. Cordey, et al. Iter l mode confinement database. *Nuclear Fusion*, 37(9):1303, 1997.
- [214] M. Keilhacker, A. Gibson, C. Gormezano, P. J. Lomas, P. R. Thomas, M. L. Watkins, P. Andrew, B. Balet, D. Borba, C. D. Challis, I. Coffey, G. A. Cottrell, H. P. L. D. Esch, N. Deliyannis, A. Fasoli, C. W. Gowers, H. Y. Guo, G. T. A. Huysmans, T. T. C. Jones, W. Kerner, R.W.T König, M.J Loughlin, A Maas, F.B Marcus, M.F.F Nave, F.G Rimini, G.J Sadler, S.E Sharapov, G Sips, P Smeulders, F.X Söldner, A Taroni, B.J.D Tubbing, M.G. von Hellermann, D.J Ward, and JET Team. High fusion performance from deuterium-tritium plasmas in JET. *Nuclear Fusion*, 39(2):209, 1999.
- [215] D. Kennedy, M. Giacomini, F. Casson, D. Dickinson, W. Hornsby, B. Patel, and C. Roach. Electromagnetic gyrokinetic instabilities in step. *Nuclear Fusion*, 63(12):126061, 11 2023.
- [216] M. Kikuchi, T. Takizuka, S. Medvedev, T. Ando, D. Chen, J. X. Li, M. Austin, O. Sauter, L. Villard, A. Merle, et al. L-mode-edge negative triangularity tokamak reactor. *Nuclear Fusion*, 59(5):056017, 2019.
- [217] P. Kim, S. Buller, R. Conlin, W. Dorland, D. W. Dudt, R. Gaur, R. Jorge, E. Kolen, M. Landreman, N. R. Mandell, et al. Optimization of nonlinear turbulence in stellarators. *Journal of Plasma Physics*, 90(2):905900210, 2024.
- [218] J. E. Kinsey, R. E. Waltz, and J. Candy. Nonlinear gyrokinetic turbulence simulations of  $E \times B$  shear quenching of transport. *Physics of Plasmas*, 12(6), 2005.
- [219] V. Kiptily, C. Challis, R. Dumont, M. Fitzgerald, J. Garcia, L. Garzotti, Z. Ghani, J. Hobirk, P. Jacquet, A. Kappatou, et al. Observation of alpha-particles in recent d-t experiments on jet. *Nuclear Fusion*, 64(8):086059, 2024.
- [220] V. G. Kiptily, R. Dumont, M. Fitzgerald, D. Keeling, S. E. Sharapov, M. Poradzinski, et al. Evidence of electron heating by alpha particles in jet deuterium-tritium plasmas. *Physical Review Letters*, 131(7):075101, 2023.

- [221] A. Kirk, E. Nardon, R. Akers, Bé, M.coulet, G. De Temmerman, B. Dudson, B. Hnat, Y.Q. Liu, R. Martin, P. Tamain, D. Taylor, and the MAST team. Resonant magnetic perturbation experiments on mast using external and internal coils for elm control. *Nuclear Fusion*, 50(3):034008, feb 2010.
- [222] A. Kirk, H. R. Wilson, G. F. Counsell, R. Akers, E. Arends, S. C. Cowley, J. Dowling, B. Lloyd, M. Price, M. Walsh, and M. Team. Spatial and temporal structure of edge-localized modes. *Physical Review Letters*, 92, 2004.
- [223] M. Kotschenreuther, X. Liu, D. R. Hatch, S. Mahajan, L. Zheng, A. Diallo, R. Groebner, J. C. Hillesheim, C. F. Maggi, C. Giroud, F. Koechl, V. Parail, S. Saarelma, E. Solano, A. Chankin, A. Chankin, and J. Contributors. Gyrokinetic analysis and simulation of pedestals to identify the culprits for energy losses using ‘fingerprints’. *Nuclear Fusion*, 59(9):096001, 2019.
- [224] M. Kovari, M. Coleman, I. Cristescu, and R. Smith. Tritium resources available for fusion reactors. *Nuclear Fusion*, 58, 2018.
- [225] N. A. Krall and M. N. Rosenbluth. Universal instability in complex field geometries. *Physics of Fluids*, 8(8):1488, 1965.
- [226] G. Kramer, A. Bortolon, A. Diallo, and R. Maingi. The formation of an radial edge electric field due to finite ion orbit width effects is the possible root cause of the h-mode edge. *Nuclear Fusion*, 64(10):106035, 2024.
- [227] J. A. Krommes. Fundamental statistical descriptions of plasma turbulence in magnetic fields. *Physics Reports*, 360(1-4):1–352, 2002.
- [228] S. Ku, C. Chang, R. Hager, R. Churchill, G. Tynan, I. Cziegler, M. Greenwald, J. Hughes, S. E. Parker, M. Adams, et al. A fast low-to-high confinement mode bifurcation dynamics in the boundary-plasma gyrokinetic code xgc1. *Physics of Plasmas*, 25(5), 2018.
- [229] A. Q. Kuang, S. Ballinger, D. Brunner, J. Canik, A. J. Creely, T. Gray, M. Greenwald, J. W. Hughes, J. Irby, B. Labombard, B. Lipschultz, J. D. Lore, M. L. Reinke, J. L. Terry, M. Umansky, D. G. Whyte, and S. Wukitch. Divertor heat flux challenge and mitigation in sparc. *Journal of Plasma Physics*, 2020.
- [230] R. M. Kulsrud, E. J. Valeo, and S. C. Cowley. Physics of spin-polarized plasmas. *Nuclear Fusion*, 26, 1986.
- [231] N. Kumar, Y. Camenen, S. Benkadda, C. Bourdelle, A. Loarte, A. R. Polevoi, F. Widmer, et al. Turbulent transport driven by kinetic ballooning modes in the inner core of jet hybrid h-modes. *Nuclear Fusion*, 61(3):036005, 2021.
- [232] B. LaBombard, T. Golfopoulos, J. L. Terry, D. Brunner, E. Davis, M. Greenwald, J. W. Hughes, and A. C. Team. New insights on boundary plasma turbulence and the quasi-coherent mode in Alcator C-Mod using a Mirror Langmuir Probea). *Physics of Plasmas*, 21(5):056108, 05 2014.
- [233] L. Landau. On the vibrations of the electronic plasma. *Zhurnal eksperimentalnoi i teoreticheskoi fiziki*, 16(7):574–586, 1946.

- [234] M. Landreman, T. M. Antonsen, and W. Dorland. Universal instability for wavelengths below the ion Larmor scale. *Physical Review Letters*, 114(9):095003, 2015.
- [235] M. Landreman, J. Y. Choi, C. Alves, P. Balaprakash, R. M. Churchill, R. Conlin, and G. Roberg-Clark. How does ion temperature gradient turbulence depend on magnetic geometry? insights from data and machine learning. *arXiv preprint arXiv:2502.11657*, 2025.
- [236] M. Landreman, F. I. Parra, P. J. Catto, D. R. Ernst, and I. Pusztai. Radially global  $\delta f$  computation of neoclassical phenomena in a tokamak pedestal. *Plasma Physics and Controlled Fusion*, 56(4):045005, 2014.
- [237] M. Landreman, H. M. Smith, A. Mollén, and P. Helander. Comparison of particle trajectories and collision operators for collisional transport in nonaxisymmetric plasmas. *Physics of Plasmas*, 21(4), 2014.
- [238] E. Lanti, N. Ohana, N. Tronko, T. Hayward-Schneider, A. Bottino, B. F. McMillan, A. Mishchenko, A. Scheinberg, A. Biancalani, P. Angelino, et al. Orb5: a global electromagnetic gyrokinetic code using the pic approach in toroidal geometry. *Computer Physics Communications*, 251:107072, 2020.
- [239] L. L. Lao, H. S. John, R. D. Stambaugh, A. G. Kellman, and W. Pfeiffer. Reconstruction of current profile parameters and plasma shapes in tokamaks. *Nuclear Fusion*, 25, 1985.
- [240] L. L. Lao, S. Kruger, C. Akcay, P. Balaprakash, T. A. Bechtel, E. Howell, J. Koo, J. Leddy, M. Leinhauser, Y. Q. Liu, S. Madireddy, J. McClenaghan, D. Orozco, A. Pankin, D. Schissel, S. Smith, X. Sun, and S. Williams. Application of machine learning and artificial intelligence to extend efit equilibrium reconstruction. *Plasma Physics and Controlled Fusion*, 64:074001, 2022.
- [241] H. Lashinsky. Universal instability in a fully ionized inhomogeneous plasma. *Physical Review Letters*, 12(5):121, 1964.
- [242] J. D. Lawson. Some Criteria for a Power Producing Thermonuclear Reactor. *Proceedings of the Physical Society. Section B*, 70(1):6–10, 1957.
- [243] G. Lee and P. Diamond. Theory of ion-temperature-gradient-driven turbulence in tokamaks. *The Physics of fluids*, 29(10):3291–3313, 1986.
- [244] W. Lee, J. Leem, J. Lee, Y. Nam, M. Kim, G. Yun, H. K. Park, Y. Kim, H. Park, K. Kim, et al. Microwave imaging reflectometry for density fluctuation measurement on kstar. *Nuclear Fusion*, 54(2):023012, 2014.
- [245] Y. C. Lee, J. Q. Dong, P. N. Guzdar, and C. S. Liu. Collisionless electron temperature gradient instability. *Physics of Fluids*, 30(5), 1987.
- [246] A. Lenard. On bogoliubov’s kinetic equation for a spatially homogeneous plasma. *Annals of Physics*, 10(3):390–400, 1960.
- [247] A. W. Leonard. Edge-localized-modes in tokamaks). *Physics of Plasmas*, 21(9):090501, 09 2014.

- [248] P. Li, M. Pueschel, P. Terry, and G. Whelan. On the role of mode resonances in regulating zonal-flow-moderated plasma microturbulence. *Nuclear Fusion*, 63(2):026028, 2023.
- [249] X. Z. Li, Q. M. Wei, and B. Liu. A new simple formula for fusion cross-sections of light nuclei. *Nuclear Fusion*, 48(12):125003, 2008.
- [250] P. C. Liewer. Measurements of microturbulence in tokamaks and comparisons with theories of turbulence and anomalous transport. *Nuclear Fusion*, 25(5):543, 1985.
- [251] Z. Lin, T. S. Hahm, W. W. Lee, W. M. Tang, and R. B. White. Turbulent transport reduction by zonal flows: Massively parallel simulations. *Science*, 281(5384):1835, 1998.
- [252] Y. Liu, H. Zhao, T. Zhou, X. Liu, Z. Zhu, X. Han, S. Schmuck, J. Fessey, P. Trimble, C. Domier, et al. Overview of the electron cyclotron emission measurements on east. *Fusion Engineering and Design*, 136:72–75, 2018.
- [253] T. C. Luce, K. H. Burrell, C. Holland, A. Marinoni, C. C. Petty, S. P. Smith, M. E. Austin, B. A. Grierson, and L. Zeng. Experimental challenges to stiffness as a transport paradigm. *Nuclear Fusion*, 58(2):026023, 2018.
- [254] Lü, H.tjens, A. Bondeson, and O. Sauter. The chease code for toroidal mhd equilibria. *Computer Physics Communications*, 97, 1996.
- [255] J. L. Luxon. A design retrospective of the diii-d tokamak. *Nuclear Fusion*, 42, 2002.
- [256] Y. Ma et al. Machine learning surrogate model for turbulent transport simulations in fusion plasmas. *Physics of Plasmas*, 27(4):042305, 2020.
- [257] T. Macwan, K. Barada, J. F. Parisi, R. J. Groebner, T. L. Rhodes, S. Banerjee, C. Chrystal, Q. Pratt, Z. Yan, H. Wang, L. Zeng, M. E. Austin, N. A. Crocker, and W. A. Peebles. Elm-free enhanced d-alpha h-mode with near zero nbi torque injection in diii-d tokamak. *Physics of Plasmas*, 31(12):122503, 12 2024.
- [258] S. Maeyama, N. Howard, J. Citrin, T. Watanabe, and T. Tokuzawa. Overview of multiscale turbulence studies covering ion-to-electron scales in magnetically confined fusion plasma. *Nuclear Fusion*, 64(11):112007, 2024.
- [259] S. Maeyama, Y. Idomura, T. H. Watanabe, M. Nakata, M. Yagi, N. Miyato, A. Ishizawa, and M. Nunami. Cross-scale interactions between electron and ion scale turbulence in a tokamak plasma. *Physical Review Letters*, 114(25):255002, 2015.
- [260] S. Maeyama, A. Ishizawa, T. Watanabe, M. Nakata, N. Miyato, M. Yagi, and Y. Idomura. Comparison between kinetic-ballooning-mode-driven turbulence and ion-temperature-gradient-driven turbulence. *Physics of Plasmas*, 21(5), 2014.
- [261] S. Maeyama, T. H. Watanabe, and A. Ishizawa. Suppression of Ion-Scale Microtearing Modes by Electron-Scale Turbulence via Cross-Scale Nonlinear Interactions in Tokamak Plasmas. *Physical Review Letters*, 119(19):195002, 2017.

- [262] R. Maingi. Enhanced confinement scenarios without large edge localized modes in tokamaks: control, performance, and extrapolability issues for iter. *Nuclear Fusion*, 54(11):114016, nov 2014.
- [263] R. Maingi, R. E. Bell, J. M. Canik, S. P. Gerhardt, S. M. Kaye, B. P. LeBlanc, T. H. Osborne, M. G. Bell, E. D. Fredrickson, K. C. Lee, J. E. Menard, J. Park, S. A. Sabbagh, and S. A. Sabbagh. Triggered confinement enhancement and pedestal expansion in high-confinement-mode discharges in the national spherical torus experiment. *Physical Review Letters*, 105:135004, 9 2010.
- [264] R. Maingi, R. E. Bell, B. P. LeBlanc, D. A. Gates, S. M. Kaye, J. E. Menard, S. A. Sabbagh, and H. Yuh. The enhanced pedestal h-mode in the national spherical torus experiment. *Journal of nuclear materials*, 390:440–443, 2009.
- [265] D. Maisonnier, D. Campbell, I. Cook, L. Di Pace, L. Giancarli, J. Hayward, A. Li Puma, M. Medrano, P. Norajitra, M. Roccella, P. Sardain, M.Q. Tran, and D. Ward. Power plant conceptual studies in europe. *Nuclear Fusion*, 47(11):1524, 2007.
- [266] N. R. Mandell, W. Dorland, I. Abel, R. Gaur, P. Kim, M. Martin, and T. Qian. Gx: a gpu-native gyrokinetic turbulence code for tokamak and stellarator design. *Journal of Plasma Physics*, 90(4):905900402, 2024.
- [267] P. Mantica, C. Angioni, B. Baiocchi, M. Baruzzo, M. Beurskens, J. Bizarro, R. Budny, P. Buratti, A. Casati, C. Challis, et al. Ion heat transport studies in jet. *Plasma Physics and Controlled Fusion*, 53(12):124033, 2011.
- [268] P. Mantica, C. Angioni, C. Challis, G. Colyer, L. Frassinetti, N. Hawkes, T. Johnson, M. Tsalas, P. Devries, J. Weiland, et al. A key to improved ion core confinement in the jet tokamak: Ion stiffness mitigation due to combined plasma rotation and low magnetic shear. *Physical Review Letters*, 107(13):135004, 2011.
- [269] P. Mantica, N. Bonanomi, A. Mariani, P. Carvalho, E. Delabie, J. Garcia, N. Hawkes, T. Johnson, D. Keeling, M. Sertoli, et al. The role of electron-scale turbulence in the jet tokamak: experiments and modelling. *Nuclear Fusion*, 61(9):096014, 2021.
- [270] P. Mantica, D. Strintzi, T. Tala, C. Giroud, T. Johnson, H. Leggate, E. Lerche, T. Loarer, A. G. Peeters, A. Salmi, S. Sharapov, D. Van Eester, P. C. de Vries, L. Zabeo, and K. . Zastrow. Experimental study of the ion critical-gradient length and stiffness level and the impact of rotation in the jet tokamak. *Phys. Rev. Lett.*, 102:175002, 2009.
- [271] A. Marinoni, S. Brunner, Y. Camenen, S. Coda, J. P. Graves, X. Lapillonne, A. Pochelon, O. Sauter, and L. Villard. The effect of plasma triangularity on turbulent transport: Modeling TCV experiments by linear and non-linear gyrokinetic simulations. *Plasma Physics and Controlled Fusion*, 51(5):055016, 2009.
- [272] S. Matsuoka, S. Satake, M. Yokoyama, A. Wakasa, and S. Murakami. Neoclassical electron transport calculation by using  $\delta f$  monte carlo method. *Physics of Plasmas*, 18(3), 2011.

- [273] S. Mazzi, Y. Camenen, J. Garcia, D. Zarzoso, D. Frigione, L. Garzotti, F. Rimini, D. Van Eester, and J. Contributors. Effects of the parallel flow shear on the itg-driven turbulent transport in tokamak plasmas. *Nuclear Fusion*, 62(9):096024, 2022.
- [274] S. Mazzi, J. Garcia, D. Zarzoso, Y. O. Kazakov, J. Ongena, M. Dreval, M. Nocente, et al. Enhanced performance in fusion plasmas through turbulence suppression by megaelectronvolt ions. *Nature Physics*, 18(7):776–782, 2022.
- [275] E. Mazzucato. Microwave imaging reflectometry for the visualization of turbulence in tokamaks. *Nuclear Fusion*, 41(2):203, 2001.
- [276] G. McKee, R. Ashley, R. Durst, R. Fonck, M. Jakubowski, K. Tritz, K. Burrell, C. Greenfield, and J. Robinson. The beam emission spectroscopy diagnostic on the diii-d tokamak. *Review of scientific instruments*, 70(1):913–916, 1999.
- [277] G. McKee, R. Fonck, M. Jakubowski, K. Burrell, K. Hallatschek, R. Moyer, W. Nevins, D. Rudakov, and X. Xu. Observation and characterization of radially sheared zonal flows in diii-d. *Plasma physics and controlled fusion*, 45(12A):A477, 2003.
- [278] I. McKinney, M. Pueschel, B. Faber, C. Hegna, A. Ishizawa, and P. Terry. Kinetic-ballooning-mode turbulence in low-average-magnetic-shear equilibria. *Journal of Plasma Physics*, 87(3):905870311, 2021.
- [279] J. E. Menard, T. Brown, L. El-Guebaly, M. Boyer, J. Canik, B. Colling, R. Raman, Z. Wang, Y. Zhai, P. Buxton, B. Covele, C. D’Angelo, A. Davis, S. Gerhardt, M. Gryaznevich, M. Harb, T. C. Hender, S. Kaye, D. Kingham, M. Kotschenreuther, S. Mahajan, R. Maingi, E. Marriott, E. T. Meier, L. Mynsberge, C. Neumeyer, M. Ono, J. K. Park, S. A. Sabbagh, V. Soukhanovskii, P. Valanju, and R. Woolley. Fusion nuclear science facilities and pilot plants based on the spherical tokamak. *Nuclear Fusion*, 56:106023, 2016.
- [280] A. Merle, O. Sauter, and S. Y. Medvedev. Pedestal properties of h-modes with negative triangularity using the eped-ch model. *Plasma Physics and Controlled Fusion*, 59:104001, 2017.
- [281] S. Meschini, S. E. Ferry, Rémi Delaporte-Mathurin, and Dennis G. Whyte. Modeling and analysis of the tritium fuel cycle for arc- and step-class d-t fusion power plants. *Nuclear Fusion*, 63, 2023.
- [282] H. Meyer and S. P. Team. Plasma burn—mind the gap. *Philosophical Transactions A*, 382(2280):20230406, 2024.
- [283] D. Mikkelsen and W. Dorland. Dimits shift in realistic gyrokinetic plasma-turbulence simulations. *Physical review letters*, 101(13):135003, 2008.
- [284] P. Molina Cabrera, S. Coda, L. Porte, N. Offeddu, P. Lavanchy, M. Silva, M. Tous-saint, T. Team, et al. V-band doppler backscattering diagnostic in the tcv tokamak. *Review of Scientific Instruments*, 89(8), 2018.

- [285] A. Morris, R. Akers, M. Cox, F. Militello, E. Surrey, C. Waldon, H. Wilson, and H. Zohm. Towards a fusion power plant: integration of physics and technology. *Plasma Physics and Controlled Fusion*, 64(6):064002, 2022.
- [286] N. F. Mott and H. S. W. Massey. *The Theory Of Atomic Collisions*. The International Series Of Monographs On Physics. Clarendon Press, Oxford, 3rd ed. edition, 1965.
- [287] S. I. Muldrew, C. Harrington, J. Keep, C. Waldon, C. Ashe, R. Chapman, C. Griesel, A. J. Pearce, F. Casson, S. P. Marsden, and E. Tholerus. Conceptual design workflow for the step prototype powerplant. *Fusion Engineering and Design*, 201:114238, 2024.
- [288] P. Mulholland, M. Pueschel, J. Proll, K. Aleynikova, B. Faber, P. Terry, C. Hegna, and C. Nührenberg. Finite- $\beta$  turbulence in wendelstein 7-x enhanced by sub-threshold kinetic ballooning modes. *Nuclear Fusion*, 65(1):016022, 2024.
- [289] T. Munsat, E. Mazzucato, H. Park, B. Deng, C. Domier, N. Luhmann Jr, J. Wang, Z. Xia, AJH Donné, and M van de Pol. Microwave imaging reflectometer for textor. *Review of scientific instruments*, 74(3):1426–1432, 2003.
- [290] M. Muraca, E. Fable, C. Angioni, T. Luda, P. David, H. Zohm, A. Di Siena, A. U. Team, et al. Reduced transport models for a tokamak flight simulator. *Plasma Physics and Controlled Fusion*, 65(3):035007, 2023.
- [291] T. Nakayama, M. Nakata, M. Honda, M. Nunami, and S. Matsuoka. Nonlinear functional relation covering near-and far-marginal stability in ion temperature gradient driven turbulence. *Plasma Physics and Controlled Fusion*, 64(7):075007, 2022.
- [292] A. Nelson, C. Paz-Soldan, and S. Saarelma. Prospects for h-mode inhibition in negative triangularity tokamak reactor plasmas. *Nuclear Fusion*, 62:096020, 2022.
- [293] A. Nelson, L. Schmitz, C. Paz-Soldan, K. E. Thome, T. B. Cote, N. Leuthold, F. Scotti, M. E. Austin, A. Hyatt, and T. Osborne. Robust avoidance of edge-localized modes alongside gradient formation in the negative triangularity tokamak edge robust avoidance of edge-localized modes alongside gradient formation in the negative triangularity tokamak edge. *Physical Review Letters*, 131:195101, 2023.
- [294] A. Nelson, C. Vincent, H. Anand, J. Lovell, J. Parisi, H. Wilson, K. Imada, W. Wehner, M. Kochan, S. Blackmore, G. McArdle, S. Guizzo, L. Rondini, S. Freiburger, C. Paz-Soldan, and T. M. Team. First access to elm-free negative triangularity at low aspect ratio. *Nuclear Fusion*, 64(12):124004, 2024.
- [295] A. O. Nelson, L. Schmitz, T. Cote, J. F. Parisi, S. Stewart, C. Paz-Soldan, K. E. Thome, M. E. Austin, F. Scotti, J. L. Barr, A. Hyatt, N. Leuthold, A. Marinoni, T. Neiser, T. Osborne, N. Richner, A. S. Welander, W. P. Wehner, R. Wilcox, T. M. Wilks, J. Yang, and T. D. Team. Characterization of the elm-free negative triangularity edge on diiii-d. *Plasma Physics and Controlled Fusion*, 66(10):105014, sep 2024.
- [296] S. L. Newton, S. C. Cowley, and N. F. Loureiro. Understanding the effect of sheared flow on microinstabilities. *Plasma Physics and Controlled Fusion*, 52(12):125001, 2010.



- [297] R. Nies, F. Parra, M. Barnes, N. Mandell, and W. Dorland. Saturation of magnetised plasma turbulence by propagating zonal flows. *arXiv preprint arXiv:2409.02283*, 2024.
- [298] H. Nordman, J. Weiland, and A. Jarmén. Simulation of toroidal drift mode turbulence driven by temperature gradients and electron trapping. *Nuclear Fusion*, 30(6):983, 1990.
- [299] M. Nunami, T. H. Watanabe, H. Sugama, and K. Tanaka. Linear gyrokinetic analyses of itg modes and zonal flows in lhd with high ion temperature. *Plasma and Fusion Research*, 6, 2011.
- [300] National Academies of Sciences. *Bringing fusion to the US grid*. 2021.
- [301] N. Offeddu, C Wüthrich, W Han, C Theiler, T Golfinopoulos, JL Terry, E Marmar, C Galperti, Y Andrebe, BP Duval, et al. Gas puff imaging on the tcv tokamak. *Review of Scientific Instruments*, 93(12), 2022.
- [302] J. Ongena, R. Koch, R. Wolf, and H. Zohm. Magnetic-confinement fusion. *Nature Physics*, 12(5):398–410, 2016.
- [303] M. Ono, S. Kaye, Y. Peng, G. Barnes, W. Blanchard, M. Carter, J. Chrzanowski, L. Dudek, R. Ewig, D. Gates, R. Hatcher, T. Jarboe, S. Jardin, D. Johnson, R. Kaita, M. Kalish, C. Kessel, H. Kugel, R. Maingi, R. Majeski, J. Manickam, B. McCormack, J. Menard, D. Mueller, B. Nelson, B. Nelson, C. Neumeyer, G. Oliaro, F. Paoletti, R. Parsells, E. Perry, N. Pomphrey, S. Ramakrishnan, R. Raman, G. Rewoldt, J. Robinson, A. Roquemore, P. Ryan, S. Sabbagh, D. Swain, E. Synakowski, M. Viola, M. Williams, J. Wilson, and N. Team. Exploration of spherical torus physics in the nstx device. *Nuclear Fusion*, 40(3Y):557, mar 2000.
- [304] S. A. Orszag. Analytical theories of turbulence. *Journal of Fluid Mechanics*, 41(2):363–386, 1970.
- [305] D. Panici, R. Conlin, D. W. Dudt, K. Unalmis, and E. Kolemen. The desc stellarator code suite. part 1. quick and accurate equilibria computations. *Journal of Plasma Physics*, 89(3):955890303, 2023.
- [306] A. Pankin, J. Breslau, M. Gorelenkova, R. Andre, B. Grierson, J. Sachdev, M. Goliyad, and G. Perumpilly. Transp integrated modeling code for interpretive and predictive analysis of tokamak plasmas. *arXiv preprint arXiv:2406.07781*, 2024.
- [307] J. Parisi and J. Ball. *The Future of Fusion Energy*. World Scientific, London, 2019.
- [308] J. Parisi, J. Berkery, A. Sladkomedova, S. Guizzo, M. Hardman, J. Ball, A. Nelson, S. Kaye, M. Anastopoulos-Tzanis, S. McNamara, et al. Doubling fusion power with volumetric optimization in magnetic confinement fusion devices. *Physical Review Research*, 7(1):013139, 2025.
- [309] J. Parisi, A. Diallo, and J. Schwartz. Simultaneous enhancement of tritium burn efficiency and fusion power with low-tritium spin-polarized fuel. *Nuclear Fusion*, 64(12):126019, oct 2024.

- [310] J. F. Parisi. *Microinstability in the Pedestal*. PhD thesis, University of Oxford, 2020.
- [311] J. F. Parisi, J. W. Berkery, K. Imada, A. O. Nelson, S. M. Kaye, P. B. Snyder, M. Lampert, and A. Kleiner. Prediction of elm-free operation in spherical tokamaks with high plasma squareness, 2025.
- [312] J. F. Parisi, S. Meschini, A. Rutkowski, and A. Diallo. Tritium-lean fusion power plants with asymmetric deuterium-tritium transport and pumping, 2025.
- [313] J. F. Parisi, F. I. Parra, C. M. Roach, C. Giroud, W. Dorland, D. R. Hatch, M. Barnes, J. C. Hillesheim, N. Aiba, J. Ball, and P. G. Ivanov. Toroidal and slab ETG instability dominance in the linear spectrum of JET-ILW pedestals. *Nuclear Fusion*, 60:126045, 2020.
- [314] J. F. Parisi, F. I. Parra, C. M. Roach, M. R. Hardman, A. A. Schekochihin, I. G. Abel, N. Aiba, J. Ball, M. Barnes, B. Chapman-Oplopoiou, D. Dickinson, W. Dorland, C. Giroud, D. Hatch, J. Hillesheim, J. R. Ruiz, S. Saarelma, D. St-Onge, and J. Contributors. Three-dimensional inhomogeneity of electron-temperature-gradient turbulence in the edge of tokamak plasmas. *Nuclear Fusion*, 62(8):086045, 2022.
- [315] H. Park, C. Chang, B. Deng, C. Domier, AJH Donné, K Kawahata, C Liang, XP Liang, HJ Lu, NC Luhmann Jr, et al. Recent advancements in microwave imaging plasma diagnostics. *Review of scientific instruments*, 74(10):4239–4262, 2003.
- [316] F. I. Parra. Electrostatic drift kinetics and drift waves, January 2019.
- [317] F. I. Parra and M. Barnes. Intrinsic rotation in tokamaks: theory. *Plasma Physics and Controlled Fusion*, 57(4):045002, 2015.
- [318] F. I. Parra and P. J. Catto. Limitations of gyrokinetics on transport time scales. *Plasma Physics and Controlled Fusion*, 50(6):065014, 2008.
- [319] F. I. Parra and P. J. Catto. Transport of momentum in full f gyrokinetics. *Physics of Plasmas*, 17(5), 2010.
- [320] B. Patel, M. R. Hardman, D. Kennedy, M. Giacomini, D. Dickinson, and C. Roach. The impact of  $e \times b$  shear on microtearing based transport in spherical tokamaks. *Nuclear Fusion*, 65(2):026063, 2025.
- [321] C. Paz-Soldan, C. Chrystal, P. Lunia, A. Nelson, K. Thome, M. Austin, T. Cote, A. Hyatt, N. Leuthold, A. Marinoni, T. Osborne, M. Pharr, O. Sauter, F. Scotti, T. Wilks, and H. Wilson. Simultaneous access to high normalized density, current, pressure, and confinement in strongly-shaped diverted negative triangularity plasmas. *Nuclear Fusion*, 64(9):094002, aug 2024.
- [322] A. Peeters, Y. Camenen, F. J. Casson, W. Hornsby, A. Snodin, D. Strintzi, and G. Szepesi. The nonlinear gyro-kinetic flux tube code gkw. *Computer physics communications*, 180(12):2650–2672, 2009.

- [323] A. G. Peeters and C. Angioni. Linear gyrokinetic calculations of toroidal momentum transport in a tokamak due to the ion temperature gradient mode. *Physics of Plasmas*, 12(7):072515, 2005.
- [324] M. Peret, J. Guterl, T. N. Bernard, F. D. Halpern, and N. Fedorczak. Predictive turbulence-driven flux model of scrape-off layer widths across confinement regimes in tokamaks. *Nuclear Fusion*, 65(5):056043, apr 2025.
- [325] J. L. Peterson, K. D. Humbird, J. E. Field, S. T. Brandon, S. H. Langer, R. C. Nora, B. K. Spears, and P. Springer. Zonal flow generation in inertial confinement fusion implosions. *Physics of Plasmas*, 24(3), 2017.
- [326] A. Piccione, J. Berkery, S. Sabbagh, and Y. Andreopoulos. Physics-guided machine learning approaches to predict the ideal stability properties of fusion plasmas. *Nuclear Fusion*, 60(4):046033, 2020.
- [327] A. Piccione, J. Berkery, S. Sabbagh, and Y. Andreopoulos. Predicting resistive wall mode stability in nstx through balanced random forests and counterfactual explanations. *Nuclear Fusion*, 62(3):036002, 2022.
- [328] G. G. Plunk, P. Helander, P. Xanthopoulos, and J. W. Connor. Collisionless microinstabilities in stellarators. III. the ion-temperature-gradient mode. *Physics of Plasmas*, 2014.
- [329] M. Podesta, M. Gorelenkova, and R. B. White. A reduced fast ion transport model for the tokamak transport code transp. *Plasma Physics and Controlled Fusion*, 56(5):055003, 2014.
- [330] F. Porcelli. Fast particle stabilisation. *Plasma Physics and Controlled Fusion*, 33(13):1601, 1991.
- [331] E. J. Powers. Spectral techniques for experimental investigation of plasma diffusion due to polychromatic fluctuations. *Nuclear Fusion*, 14(5):749, 1974.
- [332] M. Pueschel, P. Li, and P. Terry. Predicting the critical gradient of itg turbulence in fusion plasmas. *Nuclear Fusion*, 61(5):054003, 2021.
- [333] M. J. Pueschel, D. R. Hatch, M. Kotschenreuther, A. Ishizawa, and G. Merlo. Multi-scale interactions of microtearing turbulence in the tokamak pedestal. *Nuclear Fusion*, 60(12):124005, 2020.
- [334] M. J. Pueschel, M. Kammerer, and F. Jenko. Gyrokinetic turbulence simulations at high plasma beta. *Physics of Plasmas*, 15, 2008.
- [335] T. Pütterich, R. Dux, MA Janzer, RM McDermott, ASDEX Upgrade Team, et al. Elm flushing and impurity transport in the h-mode edge barrier in asdex upgrade. *Journal of Nuclear Materials*, 415(1):S334–S339, 2011.
- [336] L. Radovanovic, M. Dunne, E. Wolfrum, G. Harrer, M. Faitsch, R. Fischer, F. Aumayr, T. A. U. Team, and T. E. M. Team. Developing a physics understanding of the quasi-continuous exhaust regime: pedestal profile and ballooning stability analysis. *Nuclear Fusion*, 62(8):086004, may 2022.

- [337] T. Rafiq, J. Weiland, A. Kritz, L. Luo, and A. Pankin. Microtearing modes in tokamak discharges. *Physics of Plasmas*, 23(6), 2016.
- [338] D. Reiter, H. Kever, G. Wolf, M. Baelmans, R. Behrisch, and R. Schneider. Helium removal from tokamaks. *Plasma Physics and Controlled Fusion*, 33(13):1579, 1991.
- [339] D. Reiter, G. H. Wolf, and H. Kever. Burn condition, helium particle confinement and exhaust efficiency. *Nuclear Fusion*, 30(10):2141, 1990.
- [340] Y. Ren, W. Guttenfelder, S. Kaye, E. Mazzucato, R. Bell, A. Diallo, C. Domier, B. LeBlanc, K. Lee, D. Smith, et al. Experimental study of parametric dependence of electron-scale turbulence in a spherical tokamak. *Physics of Plasmas*, 19(5), 2012.
- [341] Y. Ren, W. Guttenfelder, S. M. Kaye, and W. X. Wang. Transport from electron-scale turbulence in toroidal magnetic confinement devices. *Reviews of Modern Plasma Physics*, 8(1):5, 2024.
- [342] T. Rhodes, K. Barada, W. Peebles, and N. Crocker. Simultaneous measurement of magnetic and density fluctuations via cross-polarization scattering and doppler backscattering on the diii-d tokamak. *Review of Scientific Instruments*, 87(11), 2016.
- [343] T. Rhodes, C. Holland, S. Smith, A. White, K. Burrell, J. Candy, J. DeBoo, E. Doyle, J. Hillesheim, J. Kinsey, et al. L-mode validation studies of gyrokinetic turbulence simulations via multiscale and multifield turbulence measurements on the diii-d tokamak. *Nuclear Fusion*, 51(6):063022, 2011.
- [344] J. Rice, A. Ince-Cushman, J. Degraessie, L. Eriksson, Y. Sakamoto, A. Scarabosio, A. Bortolon, K. Burrell, B. Duval, C. Fenzi-Bonizec, et al. Inter-machine comparison of intrinsic toroidal rotation in tokamaks. *Nuclear Fusion*, 47(11):1618, 2007.
- [345] C. M. Roach, I. G. Abel, R. J. Akers, W. Arter, M. Barnes, Y. Camenen, F. J. Casson, G. Colyer, J. W. Connor, S. C. Cowley, D. Dickinson, W. Dorland, A. R. Field, W. Guttenfelder, G. W. Hammett, R. J. Hastie, E. Highcock, N. F. Loureiro, A. G. Peeters, M. Reshko, S. Saarelma, A. A. Schekochihin, M. Valovic, and H. R. Wilson. Gyrokinetic simulations of spherical tokamaks. *Plasma Physics and Controlled Fusion*, 51(12):124020, 2009.
- [346] E. Rodriguez and A. Zocco. The kinetic ion-temperature-gradient-driven instability and its localisation. *Journal of Plasma Physics*, 91(1):E21, 2025.
- [347] P. Rodriguez-Fernandez, A. J. Creely, M. J. Greenwald, D. Brunner, S. B. Ballinger, C. P. Chrobak, D. T. Garnier, R. Granetz, Z. S. Hartwig, N. T. Howard, J. W. Hughes, J. H. Irby, V. A. Izzo, A. Q. Kuang, Y. Lin, E. S. Marmor, R. T. Mumgaard, C. Rea, M. L. Reinke, V. Riccardo, J. E. Rice, S. D. Scott, B. N. Sorbom, J. A. Stillerman, R. Sweeney, R. A. Tinguely, D. G. Whyte, J. C. Wright, and D. V. Yuryev. Overview of the SPARC physics basis towards the exploration of burning-plasma regimes in high-field, compact tokamaks. *Nuclear Fusion*, 62(042003), 2022.

- [348] P. Rodriguez-Fernandez, N. Howard, M. Greenwald, A. Creely, J. Hughes, J. Wright, C. Holland, Y. Lin, F. Sciortino, S. Team, et al. Predictions of core plasma performance for the sparc tokamak. *Journal of Plasma Physics*, 86(5):865860503, 2020.
- [349] B. N. Rogers, W. Dorland, and M. Kotschenreuther. Generation and stability of zonal flows in ion-temperature-gradient mode turbulence. *Physical Review Letters*, 2000.
- [350] F. Romanelli. Ion temperature-gradient-driven modes and anomalous ion transport in tokamaks. *Physics of Fluids B: Plasma Physics*, 1(5):1018–1025, 1989.
- [351] M. Romanelli, A. Zocco, F. Crisanti, J. Contributors, et al. Fast ion stabilization of the ion temperature gradient driven modes in the joint european torus hybrid-scenario plasmas: a trigger mechanism for internal transport barrier formation. *Plasma Physics and Controlled Fusion*, 52(4):045007, 2010.
- [352] D. W. Ross and W. Dorland. Comparing simulation of plasma turbulence with experiment. ii. gyrokinetic simulations. *Physics of Plasmas*, 9(12):5031–5035, 2002.
- [353] D. W. Ross and S. M. Mahajan. Are drift-wave eigenmodes unstable? *Physical Review Letters*, 1978.
- [354] J. Roth, E. Tsitrone, T. Loarer, V. Philipps, S. Brezinsek, A. Loarte, G. F. Counsell, R. P. Doerner, K. Schmid, O. V. Ogorodnikova, and R. A. Causey. Tritium inventory in iter plasma-facing materials and tritium removal procedures. *Plasma Physics and Controlled Fusion*, 50, 2008.
- [355] V. Rozhansky and M. Tendler. Plasma rotation in tokamaks. *Reviews of Plasma Physics*, 19:147, 1996.
- [356] L. I. Rudakov and R. Z. Sagdeev. On the instability of a nonuniform rarefied plasma in a strong magnetic field. *Soviet Physics Doklady*, 6:415, 1961.
- [357] F. Ryter, C. Angioni, A. G. Peeters, F. Leuterer, H. . Fahrbach, and W. Suttrop. Experimental study of trapped-electron-mode properties in tokamaks: Threshold and stabilization by collisions. *Phys. Rev. Lett.*, 95:085001, 2005.
- [358] F. Ryter, W. Suttrop, B. Brückner, M. Kaufmann, V. Mertens, H. Murmann, A. G. Peeters, J. Stober, J. Schweinzer, H. Zohm, et al. H-mode power threshold and transition in asdex upgrade. *Plasma physics and controlled fusion*, 40(5):725, 1998.
- [359] J. Sachdev, N. Mandell, T. Qian, et al. Trinity3d: a time dependent turbulent profile predictor for stellarators and tokamaks. *Bulletin of the American Physical Society*, 2024.
- [360] Y. Sakamoto, H. Shirai, T. Fujita, S. Ide, T. Takizuka, N. Oyama, and Y. Kamada. Impact of toroidal rotation on elm behaviour in the h-mode on jt-60u. *Plasma Physics and Controlled Fusion*, 46(5A):A299, apr 2004.

- [361] A. Sakasai, H. Takenaga, N. Hosogane, S. Sakurai, N. Akino, H. Kubo, S. Higashijima, H. Tamai, N. Asakura, K. Itami, and K. Shimizu. Helium exhaust in elmy h-mode plasmas with w-shaped pumped divertor of jt-60u. *Journal of Nuclear Materials*, 266, 1999.
- [362] Á Sá,nchez-Villar, Z Bai, N Bertelli, EW Bethel, J Hillairet, T Perciano, S Shiraiwa, GM Wallace, and JC Wright. Real-time capable modeling of icrf heating on nstx and west via machine learning approaches. *Nuclear Fusion*, 64(9):096039, 2024.
- [363] Y. Sarazin, G. Dif-Pradalier, X. Garbet, P. Ghendrih, A. Berger, C. Gillot, V. Grandgirard, K. Obrejan, R. Varennes, L. Vermare, et al. Key impact of phase dynamics and diamagnetic drive on reynolds stress in magnetic fusion plasmas. *Plasma Physics and Controlled Fusion*, 63(6):064007, 2021.
- [364] O. Sauter, S. Brunner, D. Kim, G. Merlo, R. Behn, Y. Camenen, S. Coda, B. P. Duval, L. Federspiel, T. P. Goodman, A. Karpushov, A. Merle, and T. Team. On the non-stiffness of edge transport in L-mode tokamak plasmas). *Physics of Plasmas*, 21(5):055906, 05 2014.
- [365] A. A. Schekochihin, S. C. Cowley, W. Dorland, G. W. Hammett, G. G. Howes, G. G. Plunk, E. Quataert, and T. Tatsuno. Gyrokinetic turbulence: a nonlinear route to dissipation through phase space. *Plasma Physics and Controlled Fusion*, 50(12), 2008.
- [366] A. A. Schekochihin, E. G. Highcock, and S. C. Cowley. Subcritical fluctuations and suppression of turbulence in differentially rotating gyrokinetic plasmas. *Plasma Physics and Controlled Fusion*, 54(5):055011, 2012.
- [367] L. Schmitz. The role of turbulence–flow interactions in l-to h-mode transition dynamics: recent progress. *Nuclear Fusion*, 57(2):025003, 2017.
- [368] O. Schmitz, I. Beigman, L. Vainshtein, B. Schweer, M. Kantor, A. Pospieszczyk, Y. Xu, M. Krychowiak, M. Lehnen, U. Samm, et al. Status of electron temperature and density measurement with beam emission spectroscopy on thermal helium at textor. *Plasma physics and controlled fusion*, 50(11):115004, 2008.
- [369] J. A. Schwartz, W. Ricks, E. Kolemen, and J. D. Jenkins. The value of fusion energy to a decarbonized united states electric grid. *Joule*, 7(4):675–699, 2023.
- [370] B. D. Scott. Tokamak edge turbulence: background theory and computation. *Plasma Physics and Controlled Fusion*, 49(7):S25, 2007.
- [371] B. Shanahan, D. Bold, and B. Dudson. Global fluid turbulence simulations in the scrape-off layer of a stellarator island divertor. *Journal of Plasma Physics*, 90(2):905900216, 2024.
- [372] S. Sharapov, L. Eriksson, A. Fasoli, G. Gorini, Jan Kä,llne, VG Kiptily, AA Korotkov, A Murari, SD Pinches, DS Testa, et al. Chapter 5: burning plasma studies at jet. *Fusion science and technology*, 53(4):989–1022, 2008.
- [373] J. Sheffield, W. Brown, G. Garrett, J. Hilley, D. McCloud, J. Ogden, T. Shields, and L. Waganer. A study of options for the deployment of large fusion power plants. *Fusion science and technology*, 40(1):1–36, 2001.

- [374] I. Shesterikov, Y. Xu, M. Berte, P. Dumortier, M. Van Schoor, M. Vergote, B. Schweer, and G. Van Oost. Development of the gas-puff imaging diagnostic in the textor tokamak. *Review of Scientific Instruments*, 84(5), 2013.
- [375] M. Shimada, D. J. Campbell, V. Mukhovatov, M. Fujiwara, N. Kirneva, K. Lackner, M. Nagami, V. D. Pustovitov, N. Uckan, J. Wesley, N. Asakura, A. E. Costley, A. J.H. Donné, E. J. Doyle, A. Fasoli, C. Gormezano, Y. Gribov, O. Gruber, T. C. Hender, W. Houlberg, S. Ide, Y. Kamada, A. Leonard, B. Lipschultz, A. Loarte, K. Miyamoto, V. Mukhovatov, T. H. Osborne, A. Polevoi, and A. C.C. Sips. Chapter 1: Overview and summary. *Nuclear Fusion*, 47(6), 2007.
- [376] D. Smith, H. Feder, R. Feder, R. Fonck, G. Labik, G. McKee, N. Schoenbeck, B. Stratton, I. Uzun-Kaymak, and G. Winz. Overview of the beam emission spectroscopy diagnostic system on the national spherical torus experiment. *Review of Scientific Instruments*, 81(10), 2010.
- [377] D. R. Smith, R. J. Fonck, G. R. McKee, D. S. Thompson, R. E. Bell, A. Diallo, W. Guttenfelder, S. M. Kaye, B. P. Leblanc, and M. Podesta. Characterization and parametric dependencies of low wavenumber pedestal turbulence in the National Spherical Torus Experiment. *Physics of Plasmas*, 20(5):055903, 2013.
- [378] P. B. Snyder, N. Aiba, M. Beurskens, R. J. Groebner, L. D. Horton, A. E. Hubbard, J. W. Hughes, G. T. A. Huysmans, Y. Kamada, A. Kirk, C. Konz, A. W. Leonard, J. Lönnroth, C. F. Maggi, R. Maingi, T. H. Osborne, N. Oyama, A. Pankin, S. Saarelma, G. Saibene, J. L. Terry, H. Urano, and H. R. Wilson. Pedestal stability comparison and ITER pedestal prediction. *Nuclear Fusion*, 49(8):085035, 2009.
- [379] P. B. Snyder and G. W. Hammett. Electromagnetic effects on plasma microturbulence and transport. *Physics of Plasmas*, 8(3), 2001.
- [380] P. B. Snyder, H. R. Wilson, J. R. Ferron, L. L. Lao, A. W. Leonard, T. H. Osborne, A. D. Turnbull, D. Mossessian, M. Murakami, and X. Q. Xu. Edge localized modes and the pedestal: A model based on coupled peeling–ballooning modes. *Physics of Plasmas*, 9(5):2037, 2002.
- [381] W. Solomon, K. Burrell, A. Garofalo, S. Kaye, R. Bell, A. Cole, J. DeGrassie, P. Diamond, T. Hahm, G. Jackson, et al. Mechanisms for generating toroidal rotation in tokamaks without external momentum input. *Physics of Plasmas*, 17(5), 2010.
- [382] P. Sonato, P. Agostinetti, T. Bolzonella, F. Cismondi, U. Fantz, A. Fassina, T. Franke, I. Furno, C. Hopf, I. Jenkins, et al. Conceptual design of the demo neutral beam injectors: main developments and r&d achievements. *Nuclear Fusion*, 57(5):056026, 2017.
- [383] B. N. Sorbom, J. Ball, T. R. Palmer, F. J. Mangiarotti, J. M. Sierchio, P. Bonoli, C. Kasten, D. A. Sutherland, H. S. Barnard, C. B. Haakonsen, J. Goh, C. Sung, and D. G. Whyte. ARC: A compact, high-field, fusion nuclear science facility and demonstration power plant with demountable magnets. *Fusion Engineering and Design*, 100:378–405, 2015.

- [384] G. M. Staebler, J. E. Kinsey, and R. E. Waltz. A theory-based transport model with comprehensive physics. *Physics of Plasmas*, 14(5):055909, 05 2007.
- [385] J. Stober, O. Gruber, A. Kallenbach, V. Mertens, F. Ryter, A. Stäbeler, W. Suttrop, W. Treutner, ASDEX Upgrade Team, et al. Effects of triangularity on confinement, density limit and profile stiffness of h-modes on asdex upgrade. *Plasma Physics and Controlled Fusion*, 42(5A):A211, 2000.
- [386] J. D. Strachan, H. Adler, P. Alling, C. Ancher, H. Anderson, J. L. Anderson, D. Ashcroft, C. W. Barnes, G. Barnes, S. Batha, M. G. Bell, R. Bell, M. Bitter, W. Blanchard, N. L. Bretz, R. Budny, C. E. Bush, R. Camp, M. Caorlin, S. Cauffman, Z. Chang, C. Z. Cheng, J. Collins, G. Coward, D. S. Darrow, J. DeLooper, H. Duong, L. Dudek, R. Durst, P. C. Efthimion, D. Ernst, R. Fisher, R. J. Fonck, E. Fredrickson, N. Fromm, G. Y. Fu, H. P. Furth, C. Gentile, N. Gorelenkov, B. Grek, L. R. Grisham, G. Hammett, G. R. Hanson, R. J. Hawryluk, W. Heidbrink, H. W. Herrmann, K. W. Hill, J. Hosea, H. Hsuan, A. Janos, D. L. Jassby, F. C. Jobes, D. W. Johnson, L. C. Johnson, J. Kamperschroer, H. Kugel, N. T. Lam, P. H. Lamarche, M. J. Loughlin, B. LeBlanc, M. Leonard, F. M. Levinton, J. MacHuzak, D. K. Mansfield, A. Martin, E. Mazzucato, R. Majeski, E. Marmor, J. McChesney, B. McCormack, D. C. McCune, K. M. McGuire, G. McKee, D. M. Meade, S. S. Medley, D. R. Mikkelsen, D. Mueller, M. Murakami, A. Nagy, R. Nazikian, R. Newman, T. Nishitani, M. Norris, T. O'Connor, M. Oldaker, M. Osakabe, D. K. Owens, H. Park, W. Park, S. F. Paul, G. Pearson, E. Perry, M. Petrov, C. K. Phillips, S. Pitcher, A. T. Ramsey, D. A. Rasmussen, M. H. Redi, D. Roberts, J. Rogers, R. Rossmassler, A. L. Roquemore, E. Ruskov, S. A. Sabbagh, M. Sasao, G. Schilling, J. Schivell, G. L. Schmidt, S. D. Scott, R. Sissingh, C. H. Skinner, J. A. Snipes, J. Stevens, T. Stevenson, B. C. Stratton, E. Synakowski, W. Tang, G. Taylor, J. L. Terry, M. E. Thompson, M. Tuszewski, C. Vannoy, A. V. Halle, S. V. Goeler, D. Voorhees, R. T. Walters, R. Wieland, J. B. Wilgen, M. Williams, J. R. Wilson, K. L. Wong, G. A. Wurden, M. Yamada, K. M. Young, M. C. Zarnstorff, and S. J. Zweben. Fusion power production from tftr plasmas fueled with deuterium and tritium. *Physical Review Letters*, 72, 1994.
- [387] J. D. Strachan et al. Fusion power production from tftr plasmas fueled with deuterium and tritium. *Physical Review Letters*, 72, 1994.
- [388] E. Strait, J. L. Barr, M. Baruzzo, J. Berkery, R. J. Buttery, P. C. de Vries, N. W. Eidietis, R. Granetz, J. M. Hanson, C. T. Holcomb, et al. Progress in disruption prevention for iter. *Nuclear Fusion*, 59(11):112012, 2019.
- [389] U. Stroth, M. Murakami, R. Dory, H. Yamada, S. Okamura, F. Sano, and T. Obiki. Energy confinement scaling from the international stellarator database. *Nuclear Fusion*, 36(8):1063, 1996.
- [390] S. Sudo, Y. Takeiri, H. Zushi, F. Sano, K. Itoh, K. Kondo, and A. Iiyoshi. Scalings of energy confinement and density limit in stellarator/heliotron devices. *Nuclear Fusion*, 30(1):11, 1990.
- [391] H. Sugama. Gyrokinetic field theory. *Physics of Plasmas*, 7(2):466–480, 2000.



- [392] H. Sugama and W. Horton. Nonlinear electromagnetic gyrokinetic equation for plasmas with large mean flows. *Physics of Plasmas*, 5(7):2560–2573, 07 1998.
- [393] H. Sugama, M. Okamoto, W. Horton, and M. Wakatani. Transport processes and entropy production in toroidal plasmas with gyrokinetic electromagnetic turbulence. *Physics of Plasmas*, 3(6):2379–2394, 1996.
- [394] W. Suttrop, Hynö, V.nen, T. Kurki-Suonio, P.T. Lang, M. Maraschek, R. Neu, A. Stäbler, G.D. Conway, S. Hacquin, M. Kempenaars, P.J. Lomas, M.F.F. Nave, R.A. Pitts, K.-D. Zastrow, the ASDEX Upgrade team, and contributors to the JET-EFDA workprogramme. Studies of the ‘quiescent h-mode’ regime in asdex upgrade and jet. *Nuclear Fusion*, 45(7):721, jul 2005.
- [395] E. Synakowski, R. Bell, R. Budny, C. Bush, P. Efthimion, B. Grek, D. Johnson, L. Johnson, B. LeBlanc, H. Park, et al. Measurements of the production and transport of helium ash in the tftr tokamak. *Physical review letters*, 75(20):3689, 1995.
- [396] E. Synakowski, B. Stratton, P. Efthimion, R. Fonck, R. Hulse, D. Johnson, D. Mansfield, H. Park, S. Scott, and G. Taylor. Measurements of radial profiles of he 2+ transport coefficients on the tftr tokamak. *Physical review letters*, 65(18):2255, 1990.
- [397] T. Tanabe. *Tritium: Fuel of fusion reactors*. Springer, 2017.
- [398] W. M. Tang, J. W. Connor, and R. J. Hastie. Kinetic-ballooning-mode theory in general geometry. *Nuclear Fusion*, 20(11):1439, 1980.
- [399] T. Taylor. Physics of advanced tokamaks. *Plasma Physics and Controlled Fusion*, 39(12B):B47, 1997.
- [400] J. L. Terry, S. J. Zweben, K. Hallatschek, B. LaBombard, R. J. Maqueda, B. Bai, C. J. Boswell, M. Greenwald, D. Kopon, W. M. Nevins, C. S. Pitcher, B. N. Rogers, D. P. Stotler, and X. Q. Xu. Observations of the turbulence in the scrape-off-layer of alcator c-mod and comparisons with simulation. *Physics of Plasmas*, 10(5):1739–1747, 05 2003.
- [401] D. Told, F. Jenko, P. Xanthopoulos, L. D. Horton, E. Wolfrum, and A. U. Team. Gyrokinetic microinstabilities in ASDEX Upgrade edge plasmas. *Physics of Plasmas*, 15(10):102306, 2008.
- [402] A. D. Turnbull, Y. R. Lin-Liu, R. L. Miller, T. S. Taylor, and T. N. Todd. Improved magnetohydrodynamic stability through optimization of higher order moments in cross-section shape of tokamaks. *Physics of Plasmas*, 6(4):1113–1116, 04 1999.
- [403] G. Tynan, A. Fujisawa, and G. McKee. A review of experimental drift turbulence studies. *Plasma Physics and Controlled Fusion*, 51(11):113001, 2009.
- [404] N. A. Uckan, J. S. Tolliver, W. A. Houlberg, and S. E. Attenberger. Influence of fast alpha diffusion and thermal alpha buildup on tokamak reactor performance. *Fusion technology*, 13(3):411–422, 1988.

- [405] M. Umansky, R. Bulmer, R. Cohen, T. Rognien, and D. Ryutov. Analysis of geometric variations in high-power tokamak divertors. *Nuclear Fusion*, 49(7):075005, 2009.
- [406] K. L. van de Plassche, J. Citrin, C. Bourdelle, Y. Camenen, F. J. Casson, V. I. Dagnelie, F. Felici, A. Ho, S. Van Mulders, and J. Contributors. Fast modeling of turbulent transport in fusion plasmas using neural networks. *Physics of Plasmas*, 27(2), 2020.
- [407] G. Verdoolaege, S. M. Kaye, C. Angioni, O. J. W. F. Kardaun, M. Maslov, M. Romanelli, F. Ryter, K. Thomsen, T. ASDEX Upgrade Team, T. EUROfusion MST1 Team, and J. Contributors. The updated itpa global h-mode confinement database: description and analysis. *Nuclear Fusion*, 61(7):076006, may 2021.
- [408] V. Vershkov, S. Soldatov, D. Shelukhin, and V. Chistiakov. Experimental investigation of ion-temperature-gradient-like turbulence characteristics in t-10 core plasmas with toroidal and poloidal correlation reflectometry. *Nuclear Fusion*, 39(11Y):1775, 1999.
- [409] Eleonora Viezzer, ME Austin, M Bernert, KH Burrell, Pilar Cano-Megias, X Chen, Diego José Cruz-Zabala, S Coda, M Faitsch, O Février, et al. Prospects of core-edge integrated no-elm and small-elm scenarios for future fusion devices. *Nuclear Materials and Energy*, 34:101308, 2023.
- [410] M. Wade, W. Houlberg, and L. Baylor. Experimental confirmation of impurity convection driven by the ion-temperature gradient in toroidal plasmas. *Physical review letters*, 84(2):282, 2000.
- [411] M. R. Wade and J. A. Leuer. Cost drivers for a tokamak-based compact pilot plant. *Fusion Science and Technology*, 77(2):119–143, 2021.
- [412] F. Waelbroeck and L. Chen. Ballooning instabilities in tokamaks with sheared toroidal flows. *Physics of Fluids B: Plasma Physics*, 3(3):601–610, 1991.
- [413] F. Wagner, G. Becker, K. Behringer, D. Campbell, A. Eberhagen, W. Engelhardt, G. Fussmann, O. Gehre, J. Gernhardt, G. V. Gierke, G. Haas, M. Huang, F. Karger, M. Keilhacker, O. Klüber, M. Kornherr, K. Lackner, G. Lisitano, G. G. Lister, H. M. Mayer, D. Meisel, E. R. Müller, H. Murmann, H. Niedermeyer, W. Poschenrieder, H. Rapp, H. Röhr, F. Schneider, G. Siller, E. Speth, A. Stäbler, K. H. Steuer, G. Venus, O. Vollmer, and Z. Yü. Regime of Improved Confinement and High Beta in Neutral-Beam-Heated Divertor Discharges of the ASDEX Tokamak. *Physical Review Letters*, 49(19):1408, 1982.
- [414] C. Wahlberg and A. Bondeson. Stabilization of the internal kink mode in a tokamak by toroidal plasma rotation. *Physics of Plasmas*, 7(3):923–930, 2000.
- [415] G. Wallace, Z. Bai, R. Sadre, T. Perciano, N. Bertelli, S. Shiraiwa, E. Bethel, and J. Wright. Towards fast and accurate predictions of radio frequency power deposition and current profile via data-driven modelling: applications to lower hybrid current drive. *Journal of Plasma Physics*, 88(4):895880401, 2022.

- [416] R. Waltz and R. Miller. Ion temperature gradient turbulence simulations and plasma flux surface shape. *Physics of Plasmas*, 6(11):4265–4271, 1999.
- [417] R. E. Waltz, G. M. Staebler, W. Dorland, G. W. Hammett, M. Kotschenreuther, and J. A. Konings. A gyro-Landau-fluid transport model. *Physics of Plasmas*, 4:2482, 1998.
- [418] E. Wang, X. Xu, J. Candy, R. J. Groebner, P. B. Snyder, Y. Chen, S. E. Parker, W. Wan, G. Lu, and J. Q. Dong. Linear gyrokinetic analysis of a DIII-D H-mode pedestal near the ideal ballooning threshold. *Nuclear Fusion*, 52(10):103015, 2012.
- [419] T. Watanabe and H. Sugama. Velocity–space structures of distribution function in toroidal ion temperature gradient turbulence. *Nuclear Fusion*, 46(1):24, 2005.
- [420] J. Wesson, R. Gill, M. Hugon, FC Schüller, JA Snipes, DJ Ward, DV Bartlett, DJ Campbell, PA Duperrex, AW Edwards, et al. Disruptions in jet. *Nuclear Fusion*, 29(4):641, 1989.
- [421] A. White, L. Schmitz, W. Peebles, T. Carter, T. Rhodes, E. Doyle, P. Gourdain, J. Hillesheim, G. Wang, C. Holland, et al. A correlation electron cyclotron emission diagnostic and the importance of multifield fluctuation measurements for testing nonlinear gyrokinetic turbulence simulations. *Review of Scientific Instruments*, 79(10), 2008.
- [422] A. E. White, W. A. Peebles, T. L. Rhodes, C. H. Holland, G. Wang, L. Schmitz, T. A. Carter, J. C. Hillesheim, E. J. Doyle, L. Zeng, G. R. McKee, G. M. Staebler, R. E. Waltz, J. C. Deboo, C. C. Petty, and K. H. Burrell. Measurements of the cross-phase angle between density and electron temperature fluctuations and comparison with gyrokinetic simulations. *Physics of Plasmas*, 17(5), 2010.
- [423] A. E. White, L. Schmitz, G. R. McKee, C. Holland, W. A. Peebles, T. A. Carter, M. W. Shafer, M. E. Austin, K. H. Burrell, J. Candy, J. C. DeBoo, E. J. Doyle, M. A. Makowski, R. Prater, T. L. Rhodes, G. M. Staebler, G. R. Tynan, R. E. Waltz, and G. Wang. Measurements of core electron temperature and density fluctuations in DIII-D and comparison to nonlinear gyrokinetic simulations. *Physics of Plasmas*, 15(5), 2008.
- [424] D. Whyte, R. Delaporte-Mathurin, S. Ferry, and S. Meschini. Tritium burn efficiency in deuterium-tritium magnetic fusion. *Nuclear Fusion*, 63, 2023.
- [425] D. G. Whyte, A. E. Hubbard, J. W. Hughes, B. Lipschultz, J. E. Rice, E. S. Marmor, M. Greenwald, I. Cziegler, A. Dominguez, T. Golfinopoulos, N. Howard, L. Lin, R. M. McDermottb, M. Porkolab, M. L. Reinke, J. Terry, N. Tsujii, S. Wolfe, S. Wukitch, and Y. Lin. I-mode: An h-mode energy confinement regime with l-mode particle transport in alcator c-mod. *Nuclear Fusion*, 50, 2010.
- [426] D. G. Whyte, J. Minervini, B. LaBombard, E. Marmor, L. Bromberg, and M. Greenwald. Smaller and sooner: Exploiting high magnetic fields from new superconductors for a more attractive fusion energy development path. *Journal of Fusion Energy*, 35, 2016.

- [427] T. Wilks, L. Morton, D. Kriete, M. Knolker, P. Snyder, K. Barada, C. Paz-Soldan, T. Rhodes, K. Burrell, X. Chen, et al. Impact of shape on pedestal characteristics in the wide pedestal quiescent h-mode in the diii-d tokamak. *Nuclear Fusion*, 61(3):036032, 2021.
- [428] H. S. Wilson, A. O. Nelson, J. McClenaghan, P. Rodriguez-Fernandez, J. F. Parisi, and C. Paz-Soldan. Characterizing the negative triangularity reactor core operating space with integrated modeling. *Plasma Physics and Controlled Fusion*, 2024.
- [429] A. J. Wootton, B. A. Carreras, H. Matsumoto, K. McGuire, W. A. Peebles, C. P. Ritz, P. W. Terry, and S. J. Zweben. Fluctuations and anomalous transport in tokamaks. *Physics of Fluids B*, 2(12):2879, 1990.
- [430] S. E. Wurzel and S. C. Hsu. Progress toward fusion energy breakeven and gain as measured against the lawson criterion. *Physics of Plasmas*, 29, 2022.
- [431] Y. Xiao and Z. Lin. Turbulent transport of trapped-electron modes in collisionless plasmas. *Phys. Rev. Lett.*, 103:085004, Aug 2009.
- [432] X. Q. Xu and R. H. Cohen. Scrape-off layer turbulence theory and simulations. *Contributions to Plasma Physics*, 38(1-2):158–170, 1998.
- [433] M. Yamada, R. Kulsrud, and H. Ji. Magnetic reconnection. *Reviews of modern physics*, 82(1):603–664, 2010.
- [434] S. Yamaguchi, Y. Nagayama, R. Pavlichenko, S. Inagaki, Y. Kogi, and A. Mase. Microwave imaging reflectometry in lhd. *Review of scientific instruments*, 77(10), 2006.
- [435] Z. Yan, G. R. McKee, R. Fonck, P. Gohil, R. J. Groebner, and T. H. Osborne. Observation of the L-H confinement bifurcation triggered by a turbulence-driven shear flow in a tokamak plasma. *Physical Review Letters*, 112(12):125002, 2014.
- [436] L. Yao, Y. Zhou, J. Cao, B. Feng, Z. Feng, J. Luo, J. Dong, L. Yan, W. Hong, K. Li, Z. Cui, Y. Liu, E. Wang, J. Yan, and H. Team. Hydrogen cluster-like behaviour during supersonic molecular beam injection on the hl-1m tokamak. *Nuclear Fusion*, 41(7):817, jul 2001.
- [437] M. Yoshida, R. McDermott, C. Angioni, Y. Camenen, J. Citrin, M. Jakubowski, J. Hughes, Y. Idomura, P. Mantica, A. Mariani, et al. Transport and confinement physics chapter 2 of the special issue: on the path to tokamak burning plasma operation. *Nuclear Fusion*, 65(3):033001, 2025.
- [438] P. N. Yushmanov, P. N. Yushmanov, T. Takizuka, K. S. Riedel, O. J. Kardaun, J. G. Cordey, S. M. Kaye, and D. E. Post. Scalings for tokamak energy confinement. *Nuclear Fusion*, 30, 1990.
- [439] L. E. Zakharov, S. A. Galkin, S. N. Gerasimov, et al. Understanding disruptions in tokamaks. *Physics of Plasmas*, 19(5), 2012.

- [440] X. Zhang, C. Marsden, M. Moscheni, E. Maartensson, A. Rengle, M. Robinson, T. O’Gorman, H. Lowe, E. Vekshina, S. Janhunen, A. Scarabosio, P. Buxton, M. Sertoli, M. Romanelli, S. McNamara, T. Gray, and N. Lopez. Experimental observations of bifurcated power decay lengths in the near scrape-off layer of st40 high field spherical tokamak. *Nuclear Materials and Energy*, 41:101772, 2024.
- [441] H. Zhu and I. Dodin. Wave-kinetic approach to zonal-flow dynamics: recent advances. *Physics of Plasmas*, 28(3), 2021.
- [442] H. Zhu, Y. Zhou, and I. Dodin. Theory of the tertiary instability and the limits shift from reduced drift-wave models. *Physical Review Letters*, 124(5):055002, 2020.
- [443] A. Zocco, N. F. Loureiro, D. Dickinson, R. Numata, and C. M. Roach. Kinetic microtearing modes and reconnecting modes in strongly magnetised slab plasmas. *Plasma Physics and Controlled Fusion*, 57, 2015.
- [444] H. Zohm. Edge localized modes (ELMs). *Plasma Physics and Controlled Fusion*, 38(2):105, 1996.
- [445] H. Zohm. On the size of tokamak fusion power plants. *Philosophical Transactions of the Royal Society A: Mathematical, Physical and Engineering Sciences*, 377, 2019.
- [446] F. Zonca, L. Chen, S. Briguglio, G. Fogaccia, G. Vlad, and X. Wang. Nonlinear dynamics of phase space zonal structures and energetic particle physics in fusion plasmas. *New Journal of Physics*, 17(1):013052, 2015.
- [447] S. Zweben, D. Stotler, J. Terry, B. LaBombard, M. Greenwald, M. Muterspaugh, C. Pitcher, A. C. Group, K. Hallatschek, R. Maqueda, et al. Edge turbulence imaging in the alcator c-mod tokamak. *Physics of Plasmas*, 9(5):1981–1989, 2002.
- [448] S. Zweben, J. Terry, D. Stotler, and R. Maqueda. Invited review article: Gas puff imaging diagnostics of edge plasma turbulence in magnetic fusion devices. *Review of Scientific Instruments*, 88(4), 2017.